ANDRÉ LUIZ BRAZIL

AN EPIDURAL NERVE BLOCK SIMULATOR USING HAPTICS AND GAMIFICATION

Thesis submitted to the Graduation Program of Universidade Federal Fluminense, as a requirement for the fullfillment of degree of Doctor in Computer Science.
Area: Visual Computing.

Advisor: Prof. Dr. AURA CONCI

Niterói
January 24, 2017

Ficha Catalográfica elaborada pela Biblioteca da Escola de Engenharia e Instituto de Computação da UFF

B827 Brazil, André Luiz
An epidural nerve block simulator using haptics and gamification / André Luiz Brazil. – Niterói, RJ : [s.n.], 2017.
134 f.

Tese (Doutorado em Computação) - Universidade Federal Fluminense, 2017.
Orientador: Aura Conci.

1. Computação visual. 2. Anestesia epidural. 3. Dispositivo háptico. 4. Realidade virtual. I. Título.

CDD 006

ANDRÉ LUIZ BRAZIL

AN EPIDURAL NERVE BLOCK SIMULATOR USING HAPTICS AND GAMIFICATION

Thesis submitted to the Graduation Program of Universidade Federal Fluminense, as a requirement for the fullfillment of degree of Doctor in Computer Science.
Area: Visual Computing.

Approved in January 24, 2017.

DOCTORAL COMMITEE

Prof. Dr. AURA CONCI - Advisor - UFF

Prof. Dr. DÉBORA CHRISTINA MUCHALUAT SAADE - UFF

Prof. Dr. ESTEBAN GONZALEZ CLUA - UFF

Prof. Dr. JAUVANE CAVALCANTE DE OLIVEIRA - LNCC

Prof. Dr. ANSELMO CARDOSO DE PAIVA - UFMA

Prof. Dr. ALBERTO ESTEVES GEMAL - UFF

Prof. Dr. SILENA HEROLD GARCÍA – UNIVERSIDAD DEL ORIENTE

Niterói
2017

To my wife, Lúcia, for her companionship and support in all moments.

To the always present, friend, and solicit advisor, Aura.

To my son, Allan, who brings the light, the smile and look that motivate me to go on.

To professor Jauvane from LNCC, for his support, goodwill and the prompt availability of the haptic device for tests and implementations.

À minha esposa, Lúcia, pelo companheirismo e suporte em todos os momentos.
À sempre presente, amiga e solícita orientadora, Aura.
Ao meu filho Allan, que traz a luz, o sorriso e o olhar que me motivam a prosseguir.
Ao prof. Jauvane do LNCC, pelo apoio, a boa vontade e pronta disponibilidade do dispositivo háptico para a realização dos testes e das implementações.

ABSTRACT

Epidural nerve block is a blind medical procedure, where the correct place for inserting the needle is associated with a feeling of loss of resistance (LOR) when penetrating the epidural space. It aims at injecting the anesthetic fluid, avoiding the puncturing of dura-mater membrane. Since the risk of failure is high (6 to 25%), with potential damages to the patient, much training is required to minimize it. However, in some hospitals in Brazil this practice is performed directly on the patients.

This work implements an epidural nerve block simulator that unifies three main aspects as a strategy for the reduction of the failure rate on epidural procedures: The development and use of computational models, the integration of a haptic device and the gamification of user interactions.

The main contribution of this work is the development of a computational model to dimension the thickness of tissues on epidural lumbar region (skin, fat, muscle, interpinous ligament, ligamentum flavum, epidural space and dura-mater), based on the input of values for age, height and weight. This model design is based on experimental data from epidural procedures on 2000 real parturient, and the possibility to configure these values enables the creation of a wide diversity of virtual patients for the practice.

The second relevant contribution is the creation of an experiment-based needle model for epidural tissues reactions, considering the representation of its biomechanical properties (thickness, stiffness, dampening, viscosity, static and dynamic friction), the needle depth and its displacement. This model converts movements into forces, allowing real-time force feedback reactions to the needle penetration movements.

A third contribution includes a set of developed models, considering the interaction between the tissue and the needle, and taking into account its different tip types, diameters, insertion angles and direction changes on penetration. These models represent the haptic device response, in real time, to changes on the needle inclination, movement restrictions and the simulation of internal restrictions on the continuum, as well, where the needle tip corresponds to the metal edge from the haptic device.

The integrated haptic device has six degrees of freedom (DOF): three for displacements and three for rotations on orthogonal directions. This device reacts to the user interactions and reproduces the physical sensations of the needle insertions and its restrictions to movements caused by the internal tissues of the epidural lumbar region, based on the developed computational models.

The gamification strategy subdivides the epidural block procedure into tasks and includes, based on the observation of real procedures, the following main steps: the application of a local anesthesia, the Tuohy needle insertion and the saline pressure tracking. It facilitates the tracking and evaluation of the user performance and progression. The interface displays the current player score and his achievements, to motivate the practice and the student improvement.

The implemented features on the visual interface include: (1) pre-scaling and tridimensional representation of the epidural tissues and the virtual patient body in use, (2) real-time adjustment of the biomechanical tissue properties, (3) record and reproduction of needle movements, (4) computation and display of needle insertion angles, (5) display of current needle depth and applied forces, (6) simulation of syringe fit and saline fluid injection by pressing of the haptic device buttons. The implementation uses the Unity engine and C# programming language.

The gamification has not been employed yet in any currently known epidural nerve block simulators. Compared to other works, this is the only that automatically adjusts the thickness of all epidural tissues based on the patient input data. Other systems display only uni-axial answers to needle penetration, do not visually display all the epidural internal tissues or the needle angles, or even include a tutorial mode. Almost none of other works allows a free choice of the needle insertion point, a requirement to train the midline location on the patient for epidural nerve block procedures.

Keywords: Tissue modeling, haptic device interaction, gamified interface, medical procedures, serious games, loss of resistance (LOR), force model.

RESUMO

O bloqueio do nervo epidural é um procedimento médico cego onde a inserção correta da agulha está associada à sensação de perda de resistência (LOR) à penetração dos tecidos, objetivando alcançar o espaço epidural sem perfurar a membrana dura-mater. O risco de falhas é alto (6 a 25%), com a possibilidade de sérios danos ao paciente. Para reduzi-lo, é necessário muito treinamento, sendo esse feito diretamente nos pacientes, em alguns hospitais no Brasil.

Esse trabalho implementa um simulador para a prática de procedimentos de bloqueio do nervo epidural que unifica três aspectos principais como uma estratégia para a redução da taxa de falha em bloqueios do nervo epidural: o desenvolvimento e uso de modelos computacionais, a integração de um dispositivo háptico e a gamificação das interações do usuário.

A principal contribuição do trabalho consiste no desenvolvimento de um modelo para dimensionar e representar a espessura dos diversos tecidos da região lombar epidural (pele, gordura, músculo, ligamento interspinhoso, ligamento flavum, espaço epidural e dura-mater), de acordo com valores de idade, peso e altura fornecidos. Esse modelo baseia-se em dados de 2000 experimentos em parturientes reais, e a possibilidade de configuração desses valores permite gerar uma grande diversidade de pacientes virtuais de forma realista para a prática epidural.

A segunda contribuição importante é a criação de um modelo para a reação dos tecidos epidurais, baseado em experimentos de inserção de agulhas, que considera suas propriedades biomecânicas (espessura, rigidez, amortecimento, viscosidade, fricção estática e dinâmica), bem como a profundidade e o deslocamento da agulha. Esse modelo relaciona movimentos às forças e permite uma resposta em termos de reação do háptico, em tempo real, aos movimentos de penetração realizados pelo usuário.

A terceira contribuição inclui um conjunto de modelos que considera a interação entre a agulha e os tecidos, de acordo com os possíveis tipos de pontas, espessuras, ângulos de introdução e desvios da direção de inserção, algo não modelado antes em outros trabalhos. Esses modelos permitem uma resposta do dispositivo háptico, em tempo real, a mudanças de inclinação da agulha e restrições de movimento, bem como a simulação de restrições internas no contínuo, onde a ponta da agulha corresponde a ponta de metal do dispositivo háptico.

O dispositivo háptico integrado possui seis graus de liberdade (DOF): três deslocamentos e três rotações em direções ortogonais. Reage a interações do usuário e reproduz sensações físicas das penetrações com agulhas e suas restrições a movimentos, provocadas por tecidos internos da região lombar epidural, baseando-se nos modelos computacionais desenvolvidos.

A estratégia de gamificação utilizada subdivide o procedimento de bloqueio epidural em tarefas e inclui, a partir da observação de procedimentos reais, as seguintes etapas principais: a aplicação de uma anestesia local, a inserção da agulha Tuohy e o monitoramento da pressão salina. Isto facilita o acompanhamento e a avaliação do progresso e dos resultados atingidos pelo usuário. A interface exibe a pontuação atual do jogador e suas conquistas, motivando a prática e o aprimoramento do médico.

As funcionalidades implementadas na interface de visualização incluem: (1) pré-dimensionamento e representação tridimensional dos tecidos epidurais e do corpo da paciente virtual em uso, (2) Ajuste das propriedades biomecânicas dos tecidos em tempo real, (3) gravação e reprodução dos movimentos realizados, (4) cálculo e exibição dos ângulos de introdução da agulha, (5) exibição da profundidade atual da agulha e das forças aplicadas, (6) simulação do encaixe da seringa e da injeção do líquido salino, a partir pressionamento dos botões do dispositivo háptico. A implementação utiliza a engine Unity e a linguagem de programação C#.

A gamificação não havia sido aplicada ainda em nenhum dos simuladores de bloqueio de nervo epidural atualmente conhecidos. Comparado a outros trabalhos, esse é o único que realiza o ajuste automático da espessura dos tecidos epidurais, com base nos dados do paciente. Outros sistemas exibem apenas respostas uni-axiais à penetração, não apresentam uma visualização tridimensional de todos os tecidos epidurais internos, nem dos ângulos de inclinação da agulha, ou dispõem de um modo tutorial. Quase nenhum dos outros trabalhos permite a livre escolha do ponto de inserção da agulha, necessária para treinar a localização da linha mediana do paciente no procedimento epidural.

Palavras-chave: Modelagem de tecidos, perda de resistência (LOR), interface gamificada, interação com dispositivo háptico, procedimentos médicos, jogos para treinamento, modelo de forças.

LIST OF FIGURES

LIST OF TABLES

SUMMARY

1. INTRODUCTION

Anesthesia is used on a broad range of traditional medicine fields, like surgery, odontology, trauma crisis, and obstetrics. It offers support to medical procedures and its subsequent treatments, encompassing needle insertions and anesthesic fluid injections.

Success factors for anesthesia include the appropriate use of medical instruments and the correct location for application of anesthetic fluid, where both depend on the needle tip positioning, and its accuracy is improved by skill and expertise (MAURIN et al, 2004).

The epidural nerve block is commonly used in obstetric procedures such as delivery labor and cesarean section. It has been used for decades, but the failure rate remains high, from 6% to 25% (TRAN et al, 2009). Failure consequences range from headaches to a possible respiratory paralysis and, in some cases, the patient's death (LIM et al, 2005; TRAN et al, 2009).

Strategies for reduction of such failures in epidural procedures require time dedication and time of appropriate practice. Proficiency in epidural nerve block is important to avoid or reduce the rate of clinical accidents caused to patients. Medical residents generally must perform a high number of trials to acquire proficiency. A beginner usually attains epidural needle insertion competency after one year, between 1 and 85 attempts, where some may require 75 (NAIK et al, 2003). It is considered the most difficult practical anesthetic skill to acquire competence, with a mean success rate of 80% achieved after 90 attempts (KONRAD et al, 1998). Such numbers can be a challenge for the trainee, depending on the time invested on training. Usually, this medical expertise is associated with a high investment of time and money, difficult to achieve by rehearsal or even with real procedures.

Medical expertise can also be improved by observation of 2D drawings, 3D animations and video demonstrations, as mentioned in Dreidfaldt et al (2006), or practice on phantoms, artificial partial replications of human body parts, to simulate medical procedures. Figure 1 shows an example of phantom model used for epidural procedure practices. Other options listed in Lim et al (2005) include the use of cadaveric models or virtual simulators and, a practical experience on patients, guided by senior consultant (WATTERSON et al, 2007). Most hospitals in Brazil employ anesthesia practice directly on patients. There has been a shift away from this last method, due to a reduction in error tolerance of medical procedures (GRANTCHAROV and REZNIK,

2008). Continuous practice is also important: two weeks without practice can result in a significant decline in skills (KERFOOT and KISSANE, 2014). A list of advantages and drawbacks from these techniques, compiled from Coles et al (2011) and observations contained in other previously cited works, is available on Table 1.

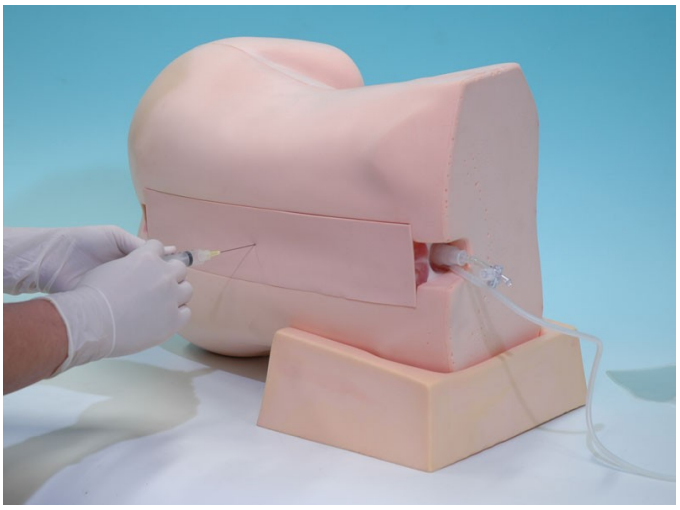

Figure 1. A phantom for the epidural procedure practice (KYOTO KAGAKU AMERICA INC., 2017).

Table 1. Comparison of main epidural procedure techniques

Technique	Advantages	Drawbacks
2D drawings	Clarity for understanding.	Lack of detail and realism.
Cadaveric models	Anatomic relationships. Allow some degree of realism of tissue behavior observations.	Limited availability and tissues displaced out from usual location.
Video demonstrations	Show clinical performance of procedures.	Require imagination of underlying body structure and tissues for the trainee
Phantom models	Replicate tactile experience. Helpful for force understanding and deformation correlations.	Lack of patient variance, difficulties for measuring needle insertion forces through their surface, inaccurate representation of biological tissues by artificial materials being used (rubber/plastic), frequent need of part replacements.
3D animations	Correct needle position and body structure tissue details visual displaied.	Lack of physical sensations.
Simulators	Inform the correct needle position and can replicate the feeling of bypassing the tissue layers. Can incorporate advantages listed for most other options.	None

Virtual simulators present a number of advantages when compared with other strategies because they can incorporate most of them (as drawings, samples and even animations, for example) in the same implementation, being able to provide a more complete learning experience. Moreover, they create a robust and secure environment

for practices with unlimited tries without any risks of accidents (CRAWFORD, 1984). This helps the medical residents to increase their skills and improve self-confidence providing an environment for executing the epidurals more close to real situations.

An increasing number of fields have explored the use of simulators for epidural and lumbar puncture anesthesia medical expertise (VAUGHAN et al, 2013). Most of them use phantoms (Figure 1), which usually present high replacement costs for the artificial body parts and tissues. Some of these lack visual feedback or do not employ an accurate force feedback model, based on human tissues properties. The use of virtual simulators may offer continuous practice and lower mantainance costs, once they usually do not require a constant replacement of parts. They support the skill development and training of medical personnel.

The objective of this work is to develop an epidural simulator, with integrated models and functionalities to support the reduction of the failure rate in epidural nerve blocks. The main work contributions include the development of computational models to correctly dimension the epidural tissues and produce force feedback responses from the haptic device to the user, both supported by real experiment data. The implemented epidural simulator (EHGS) is integrated to a haptic device and uses game elements. It associates the haptic device interactions to the developed models, emulating the epidural tissues properties and providing physical sensations for them, thus facilitating its use, practice and evaluation. The use of game elements incorporated into the simulator motivates and tracks the user progress. The simulator and its developments seek to approximate the experience to a real procedure, to provide a stimulating environment for learning and practice of medical personel before their interaction with real patients.

The development of a virtual simulator for epidural nerve block procedures is a complex task, with many important aspects to be considered. The main steps of an epidural nerve block procedure include: the search for a suitable location for the needle insertion, the application of a local anesthesia, the needle insertion and the catheter insertion (HARDAMA, 2013). The needle insertion is influenced by several factors, including: the needle diameter, its tip format and the resistance forces from penetrated epidural tissues, due to their biomechanical properties (TRAN et al, 2009). Needle movement restrictions along the procedure and the pressure measuring of the penetrated tissues, with a saline or air filled syringe are also important to simulate a correct needle placement.

The success rate of user practices on a virtual simulator is improved by the addition of force feedback, by the use of a haptic device (GEROVICH et al, 2004). Haptic devices enable sensations simulating physical restrictions and reactions of forces and moment to movements and rotations realized by operator hands. The trainee can effectively “sense” the reactions to his movements and receive immediate force feedback from actions executed by using the haptic device in the physical environment.

Haptic devices are used for a wide range of applications, including 3D modeling and realistic simulations, including medical procedures, among others. Physicians usually are not able to visualize the body interior along the epidural nerve block, so most of his interactions are oriented by tactile feedbacks (GEROVICH et al, 2004), turning the haptic device integration into an important upgrade for the simulator. This device enables the user to experiment sensations of tissue resistances when practicing the procedures within the simulator environment. It helps the practitioner to identify the transitions among tissue layers and organs, as well as their nature and properties. These interactions between the needle and tissues support the understanding of stiffness, cutting and friction mechanisms involved on a needle insertion procedure. This improves the degree of realism on virtual simulations.

Investigated models of haptic devices can be visualized in Figures 2 and 3. The Geomagic Touch (Figure 2) is the haptic device integrated to the implementations of this work. It allows a total of six (6) degrees of freedom (DOF), with three rotations and three displacements. The Novint Falcon (Figure 3 - left) is a lower cost option, but offers only 3 degrees of freedom (only displacements on 3D space). This simpler device would exclude the possibility of emulating needle inclination and rotation movements, so needle angulations. The Cybergrasp glove (Figure 3 - right) implements points of force flexion along the hand and the fingers. It can simulate the touch and grasping of different objects, but its purchase cost is very high. Moreover, the Cybergrasp glove is heavy and has big dimensions, making it a difficult target for transportations, and presents a limited avaliability for public use in scientific institutions.

Figure 4 shows the execution of the implemented simulator integrated to the use of a Geomagic Touch haptic device. The device extremity is held by the hands of the operator (user), and his actions and movements are reproduced by the black needle visible on the simulator interface. The haptic device emulates to the user the "feel" of physical sensations from the needle penetration in the tissues, as if the user were

effectively holding a real needle in his hand and feeling the resistance forces when inserting the needle through the patient body.

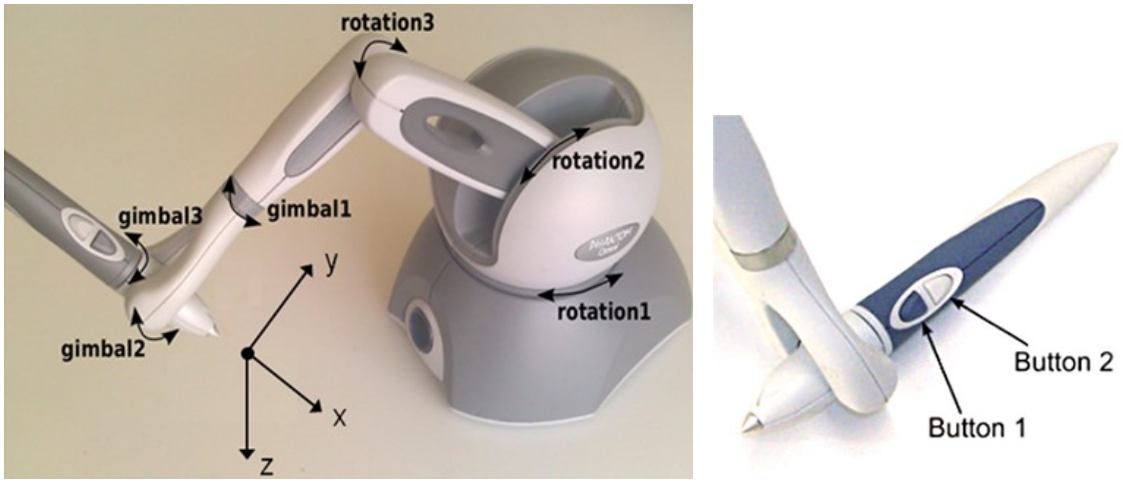

Figure 2. The Geomagic Touch haptic device, with an extremity presenting 6 degrees of freedom (DOF) and force feedback, from Sensable Technologies Inc. (2009) (left) and the needle pointer with its buttons (right).

Figure 3. Other haptic devices: The Novint Falcon haptic device (VIRTUAL REALITY SOCIETY, 2016) (left) and The Cybergrasp Glove (CYBERGLOVE SYSTEMS, 2016) (right)

Figure 5 shows the interface of the implemented simulator on execution of a needle insertion procedure, where the tissues are represented by cylindrical colored shapes. The integrated haptic device physically reproduces on the user's hand the resistance forces from each internal tissue being penetrated by the virtual needle. The simulator implementation is detailed on Chapter 5. Figure 6 shows four other developed virtual simulators with haptic device support: one with a bidimensional environment, from Gerovich et al (2004), two with a tridimensional interface, from Dubey et al (2012) and Vaughan et al (2014) works, and the last one is a hybrid solution, in that it

contains a 2D visual interface inside a phantom mannequim, from Akasum et al (2016). These works are compared to the implemented simulator in Section 6.11.

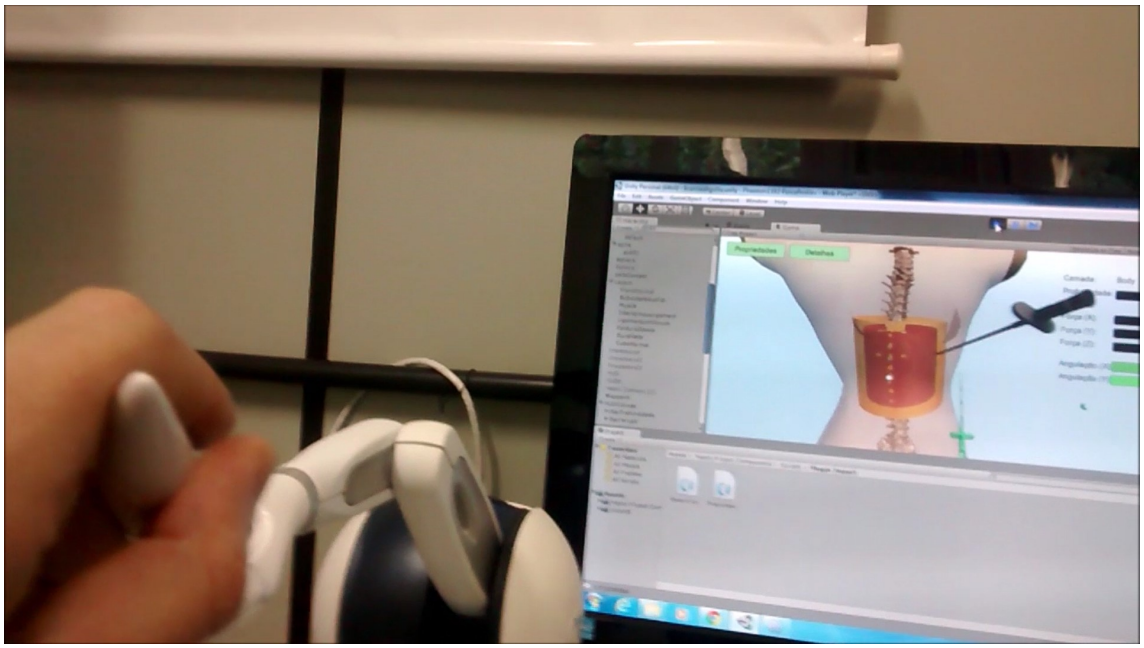

Figure 4. User hands holding a haptic device integrated to the needle movement on the simulator.

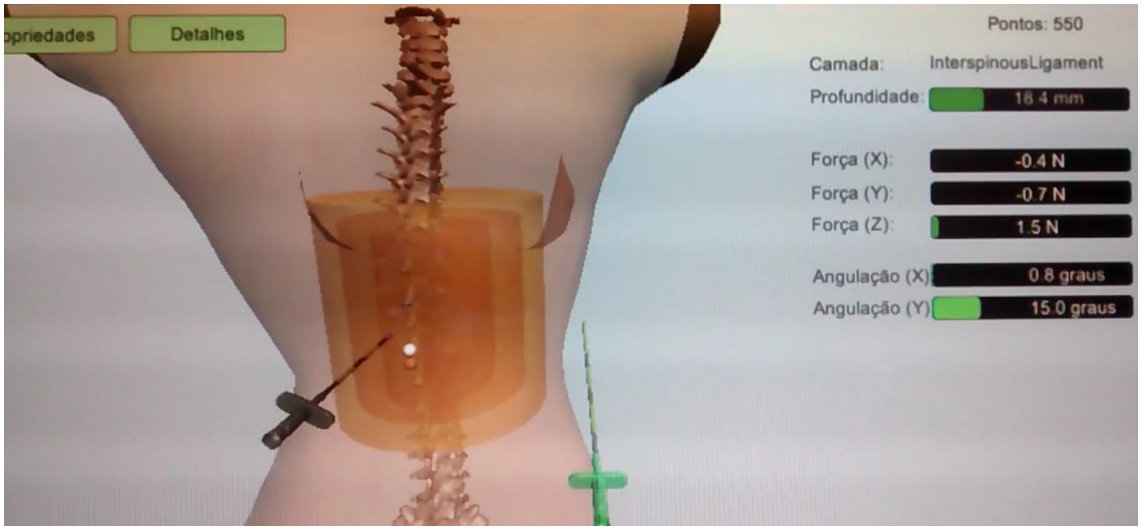

Figure 5. The interface of the implemented simulator on the execution of a needle insertion.

Critical factors for the the success of an epidural procedure also include the correct needle placement and its insertion depth (TRAN et al, 2009). Needle insertion depth can be estimated based on the thickness from tissues of epidural region. Standard thickness values for epidural tissues are provided in Dubey et al (2012) and Vaughan et

al (2014). However, experiment data from epidural needle insertion on 2000 parturient conclude that needle insertion depth changes according to the patient height, weight and age (CLINKSCALES et al, 2007). The most relevant contribution of this work is the development of a novel model to establish the proper thickness for all the relevant tissues from the epidural region, based on parturient experiment data, allowing the configuration of different virtual patients for use in the simulator, as well. This model is detailed in Section 4.1.

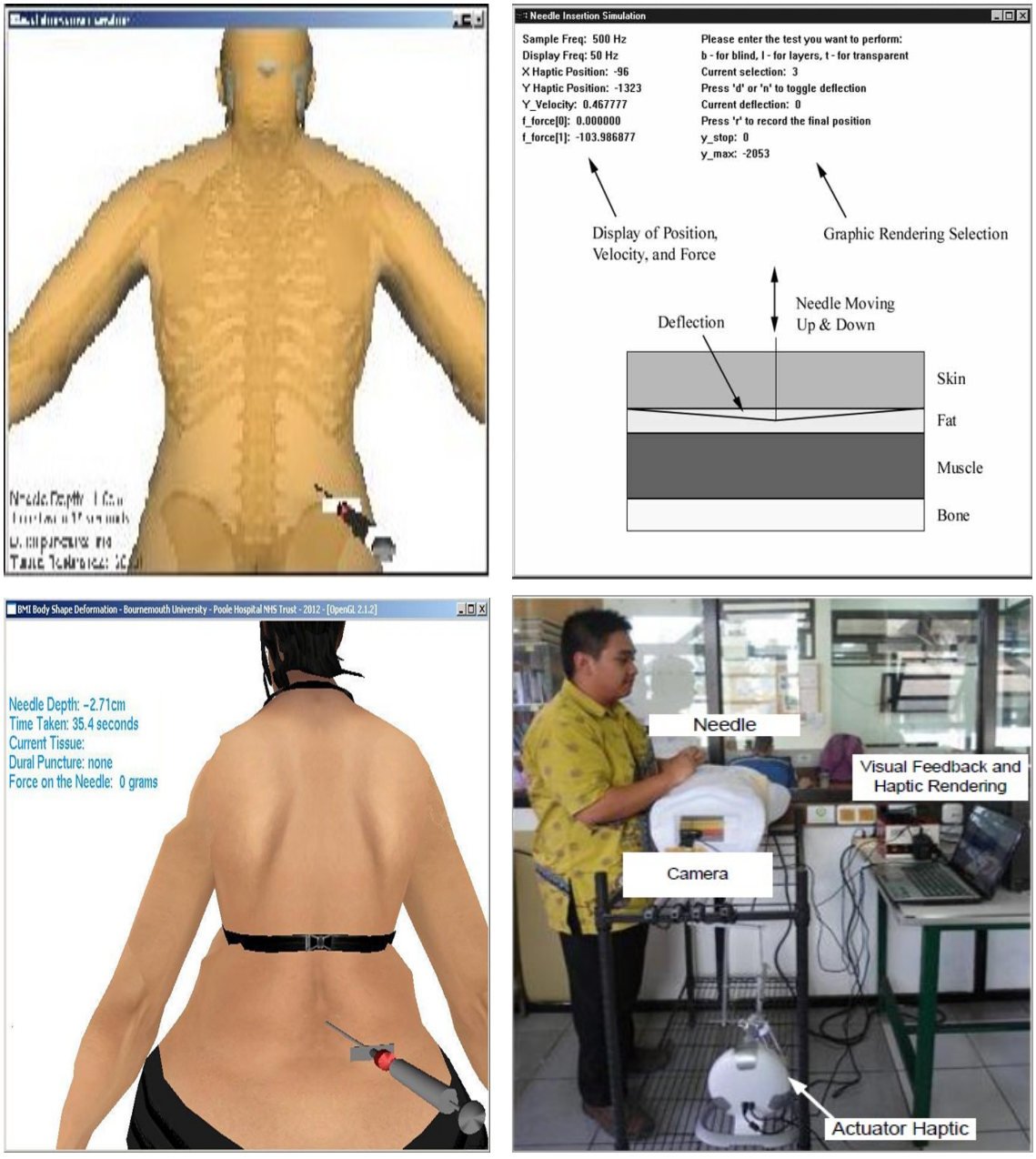

Figure 6. Visual interface of: 3D HS (DUBEY et al, 2012) (Top-Left). 2D HS (GEROVICH et al, 2004) (Top-Right). PBS (VAUGHAN et al, 2014) (Bottom-Left). Phantom mannequim integrated to a haptic device on HYS (AKASUM et al, 2016) (Bottom-Right).

The accuracy of the needle insertions forces as well as the needle deflection are also fundamental to the simulators (OKAMURA et al, 2004). They are transmitted to the haptic device and improve the realism on the emulation of physical sensations.

A proper modeling of the forces according to the needle displacement enables the production of force reactions to the user interactions. These reactions are also related to the biomechanical properties from tissues. A force model for needle insertion based on bovine liver experiment data is presented in Okamura et al (2004). It calculates the forces produced by needle displacement on the tissue, considering its stiffness, dampening and friction properties, and is detailed in Section 2.2.

Most experiment data concerning the resistance forces and biomechanical properties for human and porcine epidural tissues is scattered, presenting incomplete information, as in Tran et al (2009) and Anesthesiology (2002). This turns the research and development of force models for virtual human patients into a difficult task. The present work develops computational force models for needle insertions on humans considering all the tissues from lumbar epidural region, based on experiment data from the works found in the literature. These models are described in Sections 4.2 and 4.3.

The amount of training and the practice time invested by the physicians on the simulators are decisive factors for epidural failure rate reduction (NAIK et al, 2003; KONRAD et al, 1998). The motivation and interest of users for practice on virtual simulators can be enhanced by the incorporation of game elements. These are borrowed from games to transform the real world tasks into more ludic and meaningful experiences (HUOTARI and HAMARI, 2012). Urology residents from USA improved the amount of medical training from 3 to 84 hours by the use of gamification (KERFOOT and KISSANE, 2014).

The game elements most commonly used in gamifications are the points (P), the badges (B) and the leader boards (L) (Figure 7). These together evidence the use of the PBL mechanic, a basic and popular gamification strategy (WERBACH and HUNTER, 2012). Points indicate the current user score, a measure of experience and reputation. Badges are visual icons, associated to objectives and achievements, to track the user progress. A leader board shows the best players and the highest scores, and mobilizes the users by competition.

Figure 7. The most common game elements used in a gamification: badges (E-FRONT, 2017) (left), player score (right) and leaderboard (HOTSCHEDULES, 2016) (right).

The gamification development for the simulator focuses on the practice engagement through a gameplay experience, with specific challenges to be fulfilled, tied to the epidural procedure, and an immediate feedback composed of points, achievements and statuses, for user performance tracking and comparison. The gamification strategy implemented on the simulator is detailed in Section 5.3.

This work is divided in seven chapters. Chapter 2 includes the theorical foundation; it details the procedure of epidural anesthesia, and the relevant factors for the construction of computational models for epidural procedures, as well as definitions and main applications for gamification and serious games. Chapter 3 presents and discusses the related works, in the light of three main aspects: virtual simulators, force models and gamification strategies. Chapter 4 details the developed computational models. Chapter 5 describes the simulator implementation and its developed functionalities and features. Chapter 6 includes the achieved results and the comparisons with other investigated simulators with haptic device support. Chapter 7 focuses on the conclusions and includes and comments the future works.

2. THEORETICAL FOUNDATION

2.1. EPIDURAL NERVE BLOCK PROCEDURE

The epidural nerve block is a medical procedure for injection of anesthetic fluid in a specific location on the human body: the virtual epidural space (ES). Indications for epidural nerve block applications include: part labor or cesarean delivery on obstetrics, and surgeries related to the orthopedics, urology, gynecology, or abdominal, vascular and pelvic areas, as indicated in Chawla and Raghavendra (2015), including the pain relief treatment for women and men.

The epidural space is located inside the vertebral column, between the ligamentum flavum (Figure 1) and the dura mater, from two to nine centimeters below the skin (GRAU et al, 2001). The lumbar spine ranges from the vertebrae L1 to L5. The lumbar epidural space is situated within this range, as shown in Figure 8.

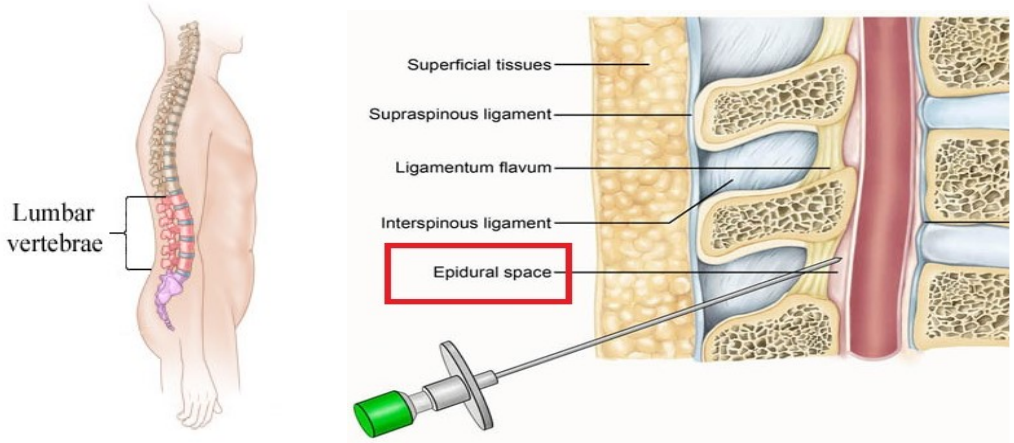

Figure 8. Lumbar epidural space region (AGENCIACULTIVA, 2016) (left) and the main tissue layers (KEVINLIMD, 2017) (right).

The epidural nerve block procedure requires a needle insertion through the patient's back, usually between the vertebrae L2 and L3 or L3 and L4, where there is a larger inter-vertebral space. To reach the epidural space (ES), the needle must trespass skin and subcutaneous fat (SF), which are superficial tissues, the supraspinous ligament (SL) (muscle), the interspinous ligament (ISL) and ligamentum flavum (LF), as shown in Figures 8 and 9. Afterwards, a catheter is introduced through the needle and, then anesthetic fluid is apllied. The vertebrae, in Figure 9, are represented by the spinous processes (SP): the bony projections located on the back of the patient body. Figure 9

shows the layers subsequent to epidural space: dura-mater (DM), cerebro-spinal fluid (CSF) and spinal cord (SC).

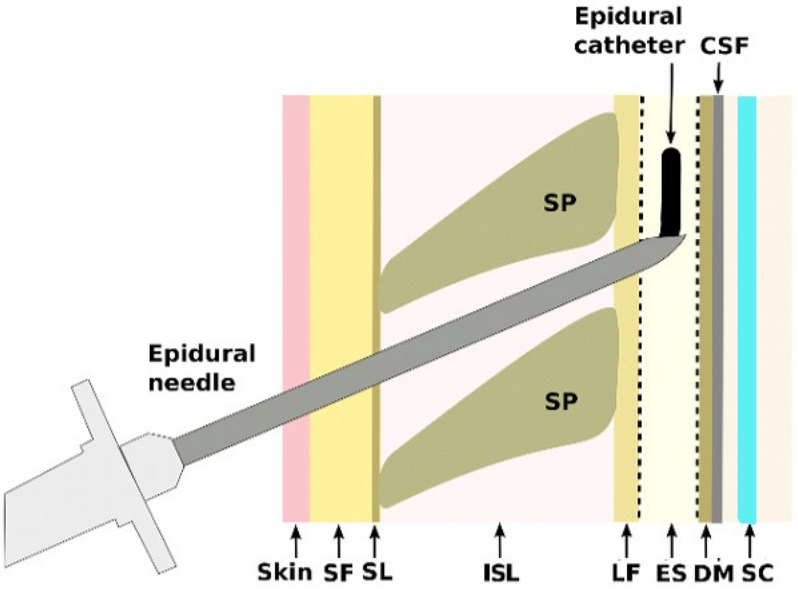

Figure 9. Lumbar epidural region with the epidural space (ES) and the other tissue layers (SOTO-ASTORGA, 2013).

The identification of the epidural space is a challenge, once anesthetists are not able to see through the patient's body. Although, as the needle insertion is a blind procedure, it can be oriented by a technique named loss of resistance (LOR) (WILSON, 2007). The LOR is related with the pressure of the tissues bypassed by the needle along its insertion process (Figure 10). It consists of measuring the tissue pressure with a syringe filled with a saline solution or air, attached to the needle. Tissue pressure is "felt" with the thumb on the syringe, by pressing the plunger and trying to inject the fluid or air. The ISL and LF tissue layers offer higher resistances, while ES can be detected by a sudden pressure drop. Figure 11 shows a simplified diagram, developed to facilitate the understanding and the representation of the LOR technique.

The epidural needle placement starts by inserting the needle up to the interspinous ligament (IL), located in the region between the vertebrae. The anesthetist is able to sense this region due to an increase in the force required to move any further the needle. Such forces are intensified when the physician proceeds with the needle insertion and reaches the Ligamentum Flavum (LF) tissue. Afterwards, the anesthetist stops the needle insertion and inserts a 10 ml syringe filled with 3 to 5 ml of saline or air on the back of the needle (see Figure 12). This filled syringe is used to sense the pressure of the current tissue, achieved by continuously trying to inject the fluids in the

syringe. The pressure from the current tissue can be felt by pressing the syringe's plunger with the thumb finger. Each time the anesthetist senses high pressure on the thumb, the needle must be inserted a little further. The syringe pressure test is then repeated again and again until suddenly a pressure drop occurs, meaning that the needle reached the epidural space location.

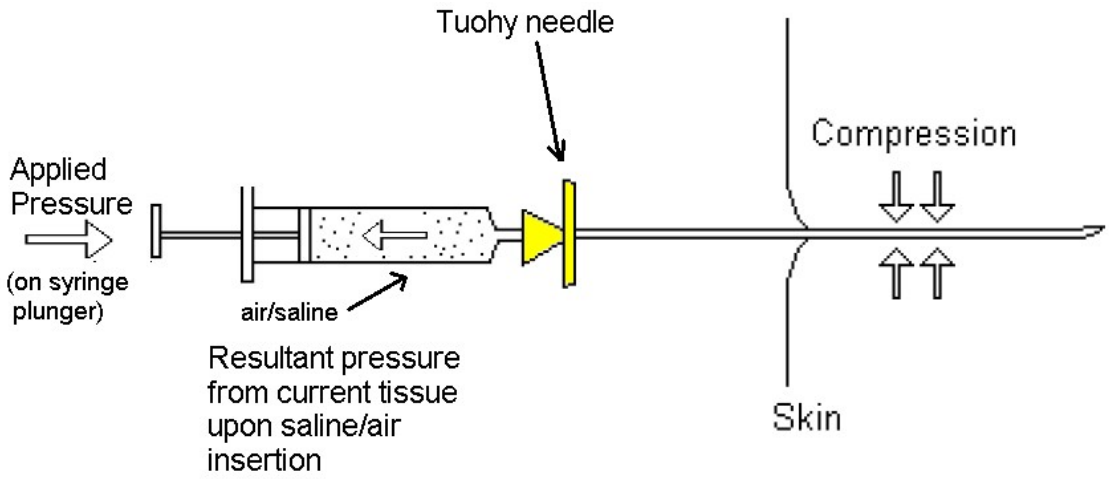

Figure 10. Applied pressure and pressure related to the loss of resistance (LOR) (VAUGHAN et al, 2013).

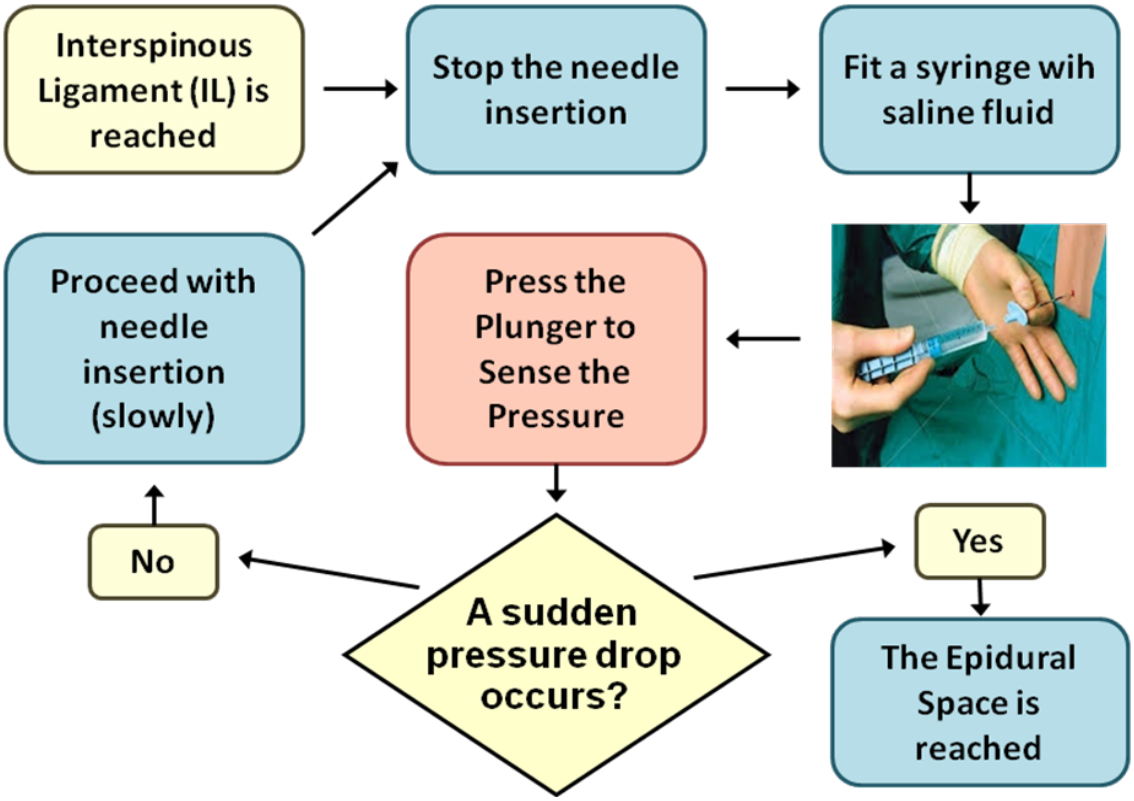

Figure 11. A simplified diagram of the loss of resistance (LOR) technique.

The epidural space location is related to a sudden sensation of drop in the pressure resistance to the fluid injection, which characterizes the loss of resistance (LOR) technique. The saline or the air in syringe is used only to test the current location to anesthesic injection. A catheter insertion occurs after the epidural space is located and is used to continuously administer the anesthesic fluid. The syringe used to test the LOR is removed. The needle is rotated until its orifice (hole) becomes pointed to the cranial direction (upwards to the patient head), and then the catheter is inserted through the needle, three to four centimeters depth, beyond epidural space. After catheter placement, the needle can be removed, because the catheter fixation is guaranteed due to combined tissues resistances along the way.

Figure 12. Insertion of saline or air filled syringe into the back of the Tuohy needle (MEDISCAN, 2017).

Serious consequences may occur when a needle surpasses the epidural space and reaches a tissue layer beyond it, like the dura-mater, cerebrospinal fluid or the spinal cord. They include neurological damage, dural puncture (leading to headache and backache) and pain. The puncture of the dura-mater can cause headache in 85% of failures, as indicated in MacArthur (1993), but there is risk of permanent paralysis or perioperative morbidity. To avoid puncturing the dura-mater membrane in the needle insertion procedure, the epidural needle (Tuohy) has a specific design for nerve block procedures (Figure 13). A curved and beveled tip helps to avoid the dura-mater membrane perforation. Its metal part has markers each 1cm apart to indicate the penetration depth to the anesthetist. Its plastic wings enable the physician to hold the needle firmly with his hand, increasing the precision on the procedure. The metal part is a long hollow tube, where a catheter or a mandrel can pass throught it. The mandrel

(Figure 13) is a thin and sharp pointed needle inserted inside the Tuohy to avoid the entrance of strange tissues into the system.

Common issues during the epidural procedure include needle insertions with wrong angles or vein tearing, by the inserted catheter. Wrong insertion angles may cause the needle to reach the spinous process (SP) (back bone structure), where bending would be necessary to proceed further. Bending the needle is dangerous, as it can break apart and remain inside the patient, causing several complications. The recommendation, in this case, is to remove the needle and restart the needle insertion in the right position. The catheter insertion can tear a vein in the epidural space. It is indicated by blood returning through the catheter, in which case, it must be removed. The needle must be rotated to slightly change its orifice orientation, so the catheter can be reintroduced without affecting the vein.

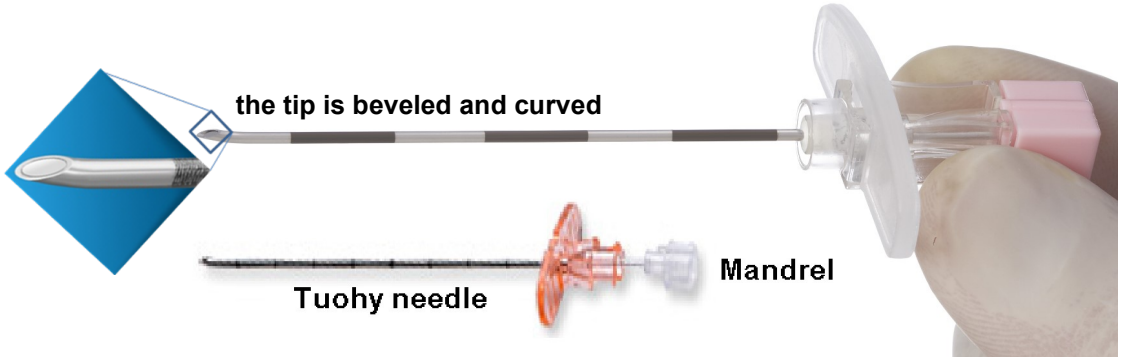

Figure 13. The Tuohy epidural needle (MYCO MEDICAL, 2017) and the mandrel (VOGT MEDICAL, 2017).

The insertion method of the needle is also important for an epidural procedure. It determines the needle inclination angles and has 2 typical approaches: the midline and paramedian (Figure 14) (VAUGHAN et al, 2013). Both techniques are usually employed. They promote the catheter fixation inside the patient body due to a higher resistance from all tissues traversed on the procedure (Figure 8), while the paramedian approach (Figure 14) is better for single shot anesthesia applications. This approach reaches the ligamentum flavum sooner after the muscle tissue, instead of cutting through interspinous ligament, but presents a higher risk of dural puncture (perforation of dura-mater). The Tuohy needle can be employed when the anesthesic fluid administration through a catheter is necessary. A syringe with anesthesic fluid is used for single shot applications.

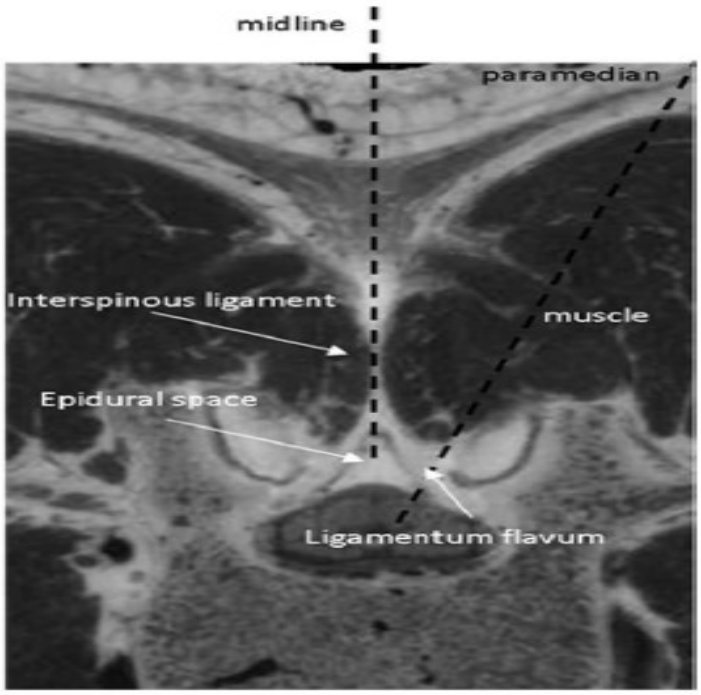

Figure 14. Midline and paramedian needle insertion approaches (TRAN et al, 2009).

2.2. FORCE MODELING

The main objective of a force model is to calculate the resulting forces to be employed at the simulations, considering input parameters. These forces are usually related to the needle insertion procedure and the biomechanical properties of the tissues.

Usually, needle insertion procedures operate in out of vision areas. Traditionally, anesthetists rely on manual (force and tactile) or even audio feedback to guide their movements (GEROVICH et al, 2004). Medical practice relies strongly on manual skill of medical personnel, challenging human accuracy, dexterity and precision, although, in some situations, visual information can be available from additional devices,

Needle insertion studies help to understand the sensibility of force perception and support the design of a haptic device interface and a more realistic simulator. Experiments results allow the establishment of force ranges involved in procedures, as well as the temporal evolution of these forces (MAURIN et al, 2004). They help in characterizing the forces and torques applied during epidural nerve block procedures.

2.2.1. NEEDLE INSERTION FORCES

Forces required for tissues penetration are significant for force modeling and simulations. Average force values for human skin puncture are 6.0 Newtons ± 0.7 Newtons (standard deviation) and 1.974 ± 0.0 Newtons for subcutaneous fat tissue in Holton and Hiemenz (2001). Porcines have a similar lumbar structure, but higher average puncture forces (12.9 ± 2.6 Newtons for skin). The use of swine models for biomaterials research is a common practice. Force values from needle insertion experiments on a porcine cadaver in Dubey et al (2012) are listed on Table 2. Force transducer measurements of the epidural needle are shown on Table 3, from Anesthesiology (2002), where the miminum, maximum, average and standard deviation values of forces in Newtons are related to four layers trespassed by the needle.

Table 2. Average thickness, depth and needle insertion forces, based on porcine and human measurements (DUBEY et al ,2012; VAUGHAN et al, 2014).

Tissue Layer	Average Tissue Thickness (mm)	Total Needle Depth (mm)	Needle Insertion Force on Porcine (N)
Skin	3	0	12.9
Subcutaneous Fat	6	3	6
Supraspinous ligament	4	9	9
Interspinous ligament	26	13	8
Ligamentum flavum	3	39	11.1
Epidural space	6	42	0
Dura	15	48	2.0

Table 3. Forces for needle penetration on human epidural tissues (ANESTHESIOLOGY, 2002).

Tissue	Average (N)	Std Dev (N)	Minimum (N)	Maximum (N)
Skin Tissue	8.5	1.4	2.5	21.1
Subcutaneous Fat	8.0	0.9	1.5	16.7
Interspinous Ligament	12.8	1.0	2.2	19.6
Ligamentum Flavum	13.8	1.5	3.4	23.0

An organized list of tissues thickness and puncture force values of experiments from needle insertion simulations is available on Table 4, constructed from results of Holton and Hiemenz (2001). Most of these experiment data values are applied on the design of the force model defined in Section 4.2, considering the force values for all the epidural tissues.

Some human puncture force values from Table 4 are estimated (they are marked with *), based on a correction factor calculated from a comparison among puncture force values from other swine and human tissues. The human muscle puncture force (4.354 N) is an estimation that uses the swine average muscle puncture force (8.407 N)

as a base value and subtracts a correction value from it. This correction value is 4.053 N, the swine average fat puncture force minus human average fat puncture force (6.027 N - 1.974 N). The ligamentum flavum human puncture force value (12.1330) is estimated based on the swine average LF puncture force value (6.1313 N), with an addition of a correction factor from the average skin puncture force value from swine (6 N). The thicknesses values were obtained from a woman MRI scan. The swine steady force is a stable force value for convergence after the tissue puncture, and along the tissue penetration.

Table 4. Human and porcine puncture forces, steady-state forces and thicknesses for tissues of epidural lumbar region (HOLTON and HIEMENZ, 2001).

Tissue	Human puncture force (N)	Thickness (mm)	Swine puncture force (N)	Swine steady-state force (N)
Skin	6.0372**	10.8	12.9***	-
Fat	1.974	2.8	6.027	-
Muscle	4.354*	1.9	8.407	3.675
Interspinous Ligament	7.467	18	-	4.053
Ligamentum Flavum	12.1330*	7.4****	6.1330	-
Epidural Space / Subdural Tissue / Dura-mater	2.437	8.6*****	-	-
Bone	8.0265******	-	-	-

* Estimated values based on swine measurings, with a correction factor calculated from other swine/human tissues puncture forces

** 6.0 ± 0.7 *** with a standard deviation of 2.6 **** 5.4 after puncture ***** 10.6 after puncture

****** The bone is impassable in this case, this is the starting force, that keeps increasing after contact

A comparison of forces required for needle insertion among the paramedian and midline approaches on human subjects and porcine cadavers was conducted in (TRAN et al, 2009). The properties of interspinous ligament and ligamentum flavum tissues are measured. The results concerning these properties indicate the average and maximum applied forces (in Newtons) required for penetrating tissues and their average and maximum pressure resistances to saline fluid injection (in kiloPascal kPa, i.e. considering the tension or the force by unit of area) , they are available on Tables 5-6. The average applied force required on the human tissue of ligamentum flavum was higher (5.0 ± 3.0 N) than on interspinous ligament (2.0 ± 1.4 N). The maximum applied force for the human ligamentum flavum was also higher (6.0 ± 3.0 N) than that for interspinous ligament tissue (4.3 ± 1.3 N).

Table 5. Applied forces and pressure resistances for tissues from porcines with values for needle insertions on midline and paramedian approaches (TRAN et al, 2009).

Tissue/Region (approach)	Applied Force (N)	Maximum Applied Force (N)	Pressure Resistance (kPa)	Maximum Pressure Resistance (kPa)
Interspinous ligament (midline)	8.9 ± 5.3	14.7 ± 6.6	31.3 ± 12.8	59.4 ± 24.1
Muscle (paramedian)	9.4 ± 5.4	13.7 ± 7.0	34.0 ± 17.4	56.2 ± 31.3
Ligamentum Flavum (midline)	8.9 ± 5.3	14.7 ± 6.6	31.3 ± 12.8	59.4 ± 24.1
Ligamentum Flavum (paramedian)	12.9 ± 5.3	16.1 ± 5.3	50.4 ± 25.8	65.6 ± 33.5
LOR (midline)	11.4 ± 8.3	18.2 ± 9.6	40.1 ± 32.7	61.2 ± 40.0
LOR (paramedian)	12.9 ± 5.1	17.4 ± 5.5	57.9 ± 28.1	82.0 ± 34.7

Table 6. Applied forces and pressure resistances for tissues from human subjects using the midline needle insertion approach (TRAN et al, 2009).

Tissue/Region (approach)	Applied Force (N)	Maximum Applied Force (N)	Pressure Resistance (kPa)	Maximum Pressure Resistance (kPa)
Interspinous ligament (midline)	2.0 ± 1.4	4.6 ± 1.3	15.5 ± 12.0	34.9 ± 17.4
Ligamentum Flavum (midline)	5.0 ± 3.0	6.0 ± 3.0	31.5 ± 28.0	39.5 ± 30.3

2.2.2. TISSUES THICKNESS AND BIOMECHANICAL PROPERTIES

Tissues thickness is relevant on force modeling and virtual simulations for epidural anesthesia. Table 2 (in Section 2.2.1) shows experiment results of needle insertions on porcine from Dubey et al (2012), and the average thickness values of epidural tissues for women, based on a MRI scan data from Vaughan et al (2014). These values are are very relevant information for specification of more realistic simulations, being applied on the development of the equation to dimension the thickness of all epidural tissues for the patient in the simulator, detailed in Section 4.1.

Subscapular skinfold thickness (Figure 15) is a common measurement applied to estimate patient body fat percentage. It can be estimated based on waist area, mass and age (VAUGHAN et al, 2014). Average women values for these parameters can be useful to calculate skinfold thickness of virtual patients with different body shapes. Epidural space thickness has an averaged value of 6 mm (VAUGHAN et al, 2014). This value matches the data reported on Table 2.

The distance from skin to epidural space (ES) is significant for simulation of epidural needle insertions. It averages 5.3 ± 1.21 (standard deviation) mm in parturients from Michigan (USA) in Clinkscales et al (2007). Average values from epidural nerve blocks realized on parturient together with weight, height and age are reported by these

authors. These values are also used as body scale parameters to formulate an equation for dimensioning the thickness of all epidural tissues for the patient in the simulation (Section 4.1). There is also a correlation of the skin to epidural space distance with the body-mass index (BMI) of patients. It ranges from 4.8 cm, on normal BMI patients, to 6.2 cm, on obese ones in Brummett et al (2009). Average epidural space depth for patients with a BMI 30 or less is 41.60 ± 5.80 (standard deviation), and 51.97 ± 5.28 for patients with a BMI superior to 30 in Ravi et al (2011).

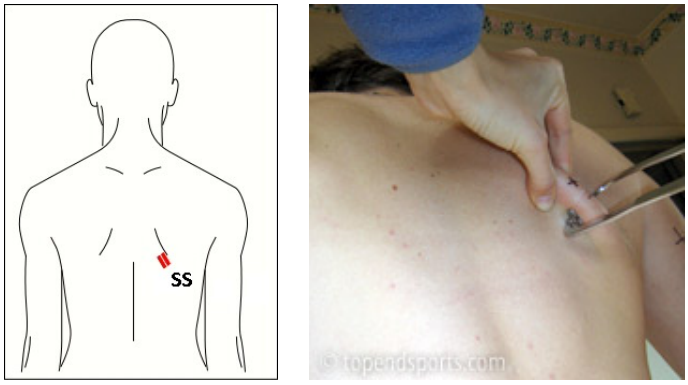

Figure 15. Subscapular skinfold (SS) area (DIGITAL HUMAN RESEARCH CENTER, 2017) (left) and how it is measured with a pinch (TOPEND SPORTS, 2017) (right).

The composition of each tissue to be penetrated in the needle insertion procedure determines its biomechanical properties. Among these are: stiffness, damping, static and dynamic friction, and resistance to perforation. Friction forces oppose lateral motion along a surface, and their magnitude is proportional to the perpendicular (normal) contact force. They can be simulated on needle insertion procedures. Physical sensations for these can be emulated by haptic devices. A detailed description of these tissue properties related to their sensations from Sensable Technologies Inc. (2009) includes**:**

- **Stiffness:** Relation between tension and deformation, or force and displacement for elastic materials (spring behavior). It represents the tissue hardiness to deformation. Maximum stiffness represents the hardest surface to deformation while minimum represents the most compliant one.
- **Damping:** The restraining of vibratory motion. Minimum damping creates a highly stable feeling. The damper is provided to reduce vibration, since it opposes motion, and its strength is proportional to the current velocity. The force felt is of restoring with a decrease in the amplitude.

- **Static Friction:** Tissue motion resistance, when moving from static (inertia). It represents the hardiness to move onto the surface starting from a static position.
- **Dynamic Friction:** Tissue motion resistance, when there is already movement (not inertia). It represents the hardiness to move onto a surface when the motion has already been engaged.
- **Resistance to perforation:** The amount of force to go through a surface. Maximum resistance will block the puncture.
- **Punctured Static Friction:** The hardiness to move inside a punctured tissue starting from a static position.
- **Punctured Dynamic Friction:** Represents the hardiness to move inside a punctured tissue when motion has already been engaged.

2.2.3. NEEDLE DEFLECTION

Needle deflection forces are another factor to be considered on force modeling and simulations. Needle tip format and diameter can influence needle insertions (OKAMURA et al, 2004). Section 4.3 details the design of a force model for the needle deflection based on these factors, and uses the experiment data available on Table 7.

Table 7. Average needle bending forces based on tip type, angles and diameter (OKAMURA et al, 2004).

Needle Tip Type	Tip Angle	Diameter (mm)	Average Force (N/s)	Standard Deviation (N/s)
beveled	14 ^{o}	0.75	-0.263	0.010
beveled	10 ^{o}	1.00	-0.308	0.009
beveled	14 ^{o}	1.00	-0.309	0.011
beveled	20 ^{o}	1.00	-0.320	0.015
beveled	14 ^{o}	1.35	-0.420	0.017
beveled	14 ^{o}	1.55	-0.469	0.033
coned	28 ^{o}	0.59	-0.276	0.006
coned	28 ^{o}	0.95	-0.328	0.015
coned	28 ^{o}	1.55	-0.552	0.005
triangular	49 ^{o}	0.59	-0.171	0.006
triangular	49 ^{o}	0.95	-0.251	0.002
triangular	49 ^{o}	1.55	-0.360	0.007

Most common needle tips are triangular, coned and beveled (Figure 16). Other needle tips and its angles can be seen in Figure 17 in Abolhassani et al (2007). A deflection can occur when the tissue around the needle tip is compressed. This can exert an unbalanced resistance against the compression, depending on the tip format (ABOLHASSANI et al, 2007). Figure 16 shows the directions of the forces exerted by symmetric tips (1 and 2) and a beveled tip (3). Triangular and coned tips are symmetrical, while beveled ones are not. Figure 16 (bottom) shows the influence of the unbalanced resulting forces upon a needle with a beveled tip on insertion.

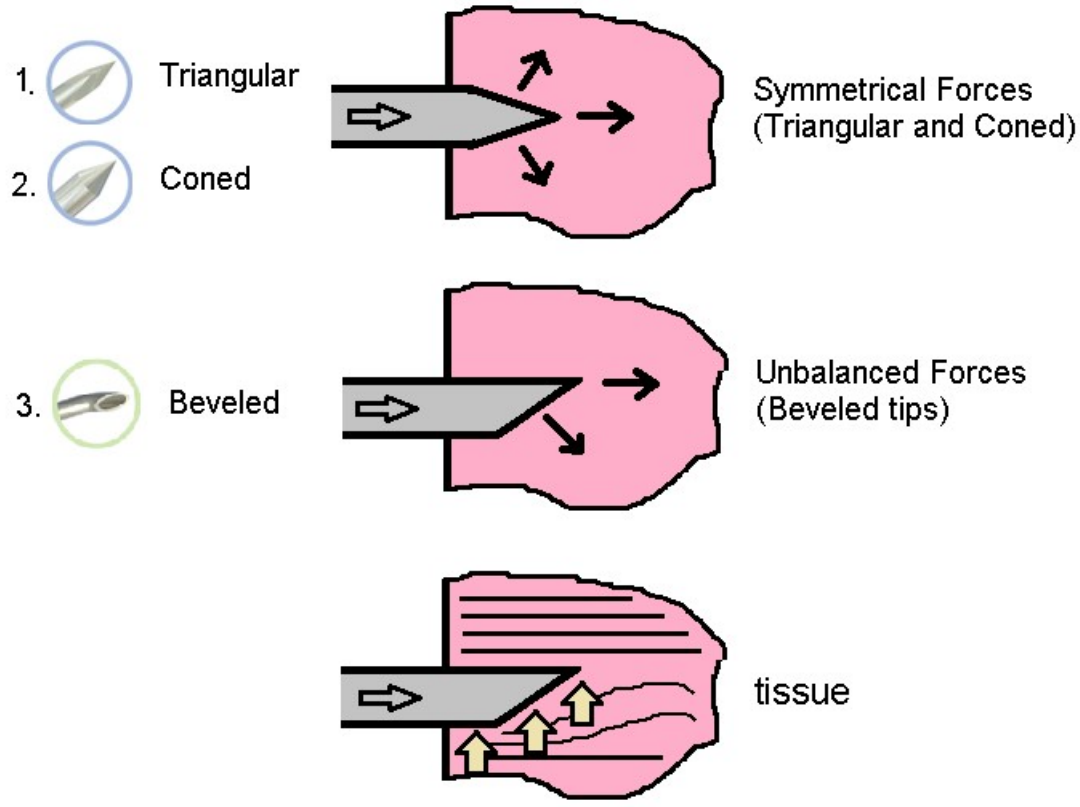

Figure 16. Symmetric triangular (1) and conic (2) tip and unbalanced beveled (3) type with their acting forces from tissue compression on needles.

Needle insertion experiments on a 10x4cm cylindrical silicone rubber piece, with stiffness properties similar to a bovine liver were conducted in Okamura et al (2004). Needles of different tips and sizes are considered with CT image analysis to measure the bending forces in tests, including the mapping of relative needle and tissue velocity experiments. Average values for bending forces vary relating and they are visible on Table 7. Coned tips produce the higher needle deflection force values, followed by beveled ones. The use of triangular tips result in reduction of the needle

deflection forces. This can be justified by the number of cutting surfaces (triangular=3, beveled=1, coned=0) that contribute for tissue ripping. Tip angle variations do not present a significant effect upon the needle slope.

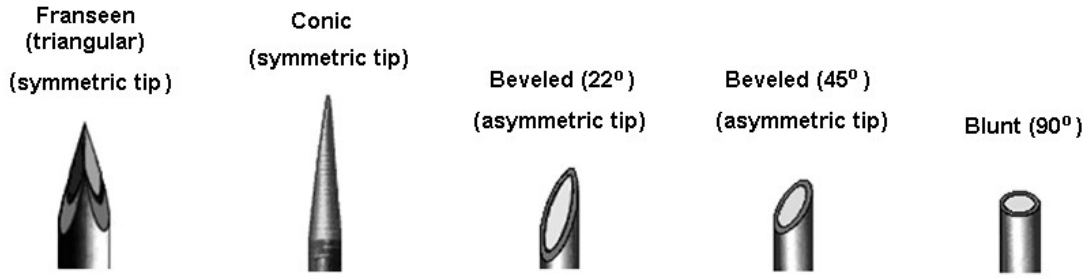

Figure 17. Needle tip types (ABOLHASSANI et al, 2007).

Needles with beveled tips tend to bend more, because they have a single cutting surface, so they tend to receive a higher force to one side. Figure 18 shows the ratio between bending force and axial force (on z axis). Bending on coned and triangular tips occur due to small density variations on rubber, since they are symmetrical, so normally would not bend at all. Beveled tips present more possible bending and susceptibility to tissue density variations. Although, they remain preferred among physicians due to their ability to rotate the needle and apply fluids in different directions (OKAMURA et al, 2004).

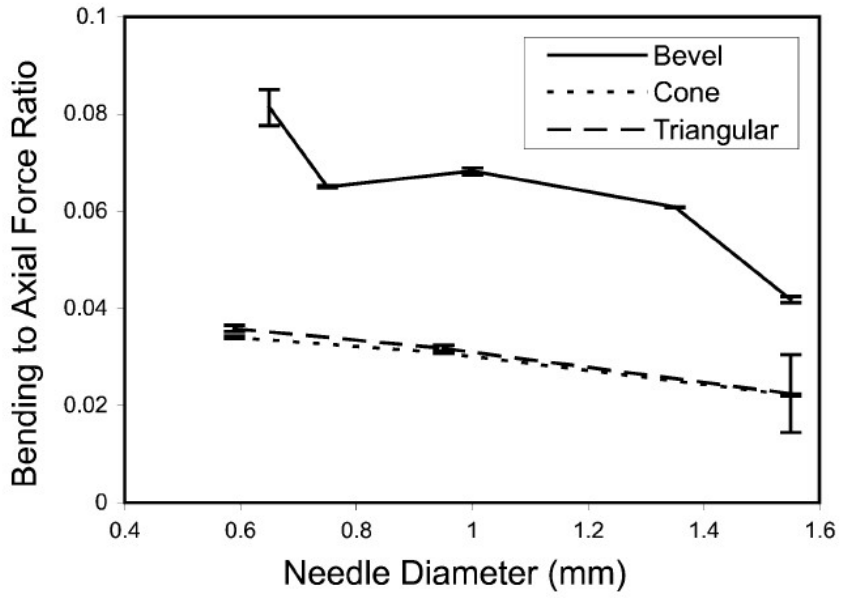

Figure 18. Needle bending force ratio and needle diameter for different tips (OKAMURA et al, 2004).

Needle diameter significantly affects average bending in a positive relation. As needle diameter increases, more tissues are compressed in the needle vicinity, which improve forces normal to the needle surface, resulting in higher friction forces. A linear relationship between needle displacement and axial forces upon needle insertion are presented for all needles, with a single exception of the 0.65mm diameter where it is represented by a second order polynomial curve in Okamura et al (2004). Needle bending effect was also studied in Okamura et al (2004). A reducing bending-axial force ratio increases the needle diameter, as usually thinner structures tend to bend more (Figure 18). Results indicate that thinner needles with beveled tips bend more than thicker ones or those with coned or triangular tips. Needles with larger diameter demand higher cutting forces on insertion which is directly related to the tissue being penetrated.

2.2.4. Pressure Resistance

The detection of the epidural space constitutes into a critical element for a successful needle insertion on an epidural nerve block procedure. The epidural space can be located by the use of the loss of resistance (LOR) technique, detailed in Section 2.1.

Pressure resistances to saline fluid and air injections on the tissues can be measured by the use of sensors. Results of pressure measuring from needle insertion experiments using a midline approach and the LOR technique in humans in Tran et al (2009) are shown in Tables 5 and 6, presenting the average and maximum forces applied and the pressure resistances for human tissues. These values are considered for the implementation of a pressure generation functionality for the epidural tissues on the simulator, described in Section 5.2.6.

The results of Figure 19 show how the needle displacement (a), average applied force (b) and estimated pressure variation (c) applied on the syringe plunger behave along the time (TRAN et al, 2009). The estimated maximum pressures values for the interspinous ligament are (15.0 ± 5.3 kPa), against (37.5 ± 20.0 kPa) for the ligamentum flavum. The epidural space is reached slightly after 20 seconds, when both a sudden force decrease (b) and a syringe pressure drop (c) occur (Figure 19).

Results of needle position and pressure versus time for the midline and paramedian approach for LOR can be compared in Figure 20. In the midline approach, the pressure drop (50 to 10 kPa) is bigger and more easily detected than in paramedian approach (60 to 40 kPa). The midline approach trespasses the ligamentum flavum

before epidural space. This tissue presents a higher pressure resistance to air and saline injection. The paramedian approach usually jumps from supraspinous ligament directly to epidural space, turning its detection by LOR more difficult (TRAN et al, 2009).

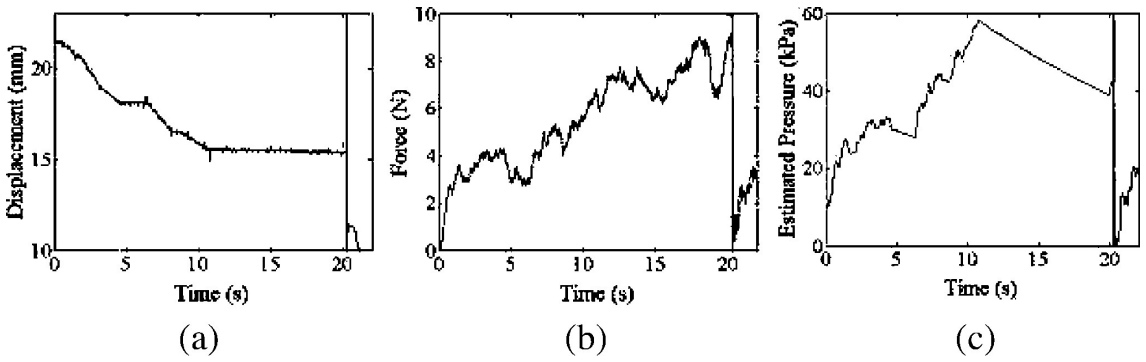

Figure 19. Graphic of (a) Displacement, (b) Force and (c) Estimated pressure for midline approach using the continuous pressure technique on humans in (TRAN et al, 2009).

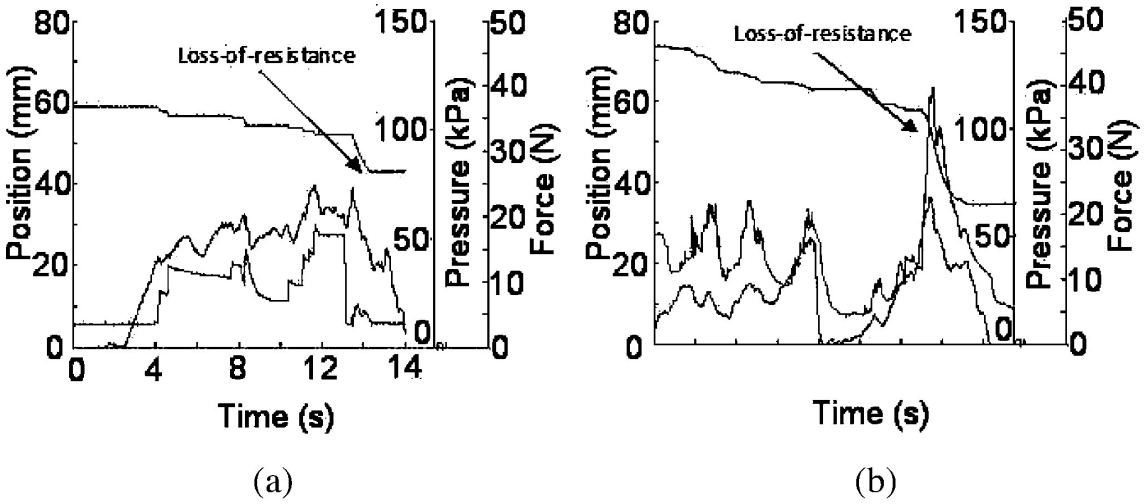

Figure 20. Graphics of displacement (highest line), pressure (bottom) and force (middle) versus time for (a) Midline and (b) Paramedian needle insertion approaches in (TRAN et al, 2009).

The graphics of Figure 21 show that pregnancy affects LOR detections for needle insertions. Pressure measurings for epidural needle insertion have shown a higher pressure (85 kPa) on non-pregnant women against 50 kPa for pregnant women using LOR in Lechner et al (2011). These graphs present the pressure (kPa) in various stages of needle insertion procedure marked with numbers 1-3 and letters A-C, where (1) represents test to verify the sensors before epidural insertion, (2) indicates the puncture start and (3) the reach of epidural space, (A) is the pressure peak before entering the epidural space, (B) is the pressure level soon after its entrance and (C) is

pressure level after a catheter insertion, for pregnant woman (left) and non-pregnant (right). Table 8 compares average pressure resistance values for penetration of ligamentum flavum and epidural space. Pregnant women have weaker resistance on LF due to their hormonal state. Difficulty for epidural anesthesia training and its learning curve were mentioned in Lechner et al (2011).

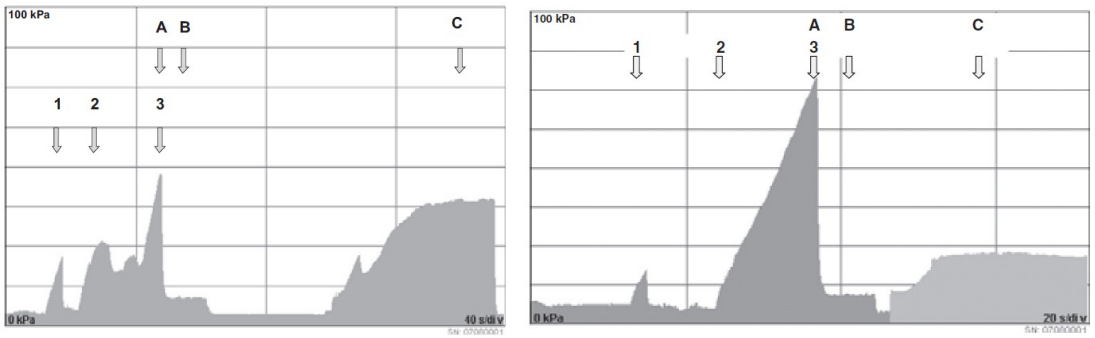

Figure 21. Pressure resistances (kPa) for epidural needle insertion events on pregnant (left) and non-pregnant (right) (LECHNER et al, 2011).

Table 8. Pressure resistances (kPa) for epidural insertions on pregnant and non-pregnant (LECHNER et al, 2011).

Event	Pressure Resistance (kPa)	
	Pregnant	Non-Pregnant
Ligamentum flavum (LF) penetration	47.4 ± 14.7	59.8 ± 11.4
Epidural space entrance	8.5 ± 1.2	7.4 ± 1.7
Catheter insertion	25.0 ± 5.2	20.7 ± 2.2

A curve of pressure versus time was developed in Dubey et al (2012), based on constant force values obtained from porcine tissues measurenents. The LOR moment is indicated by a sudden pressure drop (Figure 22). Cadaveric tissues present completely diverse biomechanical properties from the living tissues; data from them have poor utility for LOR dectection in epidural procedures (KWON et al, 2001).

2.2.5. FORCE COMPUTING

Calculation of resulting force is based on virtual patient body dimensions, tissue properties and the needle displacement. A simplified scheme of forces acting along the needle insertion procedure can be visualized in Figure 23. The force model developed in Section 4.2 used this scheme as a starting point for the subdivision of the needle insertion model in two stages: before and after the tissue puncture.

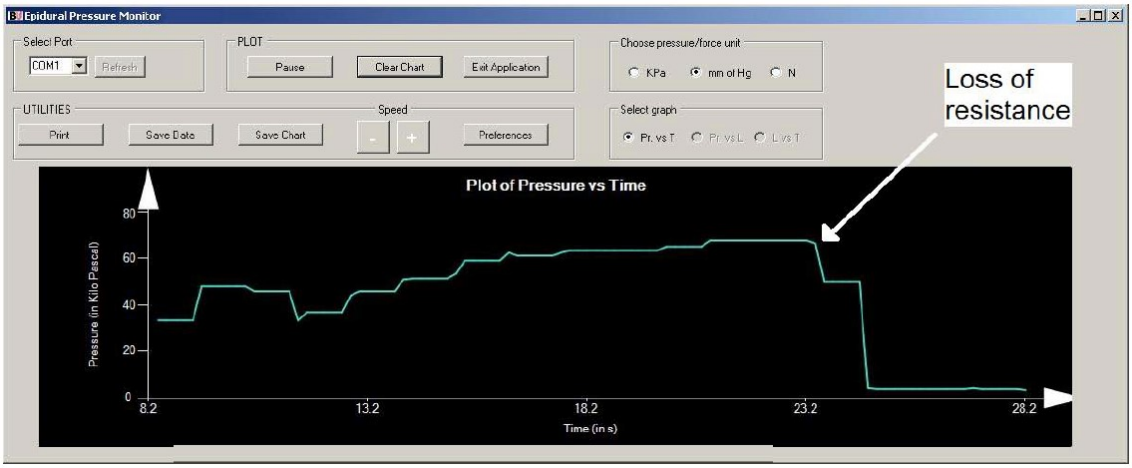

Figure 22. A pressure x time curve from porcine tissues (DUBEY et al, 2012).

The event (1) represents the moment before the contact between the needle and the tissue, where no resulting force is gererated. In (2), the needle contacts the tissue and presses it before perforation, where a stiffness force **(S_f)** occurs. After perforation, (3) indicate the needle penetration into the tissue, where cutting **(C_f)** and friction **(F_f)** forces actuate, and (4) shows a higher friction force due to a needle depth increase.

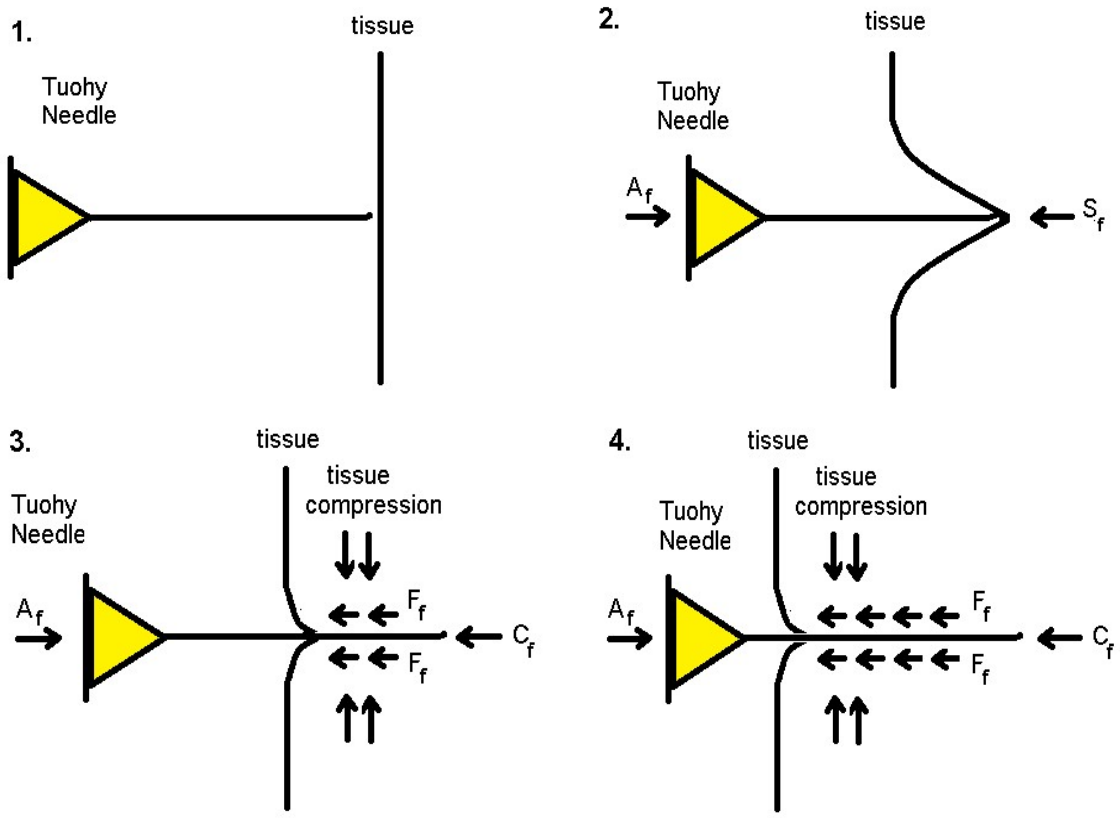

Figure 23. Main forces on a needle insertion simplified model

A force model for calculation of resultant forces based on combinations of stiffness, friction and cutting forces influence has been defined in Okamura et al (2004). This model is used to represent needle insertions in soft tissues. It was designed based on needle insertions experiments in bovine livers. It was also used with experiment data from insertions on livers of anesthetized living pigs, in Maurin et al (2004), and cited in Vaughan et al (2013) and Abolhassani et al (2007). In this model, the applied force (A_f) must be superior to the resulting force (R_f) in order to move the needle. The resulting force (R_f) is considered composed by three forces represented by equation ***(1)***:

$$R_f = S_f + C_f + F_f \qquad (1)$$

where the resulting force (R_f) is modeled as a sum of three main forces. The stiffness force (S_f) relates to tissue stiffness. It is the resistance force derived from tissue elasticity, before the tissue perforation. The stiffness force (S_f), the friction force (F_f) and the cutting force (C_f) occur after the tissue puncture. The cutting force (C_f) is related to the tissue cutting resistance, while being ripped by the needle advancement. It is produced when the tip of the needle pierces through the tissue. The friction force (F_f) is related to the friction caused by the needle movement while inside the patient tissue. It is caused by the needle shaft rubbing on the already trespassed tissue. These forces are represented in Figure 23.

The stiffness force (S_f) is the first to occur, it can produce elastic deformation in the skin surface as showed in Figure 23-2, before the applied force (A_f) be greater than the force to pierce the skin (Figure 23-3). It increases with the applied force, forcing the needle backwards until the applied force reaches a maximum value of elasticity. Then, the needle moves and the internal tissues react to this motion with friction and cutting forces (F_f and C_f) (Figure 23-4).

Stiffness force (S_f) is computed based on the needle displacement variation (Δz): i.e. the axial distance between the position of first needle contact with tissue (Z_1) and the current needle tip position (Z_{tip}) (OKAMURA et al, 2004). Maximum S_f value represents the naximum tissue elasticity before its perforation by the needle: Figure 24 illustrates this.

Calculation of friction forces (F_f) considers tissue biomechanical properties of static friction, dynamic friction and damping. Cutting force (C_f) was considered as a constant value, based on the tissue "resistance to cutting" property, it is considered with

an average value of 0.94 N (Newtons) with a standard deviation of 0.36 N, considering needle insertions in bovine livers at a speed of 3mm/second from Okamura et al (2004).

Two stages of forces were identified: The resulting force before perforation is calculated as an exponential function, based on needle displacement (Δz) (MAUREL, 1999). After perforation, a sharp rupture and a constant repulsion force (0.3 N) was measured, followed by a rising slope in Maurel (1999).

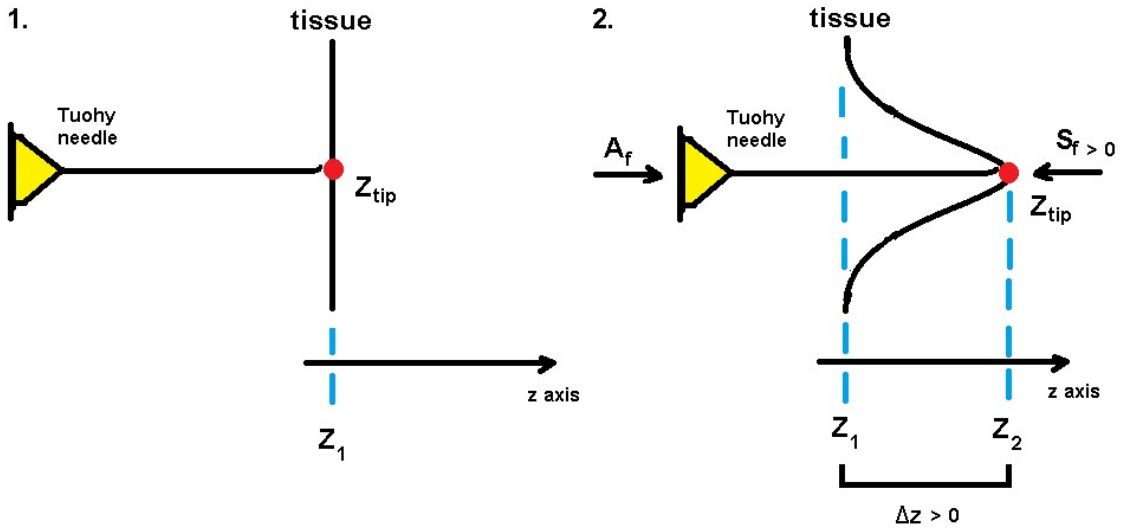

Figure 24. Needle displacement (Δz) for stiffness force (S_f) calculations (1): first contact between needle tip and tissue, and (2) tissue elasticity, based on Δz.

2.3. GAMIFICATION AND SERIOUS GAMES

The videogames industry had a great deal of evolutions in the last years. Digital and electronic games revenues have surpassed cinema income in a global scale since 2008 (GROENENDIJK, 2008). Game design mechanics and complexity level have increased along the time. Figure 25 shows an example of this change, where modern games, like the Flight Simulator X, from Seltz et al (2006), launched in 2006, include many more controls and visual details than the games from previous generations, like the Pac-Man game (IWATANI, 1980).

The game influence over players is studied by scientists and psychologists. They are embedded in the quotidian life of kids, teenagers and adults: players from the current and previous generations. Primary motivation for people engagement includes the autonomy to change the game outcome by player actions and a strong desire for victory (MCCALLUM, 2012; FERRARA, 2013). Games place the person in the center of the activity, deling with different situations to find efficient solutions, on

collaborating and acting as a team (SMITH, 2011). Some characteristics and complexities found on games are indentified as applicable to real world situations.

Figure 25: The classic Pac-Man game (IWATANI, 1980) (left). The Flight Simulator X (SELTZ et al, 2006) (right).

2.3.1. GAMIFICATION

Gamification initiatives include corporative, academic and scientific sectors of society. Their mechanisms stimulate and engage people toward objectives and ideals. Section 5.3 develops a gamification strategy used in the developed simulator, including points and achievements as game elements to motivate the practice by medical personel.

Gamification use started around 1980 (MALONE, 1980). Its use was reinforced by: The Serious Game Initiative movement (2002), the Games for Change organization (2002) and the Games for Health Project (2004), listed in Sawyer (2008). The gamification increased its popularity in 2011, when the terminology started to be used in most media (SCHELL; MCGONICAL, 2010; SMITH; RADOFF, 2011). However, gamification practices can be observed from a long time before the term definition. Examples include badges (Figure 26), medals and military patents. They are granted for merit and experience to scouts, serviceman and soldiers. They work as a reward, a performance recognition symbol (HAKULINEN et al, 2013). Airlines fidelity programs, with their points exchange for advantages or products are also listed as examples in Hamari (2013). Recent use of gamification transforms the user interface (see Figure 26) of modern videogame consoles (Xbox and Playstation), where the badges are associated to the gamer performance achievements.

The gamification is defined as an improvement by incorporation of game elements and mechanics. It borrows elements from games to transform real world tasks

into attractive and playful ones, turning the work a *gameful* (ludic and meaningful) experience (HUOTARI and HAMARI, 2012). A precursor and popular definition is the use of game elements and mechanics in non-game contexts (DETERDING, 2012). Gamification is positioned somewhere along the frontier of play and work. It improves player motivation and engagement on tasks execution. It mixes these activities together in a single pack and blurs the work *versus* play division. The duality between work and play duality is explored in Danbridge (1986). Improvement is caused by inclusion of game features when game design techniques are applied in non-game contexts (HUOTARI and HAMARI; DETERDING, 2012).

Figure 26. Badges related to achievements obtained by player in Minecraft game (BATKINGZ, 2017).

A gamified environment is different from a game. A player in a game is immersed in a virtual environment. His actions affect exclusively this environment. The actions performed in a gamified environment have a different outcome: they are associated to the execution and conclusion of real world tasks (WERBACK and HUNTER, 2012).

The gamification usually tries to influence the user decision process, directing it into third parties desirable choices (HAMARI ,2013). Although, the feeling of joy which comes from playing emerges from autonomy capacity for taking decisions, as mentioned in Ryan et al (2006), so gamification experiences should preserve user autonomy and offer significant choices for the player. Available services can incorporate value with gamification. It can be achieved by placing the user on a co-

producer position. The user indicates his preferences by the choices made inside the gamified environment. This can contribute for value production on the services (HUOTARI and HAMARI, 2012).

The user experience (gameplay) on a game or a gamification is influenced by five aspects: motivation, autonomy, balance, usability and aesthesics (FERRARA, 2013). The motivation is tied to the intrinsic (self) interests, the extrinsic (external) rewards and the core game mechanic. The autonomy is associated to in-game meaningful choices, the tactics and the overall strategy. The balance relates to the short and long-term play interactions. Usability is linked to the game controls and their mastery. Aesthesics are related to the player sensory perception: visual (graphics), sound and tactile, together with the story and the narrative of the experience.

Beyond the PBL mechanic described on the introduction (Figure 7), other examples of game elements used in gamification are the levels, the achievements and the progression bars. The use of elements must be significant and meaningful to the trainees. Proper orientation towards players' autonomy on decisions should also be considered (DETERDING, 2012).

The "reward" gamification element can be subdivided into intrinsic and extrinsic. Intrinsic rewards are related to the individual itself, and the improvement of its own skills, related to the environment context. Examples of intrinsic rewards: play given song with mastery (music school), loose weight (weight loss program), decode an enigma (game). The extrinsic rewards relate themselves to real or virtual objects or items, conquered or obtained by the individual inside the gamified environment. Extrinsic rewards examples: recognition badges, score (points), money bonuses, discount coupons, merchandise, equipment or virtual or even real items.

The "achievement" gamification resource is used to render the applications more interesting and engaging by offering instructions, objectives, reputation and status to their users. The use of a mobile device gamified application to stimulate the exploration and recognition of university campus by newcomers in Fitz-Walter et al (2011) is an example.

A universitary gamification proposition for an education at distance (EAD) environment described in Muntean (2011) exemplifies the use of different elements to engage the students. The permanent provision of the information about the course next steps acts as a motivator for keeping the students involved into the learning flux. The

continuous presence of tasks and commitments to be fulfilled in the learning environment stimulates the student activity on the platform. The use of a score and a level as comparison measures among the students turn the environment into a more social and competitive place. The "progress bar" resource offers feedback related to the student progress in a course or discipline. The environment should reward students achievements and attitudes (support to others), with badges for special actions done. The possibility to convert the obtained points or badges into virtual merchandise or discounts for institutional services can stimulate the student to increase his performance.

2.3.2. SERIOUS GAMES

Serious games are games focused into training or learning purposes, so they target real world results, as gamification does. Serious games usually include a more immersive environment (Figure 27 - left) than a gamification (Figure 27 - right). They can be improved by inclusion of game elements, to better engage the students into practice, and to accelerate the learning curve and the time required to improve skills. The developed epidural simulator detailed in Section 5.1 is an example of a serious game with game elements integrated for improvement of user feedback and practice.

Figure 27. The Detran Driving Simulator (VIDEOGAMES BRASIL, 2017) (left). The Samsung Nation (MARCABRAHAM, 2014) (right).

Othe examples of serious games include the popular Microsoft Flight Simulator X (Figure 25 - right), and the Detran Simulator (Figure 27 - left), a simulator used in Brazil to train drivers in a virtual environment, before the practical driving proof. Serious games are employed in medical field for different learning subjects, like ultrasound, x-ray, CT, MRI, pathologies, cardiology and others (PHILIPS LEARNING CONNECTION, 2016). Some examples can be seen in Figure 28. Life and Death game,

from Smith and Laabs (2016) is an older medical game example (1988), where the user assumes the role of a surgeon, diagnoses and treats a patient with a random pathology with can be from arthritis to appendicitis. The Surgeon Simulator, from Bossa Studios (2013) is also available. These games interface is visible in Figure 29.

A serious game experience is directly tied to the meanings to be transmitted, and the gameplay is used to consolidate them. A credible simulation is maintained by meaningful choices within a self-discovery environment. "Games are arguments, play is evidence" (FERRARA, 2013).

Figure 28. Medical Games (PHILIPS LEARNING CONNECTION, 2016).

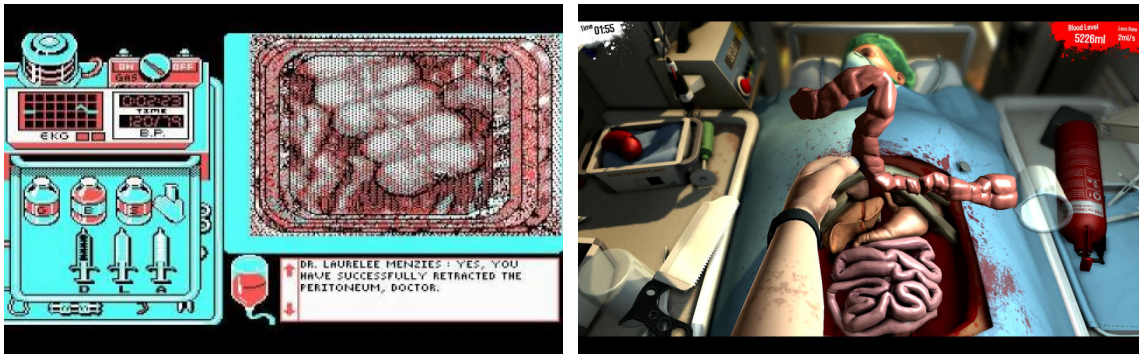

Figure 29. Life & Death game (SMITH and LAABS, 1988) (left) and Surgeon Simulator (BOSSA STUDIOS, 2013) (right).

A taxonomy for serious games associated to health care projects in McCallum (2012) can be visualized in Table 9. The investigated experiences show that the gamification approach can be an interesting resource to keep the medical students practicing for a longer time, once previous investigations detected that many attempts for epidural anesthesia normally are required by them in order to gain the skill and proficiency necessary before interaction with real patients.

Table 9. The Games for Health Taxonomy, developed by the Games for Health Project from McCallum (2012).

Area of health activity	Personal	Professional practice	Research and academia	Public health
Preventive	"Exergaming" Stress	Patient Communication	Data Collection	Public health Messages
Therapeutic	"Rehabitainment" Disease management	Pain distraction Cyberpsychology Disease management	Virtual humans	First responders
Assessment	Self-ranking	Measurement	Inducement	Interface and visualization
Educational	First Aid Medical information	Skills and training	Recruitment	Management simulations
Informatics	Personal health records	Electronic medical records	Visualization	Epidemiology

3. RELATED WORKS

3.1. EPIDURAL SIMULATORS

A review of epidural simulators is presented in (VAUGHAN et al, 2013). Epidural procedure is described together with a force model for needle insertion forces. Examples of virtual and phantom simulators are commented, with a list of desirable functionalities for them. A detailed comparison among the features and functionalities of the existing simulators from Gerovich et al (2004), Dubey et al (2012), Vaughan et al (2014), Akasum et al (2016), Dang et al (2001), Frazetto (2011), and the current implementation, is available in Section 6.11.

The desirable characteristics for virtual simulators from Vaughan et al (2013) are used here as a reference point for consideration of which relevant features shall be implemented on the simulator, as well as its evaluation. The listed features include: 3D model generated from computer tomography (CT) and magnetic ressonance image (MRI) scans, tutorial implementation, configuration of dificulty or competence levels for procedures, adjustment of patient bodies, sound and color feedbacks, recording and visualization of training execution, back and column palpation, needle gauge adjustment (size), patient column flexion (degree of difficulty or facility), adjustments or variations on virtual patient body (weight, height, position, body shape), calculation of resulting forces, precision of haptic device forces, free choice of the needle insertion point, mapping relevant positions by ultrasound or landmarks, cardiogram and respiration sound simulation of patient movement and mobility along the procedure, delivery room of a maternity hospital ambient sounds, presence or interference of a husband or a companion, patient voice and speech, simulation of false positives in loss of resistance (LOR) technique, implementation of a gradual LOR sensation spectrum instead of a discrete change on force values on the tissue transitions, immersive simulation, use of body-mass index (BMI) and performance evaluation. Many of these features are included on the developed simulator (EHGS), detailed and commented in Chapter 4.

A simple needle insertion simulator created with a 2D interface and a unique degree of freedom (1 DOF) from Gerovich et al (2004) is shown in Figure 6 (top-right) on Chapter 1. Its goal is to measure user accuracy to identify the tissue layer transitions. Users are asked to stop the needle movement once they perceived the layer to be puncture, so needle position data is recorded by the instructor. Different feedback options combinations are included on the simulator in Gerovich et al (2004): static

tissue layers display (prior to experiment), real-time visual needle tracking, real-time visual tissue deflection and haptic device force feedback. The relevance and the influence of the visual and tactile feedbacks for the needle insertion procedure performance are verified in Gerovich et al (2004). Their experiments employ the haptic device feedback for emulation of four tissue layers: skin, fat, muscle and bone, where simple force calculations are implemented for tasks executed by medical trainees and experts. The results from Gerovich et al (2004) indicate an 87% accuracy improvement for needle insertions, when real-time visual and haptic device feedbacks are active together on the simulations, and a 52% improvement rate for the single presence of the haptic device feedback alone (visual feedback disabled). The importance of force feedback increases as the quality of visual display degrades, as mentioned in Gerovich et al (2004), and their results confirm the importance of an accurate mechanical model when a real-time visual feedback is limited or absent.

A computer-based epidural procedure simulator including a low resolution 3D graphical interface with haptic device forces feedback is presented in Dubey et al (2012) (Figure 6, top-left). The user interface is tridimensional but few details concerning the needle insertion procedure are displayed. A virtual patient body is shown in the screen but the only epidural structures visually displayed are the skin tissue and the spine. This simulator integrates the use of a Novint Falcon haptic device for force feedbacks and stereo-glasses with an 800 x 600 resolution for visualization. An interesting feature detailed in Dubey et al (2012) is the use of a pressure tracking device composed of a force transducer attached to a syringe and connected to a wireless transmitter, used to measure the pressure on the plunger for in-vivo needle insertion trials and send the values to a computer system. They used the pressure tracking device to compose a curve of pressure measurements from porcine tissues versus time, plotted by the software (Figure 22). Standard thickness values for epidural tissues, available on Table 2, are also listed in Dubey et al (2012), constituting into an useful reference. Average needle insertion forces required to perforate the porcine epidural tissues are also listed. The interface of simulator lacks detailed information about all the epidural tissues and uses the porcine tissue forces to simulate the needle insertions by the haptic device.

An epidural simulator with virtual patient body generation capabilities from Vaughan et al (2014) can be visualized in Figure 6 (bottom-left). This work uses the average female waist, hip, calf, thigh and arm areas, and correlates to body-mass index values and age as parameters to compose an equation to dimension the 3D bodies for

virtual patients on the simulator. The simulator shows the 3D parametrically dimensioned virtual patient body, but reveals few details about the epidural needle insertion on its visual interface, only tracking the current needle depth, the elapsed time, the applied force (on z axis) and information about the dura-mater perforation. Information concerning the relevant epidural tissues being perforated or even the needle position and inclination are not displayed, neither are visually displayed the internal tissues from the patient.

A hybrid simulator for needle insertions on soft tissues, combining the use of a phantom mannequim with a haptic device from Akasum et al (2016) is visible in Figure 6 (bottom-right). Its visual interface is not shown. The simulator is integrated to a Novint Falcon haptic device and calculate the forces by using stiffness values from skin and liver tissues as parameters for elasticity calculations, correlated to the needle displacement. The work shows the thickness values used for skin, fat, muscle and liver tissues representation and measures the average forces required for tissue perforation on trials from 24 volunteers using the simulator. Unfortunately, this work only explores soft tissues penetration, not considering the other tissues from epidural region for the simulations.

Other investigated epidural simulators listed in Vaughan et al (2013) include: an injection simulator, combining a physical interface with a visual display of the patient back, shown in Figure 30 (left). Observe that no data concerning the needle insertion is shown by this solution and it does not present haptic device integration. A spinal anesthesia simulation with a haptic device is integrated to stereo glasses and a 2D interface, visible in Figure 30 (right) in Vaughan et al (2013), where a 16-color 2D interface only displays a little amount of needle insertion data. Both have the following drawbacks: only allow the needle insertion on a fixed point, lack a spinal anatomy for the palpation, and constitute into expensive interface solutions without any game-like features. The location of the midline is a challenging aspect of epidural anaesthesia not trainable if the needle position is fixed in the simulator (VAUGHAN et al, 2013). The implemented simulator described on Chapter 5 allows the choice of any location in the lumbar region for the needle insertion. The other two epidural simulators with haptic support listed in Vaughan et al (2013) are: the simulator from Dang et al (2001) and the EpiSIM, both included in the simulators comparison in Section 6.11.

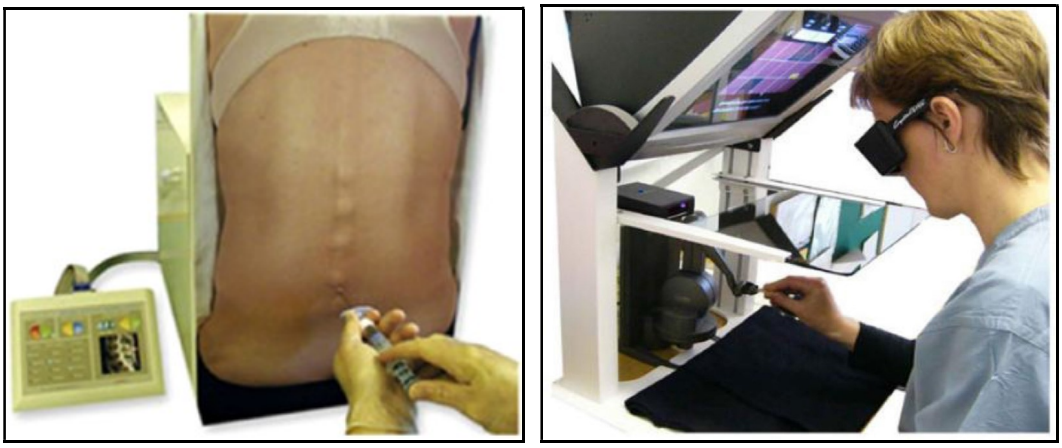

Figure 30. Epidural Injection Simulator (left) and Spinal Anesthesia Simulator (right) in Vaughan et al (2013)

3.2. FORCE MODELING

A force model for calculation of needle insertion forces based on combinations of stiffness, friction and cutting forces influence has been defined in Okamura et al (2004), used to represent needle insertions in soft tissues, based on experiments from insertions in bovine livers. The proposal for this model indicates an applied force (A_f) that must be superior to a resulting force (R_f) in order to move the needle. This work idea is interesting but only considers the bovine liver tissue for needle forces calculation. This work also presents experiment data concerning needle deflection axial forces related to the needle tip type and its diameter (Table 7). Both the developed equation and the needle deflection experiment data were useful on the design of the force models from Chapter 4. This work idea is better described in Section 2.2.5.

Experiment data from epidural needle insertions on 4 fresh porcine cadavers, human skin and fat tissues, realized with a material testing system (MTS) machine in Holton and Hiemenz (2001) shows distinct force values for the epidural tissues and subdivides the needle insertion in two stages, considering the forces before and after puncture, where forces required for epidural tissues penetration are summarized on Table 4. Needle insertions speed was 0.2 mm/s (millimeters per second). Achieved results are compared with high-resolution MR images to improve tissue identifications. They are plotted in the force versus needle displacement curve of Figure 31, for an epidural needle insertion on an average woman at lumbar vertebra 2. Some simplifications are considered for the model design: (1) the puncture forces are axial and independent of needle speed insertion, (2) the needle deflection and (3) initial insertion angles are not considered by their work. This experiment data was useful to

compose the values for the epidural tissues constants on force models designed on Chapter 4. More details about the Holton and Hiemenz (2001) work are available in Section 2.2.5.

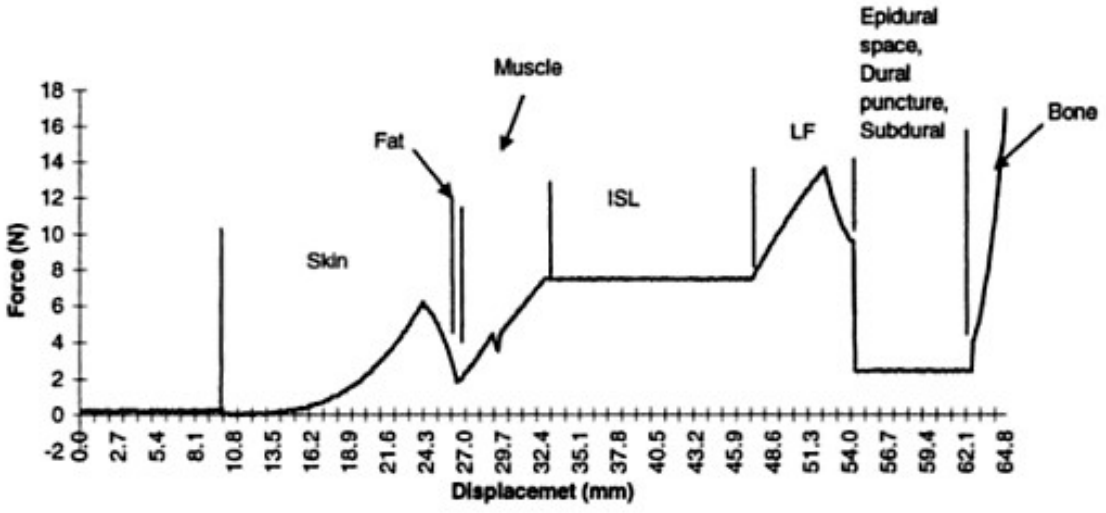

Figure 31. Force displacement curve from MRI of an average woman on needle insertion at lumbar vertebra 2 (HOLTON and HIEMENZ, 2001).

Another force model with four tissue layers (skin, fat, muscle and bone) is applied in a 2D needle insertion simulator in Gerovich et al (2004). This model uses spring and damping coefficients for tissue properties emulation on each layer. The stiffness coefficient represents tissue density and the damping coefficient for the friction among the tissue and the needle surface. Table 10 lists the values used for each tissue. Two stages are considered: upon contact and after puncture. Force feedback behavior was considered linear for stiffness (before tissue perforation) and damping (after puncture). This is a relatively simple force model, and only considers four epidural structures (skin, fat, muscle and bone) on force calculations.

Table 10. Stiffness and damping coefficients for virtual simulator tissue layers (GEROVICH et al, 2004).

Tissue	Stiffness coefficient (N/m)	Damping (Ns/m^2)
Skin	331	3
Fat	83	1
Muscle	497	3
Bone	2483	0

A comparison among the investigated models indicates that force function presented in Holton and Hiemenz (2001) are similar and a simplified versions of the model introduced in Okamura et al (2004): their stiffness force can be compared to the pre-puncture stage in Holton and Hiemenz (2001). Cutting force in Okamura et al (2004) can be associated to the constant force value from the steady-state in Holton and Hiemenz (2001). The main difference among these two models is the friction force in Okamura et al (2004), which can be related to the post-puncture stage in Holton and Hiemenz (2001). An ascendant force behavior is reported in Okamura et al (2004) for friction values after tissue puncture, while both Maurin et al (2004) and Holton and Hiemenz (2001) report a descendant one, with a steady-state afterwards in Holton and Hiemenz (2001). Functions from Holton and Hiemenz (2001) map all tissues relevant for an epidural needle insertion. The model presented in Gerovich et al (2004) is a simplified version from Okamura et al (2004) work. It considers a cumulative linear progression of stiffness and friction forces, represented by stiffness and damping coefficients, respectively. Cutting forces and needle deflection were not considered. All these models, with exception of Gerovich et al (2004), have not used computer simulation. A forces-time curve from Kwon et al (2001), a forces-displacement curve in Lee (2013) and a tissue pressure-time curve from Vaughan et al (2014) are also presented. The force progression of the needle insertions, thereby, is not linear.

A study on how pregnancy affects LOR detections for needle insertions is conducted in Lechner et al (2011), including pressure measurings for epidural needle insertions. Pressure measurings are higher on non-pregnant women when compared to the pregnant using LOR, turning the epidural space detection more challenging on pregnant women. These values are available on Table 8, and are used as reference for implementation of pressure measuring feature on the currently developed simulator (EHGS). This work is detailed in Section 2.2.4.

3.3. GAMIFICATION

Medical simulations employing gamification achieved a significant boost from 2.7 to 83.9 average practice hours with USA urology residents in Kerfoot and Kissane (2014). They trained on a simulator for minimally invasive surgeries, using exercises to improve and maintain their skill level in (KERFOOT and KISSANE, 2014). This work shows that gamification can be sucessfully applied to motivate people for medical simulator practices, increasing the time invested on thisk kind of training and, thereby,

the proficiency of medical personel. These results were considered as an evidence for the implementation of the gamification strategy defined in Section 5.3.

Corporative gamification initiatives encouraged user social interaction and participation in Farzan et al (2008) and Thom et al (2012). These experiences targetted the IBM's social intranet BeeHive (Figure 32), used by over 400.000 employees from different countries for communication and information sharing. On corporative sector, the gamification of IBM intranet by the use of points, badges and a leader board have resulted in a 40% interaction improvement in 7 weeks in Farzan et al (2008). The most important motivational factors influenced by gamification on the corporate environment are the reputation, social interaction and competition. The reputation is stimulated by the use of status titles ("Busy Bee", "Super Bee"), earned by the user after a specific number of points is achieved. The points are gained by information sharing actions (posts). The competition is promoted by a leaderboard that shows the usernames of employees with the 10 higher scores. After six months using the gamified environment, the users accumulated around three times more postings than the usual. When the gamification features were removed (10 months later) a 40% drop in the posts monthly rate was noticed. This is an extensive mapping that unifies three published works and concludes that gamification can be sucessfully applied on a large scale, and worldwide, enhancing the user performance for work-related tasks.

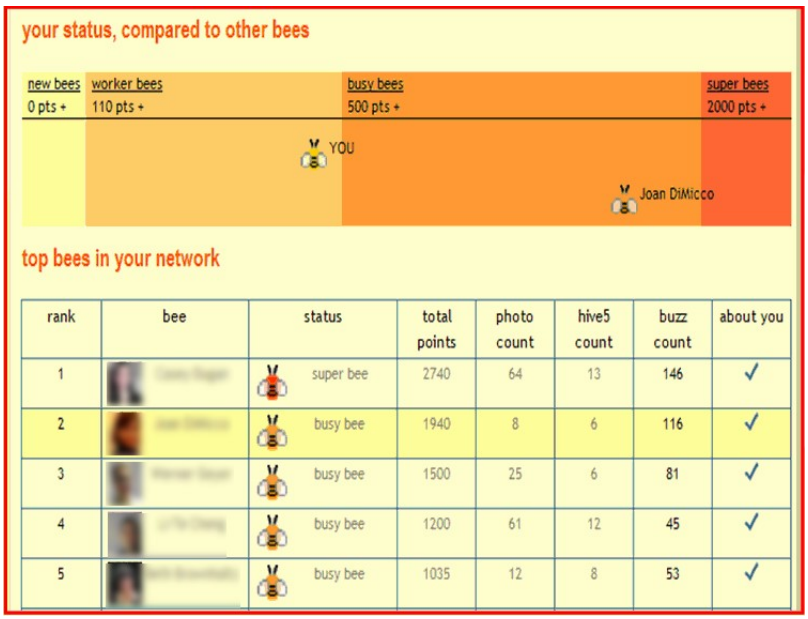

Figure 32. The Beehive's leader board, with the employees status titles and their total points (FARZAN et al, 2008).

A gamified simulation of clinical cases is the target of the UBICare project in Corriero et al (2014). It supports management of patients with chronic diseases and includes a web service to provide real patient data to help users to learn the best practices from real case studies. The players assume the roles of caregiver, patient, nurse and general and specialist physicians. The chosen role defines the objectives to be achieved, responsabilities and available interaction options within the platform. The player is challenged with clinical cases and dialogues with options for answering. A time span of 90 seconds is given for an answer, to avoid patient state degradation. At the simulation end, points and elapsed time are displayed, along with the patient condition. Good levels of user satisfaction were reported by the authors on the project. Gamification elements, process and results were poorly detailed in that work.

A serious game using a haptic device for stroke rehabilitation is the proposal of the SHRUG project (Stroke Haptic Rehabilitation Using Gaming) in Peiris et al (2014). It consists in a vertical platform composed of several hooks placed at six different heights, aligned vertically on its edges, where the patient is required to lift and place a pole by use of arm, hands and shoulder muscles structure. The patient needs to maintain the pole in a horizontal position, so the weak shoulder can be exercised with the help of the strong one. The horizontal bar pole is enhanced with feedback and recording capabilities, working as a game. Immediate feedback is provided by led lights, placed along the bar and under the hooks. These leds vary its colors to orientate the patient in rehabilitation tasks. A patient exercises his shoulder muscles by placing this bar pole at specific heights and receiving feedbacks from the pole. It is capable of displaying both the current player score as well as the player progress. Its orientation sensor keeps track of movement data. The user performance is recorded in a memory card. This work maps a serious game use integrated with a haptic device, but few game elements use.

Other serious games in medical field are used as a learning tool for: ultrasound, x-ray, CT, MRI, pathologies, cardiology and others in Philips Learning Connection (2016), with some examples shown in Figure 28.

4. DESIGNED MODELS

Computational models are important for reproduction of tissues dimensions and forces representing real experimental data in the virtual simulator.

The most significative contribution of this work is the design of a model to adjust the thickness from all epidural tissues in the simulator, detailed in Section 4.1. It is achieved by the calculation of a scale factor, based on parturient experiment data, and the configuration of attributes for a virtual patient. This scale factor is used to resize all the tissues.

Two force models are developed for needle insertions on epidural tissues, detailed and discussed in Sections 4.2 and 4.3. The first one considers the influence of stiffness, friction and cutting on its calculations. The second model considers the influence of needle attributes for needle bending, and calculates the forces that result from this. Both are also based on real experiment data. A mechanical model for calculating the needle penetration forces in a body is also designed and detailed in Section 4.4.

A model for visual deformation of the skin tissue is described in Section 4.5.

4.1. A MODEL TO DIMENSION THE THICKNESS OF EPIDURAL TISSUES

The possibility to create a set of different virtual patients is one of the desirable features for an epidural simulator, listed in Section 3.1. The dimensioning of the thickness for all tissues involved in the epidural nerve block contributes for this purpose by incorporating a diversity of challenges for skill practice in the simulator, thereby enhancing the replay value of the simulations.

An equation to resize the thickness of all the epidural tissues relevant for the simulation is developed. It calculates a tissue scale factor (S_t), based on patient height, weight and age. This equation is generated from a multiple linear regression from parturient experiment data available in Clinkscales et al (2007), considering both the body-mass index (BMI) and the age of patient in relation to the distance from skin to epidural space. Afterwards, these regression results are combined to the average needle depth value for epidural space tissue from Dubey et al (2012) and Vaughan et al (2004) to compose the equation. The proposed formula (2) to calculate the tissue scale factor (S_t) is:

$$S_t = S_0 + [(B_i\, W_p / H_p^2) - (A_i\, A_p)] / D_{se} \qquad (2)$$

where W_p is the patient weight in kilograms, H_p is the patient height in meters, and A_p is the patient age in years. Heavier and taller patients increase the scale factor, while older ones decrease it. B_i and A_i are constants related to body mass and age influences over the scale factor, with defined values of $1.1m^2/kg$ and 0.1mm/years, according to experiment data from parturient in Clinkscales et al (2007). S_0 is a constant representing an initial scale factor value of 0.625, based on experimental data, too. The D_{se} represents the distance from skin to epidural space distance. A DSE value of 42 mm is used, being the average needle depth for the epidural space tissue, reported on the Table 11.

For example, considering: a thin patient (1), with a weight of 58.2 kilograms, 1.72 meters tall and 19 years old, these would result in:

$$S_{t1} = 0.625 + [(1.1m^2/kg \times 58.2kg / 1.72m^2) - (0.1mm/year \times 19\ years)]/ 42mm = 1.095$$

and considering an obese patient (2), with a weight of 119.5 kilograms, 1.56 meters tall and 34 years old, these would result in:

$$S_{t2} = 0.625 + [(1.1m^2/kg \times 119.5kg / 1.56m^2) - (0.1mm/year \times 34\ years)]/42mm = 1.830$$

The tissue scale factors S_{t1} (for the thin patient) and S_{t2} (for the obese patient) are then used to adjust to the average thickness tissues values on the second column of Table 11. The scale factors multiply those values to rescale all relevant tissues thickness accordingly. The adjusted values are shown on rescaled tissue thickness columns of Table 11 (the last two columns at right), considering S_{t1} calculated value (1.095) for the thin patient and S_{t2} calculated value (1.830) for the obese patient. The average values for the tissue thickness and the needle depth columns on Table 11 are obtained from Dubey et al (2012) and Vaughan et al (2014).

Table 11. Original and adjusted thickness of tissue layers, based on the Scale Thickness Factor (St).

Tissue Layer	Average Tissue Thickness (mm)	Average Needle Depth (mm)	Rescaled Tissue Thickness (mm) (thin patient)	Rescaled Tissue Thickness (mm) (obese patient)
Skin	3	0	3.108	5.037
Subcutaneous Fat	6	3	6.216	10.074
Supraspinous ligament	4	9	4.144	6.716
Interspinous ligament	26	13	26.936	43.654
Ligamentum flavum	3	39	3.108	5.037
Epidural space	6	42	6.216	10.074
Dura	15	48	15.540	25.185

The patient tissue layers are represented as cylindrical three-dimensional shapes in the simulator. They will be resized by the values listed on rescaled thickness column of Table 11. Location of tissue layers is planned to be positioned in vertical axis, according to the spine three-dimensional coordinates in the simulator. Implementation results can be visualized in Figures 45 (Section 6.1) and 50 (Section 6.2).

The use of cylindrical shapes for the tissue layers allows a correlation with the mechanical model for needle penetration, designed in Section 4.4, that uses the continuum approach, cilyndrical coordinates and updated lagrangean equations to represent the epidural space and other tissues.

The distance from skin to epidural space (DSE) is used for a comparison of the implementation results with the parturient experiment data from Bassiakou et al (2011) and Clinkscales et al (2007). The DSE is calculated as the sum of the rescaled thickness values of the epidural tissues previous to the epidural space: skin, subcutaneous fat, supraspinous ligament, interspinous ligament and ligamentum flavum.

The calculated DSE values for the patients from implementation example are: 4.99 mm, for the thin patient (1), and 7.69 mm, for the obese patient (2). These values are plotted in the graph shown in Figure 33.

These implementation results (Figure 33) are compared to the DSE values obtained from experiment data with real patients in Bassiakou et al (2011). The patients picked from Bassiakou et al (2011) have approximately the same body-mass index (BMI) values than the BMI calculated for the patients used on implementation, allowing a fair comparison of generated patient DSE values. The selected patients represent two extremes on the graph, where the patient 1 represents a thin person, with a calculated BMI value of (19.67), and the patient 2 is an obese one, with a BMI value of (49.10). The corresponding patients selected in Bassiakou et al (2011) are "points out of the curve": they present the most extreme BMI reported values (the lower and higher values). It is possible to observe that even considering these patients for comparison, the DSE values from patients generated by the implementation are relatively near to the real experiment DSE values from real patient experiment data.

The minimum and maximum limits for DSE values are also plotted on the graph. These limits are based on parturient experiment data from Clinkscales et al (2007), considering the average values for each given BMI range and the addition (maximum) or subtraction (minimum) of their respective standard deviations. It is possible to detect

that DSE values from patients generated by the implementation are contained inside these limits, showing plausible DSE values for the patients as result.

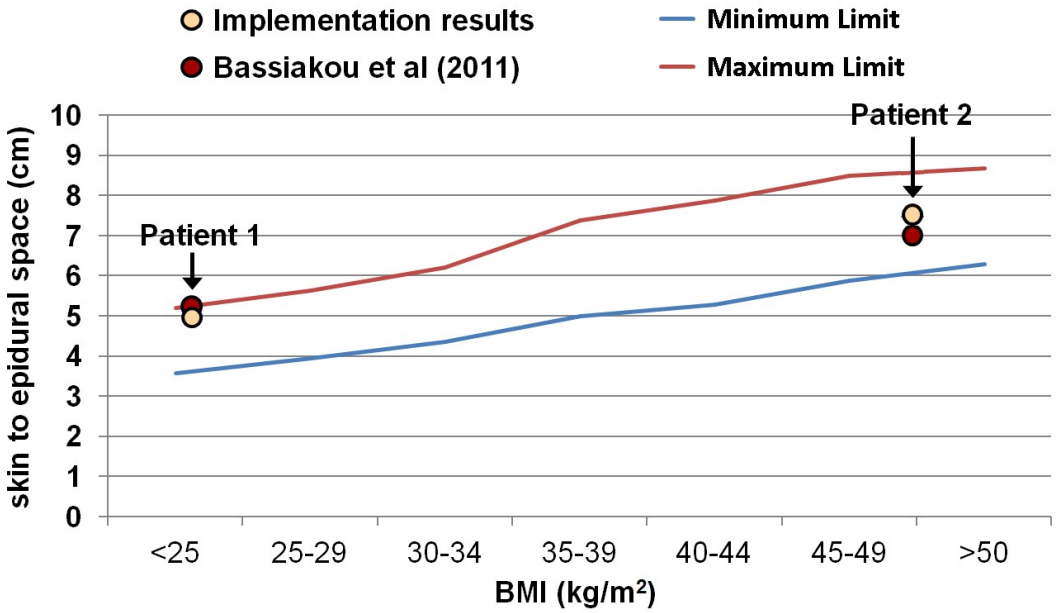

Figure 33. A comparison of DSE values for patients: thin (1) and obese (2), from implementation results, and the experiment data from Bassiakou et al (2011)

4.2. A FORCE MODEL FOR EPIDURAL NERVE BLOCK

The force models described in Sections 2.2.5 and 3.2 employed fewer constants to represent tissue properties and forces. The resulting force (R_f) can be obtained as a sum of three main forces: the stiffness force (S_f), the friction force (F_f) and the cutting force (C_f). In order to achieve more realism, two force models are designed for the emulation of the tissue-related forces, and they are integrated to the simulator. They represent two stages of the procedure: before (equation 3*)* and after tissue puncture (equation 4*)*.

Before tissue puncture, resulting force (R_f) is egual to the Stiffness force (S_f):

$$R_f = S_f = c_0 + (c_1\ \Delta d) + (c_2\ \Delta d^2) + (c_3\ \Delta d^3) \qquad (3)$$

where the constants c_0 *(Newtons – N)*, c_1 *(N/*mm*)*, c_2 *(N/*mm^2*), and* c_3 *(N/*mm^3*)* represent current tissue behaviour before puncture, according to tissue properties data available on Table 12. The constants for a tissue incorporate all previously trespassed tissues (ex.: muscle constants include the skin data). The Δd represents the needle depth before

tissue puncture, calculated as the current needle depth (in millimeters) inside the patient body minus the needle depth (mm) where current tissue was first contacted by the needle. For the first tissue (skin), ***Δd*** is calculated as the needle displacement from point where the skin was first contacted by the needle. Most tissue data provided on Table 12 were obtained from experiments in Holton and Hiemenz (2001). The values for ligament flavum were adjusted for better simulation of this tissue behaviour.

Table 12. Tissue force calculation parameters before tissue puncture

Tissue	c_0 (N)	c_1 (N/m)	c_2 (N/mm^2)	c_3 (N/mm^3)	Max. Stiffness Force (MSf) (N)
Skin	0.0235	0.0116	-0.0046	0.0025	6.0372 N
Muscle	1.9736	0.8287	0.1078	0	4.354 N
Interspinous Ligament	4.4062	0.9598	0	0	7.467 N
Ligamentum Flavum *	4.533	1.5029	-0.0583	0	12.1330 N
Epidural Space	2.437	0	0	0	2.436 N
Bone (Strike)	3.9735	2.210	1.4814	0	50 N

*** Values adjusted to conform to tissue behaviour reported in Figure 31**

After tissue puncture, the resulting force (***Rf***) equals the sum of the friction force and the cutting force (***Ff*** + ***Cf***). The resulting formula adds different tissue constants, based on tissue biomechanical properties, achieving better tissue forces behaviour on virtual simulator, after perforation stage:

$$R_f = F_f + C_f = cp_0 + (cp_1 \ \Delta \ dp) + (cp_2 \ \Delta \ dp^2) \qquad (4)$$

where cp_0 *(Newtons – N)*, cp_1 *(N/*mm) *and* cp_2 *(N/*mm^2*)* are constants reproducing current tissue behaviour after puncture, according to Table 13. The constants for a tissue consider all previously trespassed tissues (ex.: muscle constants contain the skin data). The ***Δdp*** represents the needle depth after tissue puncture, being calculated as the current needle depth (in millimetres) inside the patient body minus the needle depth (in millimetres) where the current tissue was first punctured by the needle. For the first tissue (skin), consider needle depth inside current tissue being penetrated by the needle (zero). Table 13 data was mostly obtained from experiments in Holton and Hiemenz (2001), with values adjusted to better represent ligament flavum tissue behaviour.

A curve of forces versus needle displacements for a needle insertion considering all the relevant epidural tissues is plotted in Figure 34. This curve is generated by the

equations (3) and (4), and they use the constant values for the tissues from the Tables 12 and 13. It is possible to visualize the transitions between the stages before tissue puncture (red color) and after tissue puncture (green color) in Figure 34, represented by the changes of the line color on the curve. The names of the tissues in contact are indicated by the arrows added to the the plotted curve.

Table 13. Tissue force calculation parameters after tissue puncture

Tissue	Cp_0 (N)	cp_1 (N/mm)	cp_2 (N/mm^2)	Thickness (mm)	Transition Force (Tf) (N)
Skin	6.0372	0.4516	-0.5287	N/A	1.974 N
Muscle	4.354	-2.2543	0.2902	N/A	3.675 N
Interspinous Ligament	7.467	0	0	18 mm	N/A
Ligamentum Flavum *	12.1330	-0.1693	-0.1177	7.4 mm	N/A
Epidural Space	2.437	0	0	8.6 mm	N/A
Bone	N/A	N/A	N/A	10 mm	N/A

*** Values adjusted to conform to tissue behaviour reported in Figure 31**

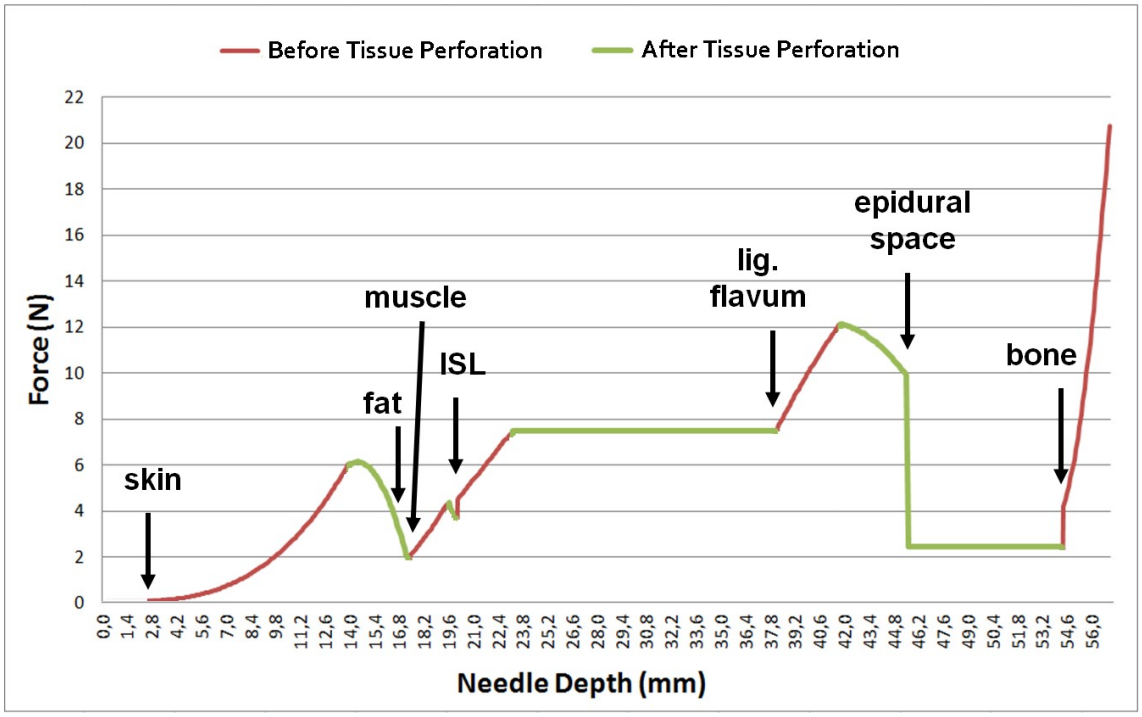

Figure 34. A force versus needle displacement curve plotted by the force models (3) and (4).

The transition from "before puncture" to "after puncture" stage occurs after the calculated force achieves the tissue maximum stiffness force (MS_f). Transitions to the next tissue happen after Δdp surpasses the tissue thickness or if the resulting force

becomes lower than the tissue transition force (T_f), whatever comes first. For instance, the transition from skin tissue to muscle tissue will occur when the R_f reaches the skin to muscle transition force value, which is 1.974 N. The tissue transition from ligament flavum to epidural space will occur after Δdp (needle depth on current tissue) reaches a value of 7.4 mm. In this case, there is not a force value listed for the tissue transition.

4.3. A NEEDLE BENDING FORCE MODEL

Needle bending is influenced by the tip format and its diameter. In a needle insertion procedure, the tissue around the tip becomes compressed, and it can exert an unbalanced resistance force against compression. An axial needle force model is proposed for these forces decurrent from needle bending. It considers the needle diameter and the needle tip type as parameters for the calculation of axial forces from needle bending (B_f):

$$B_f = \begin{cases} (0.1953\ D_n - 0.05948)\ \Delta z/2.65 \text{ (for a triangular tip),} \\ (-0.2963\ D_n - 0.08019)\ \Delta z/2.65 \text{ (for a coned tip),} \\ (-0.2665\ D_n - 0.05539)\ \Delta z/2.65 \text{ (for a beveled tip)} \end{cases} \quad (5)$$

where D_n is the needle diameter (gauge) and Δz is the needle penetration depth inside the patient body, both measured in millimeters. The tip type of needle being used determines the constants of the equations. The line 1 corresponds to a triangular tip, the line 2 is for representation of a coned tip and the line 3 is for a beveled tip (Tuohy hubber needle), the most commonly used on epidural procedures.

The bending forces calculated by this model should be considered in addition to those defined in the equations of Section 4.2, resulting in: $R_f = S_f + F_f + C_f + B_f$. Equations (5) are generated by linear regressions based on experiment data from Okamura et al (2004). Figures 35-37 show the linear regression graphics for the three needle tips, executed on the *Curve Fit* feature for these tip types using MATLAB® Software.

4.4. A MECHANICAL MODEL FOR NEEDLE PENETRATION IN A BODY

The main reason for employing a mechanical model is to provide a more precise and realistic experience for the trainees, by calculating the mechanical forces which act upon and during the anesthesia procedure, simulating the tissues to be bypassed by the epidural needle.

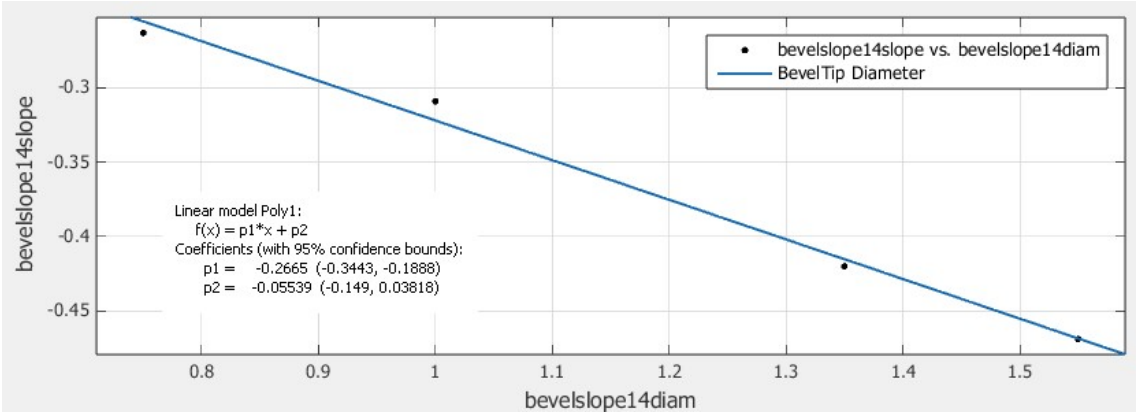

Figure 35. A linear regression graphic for a beveled tip

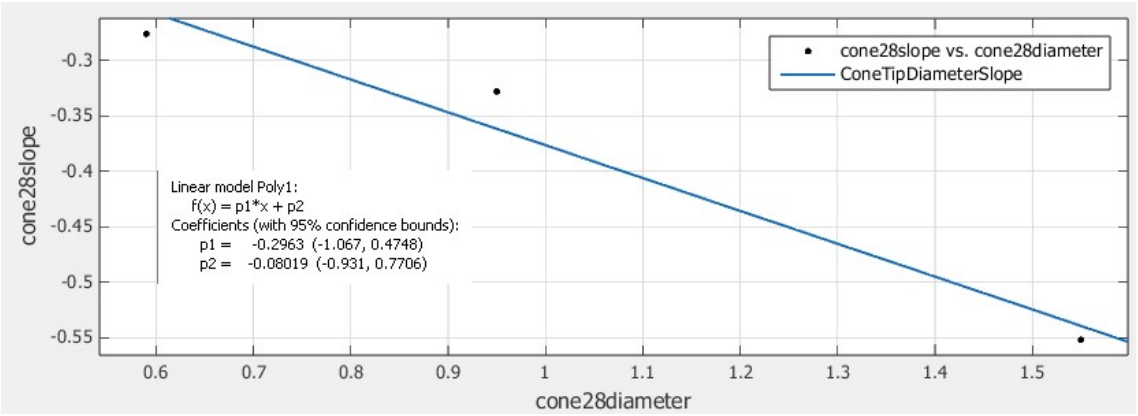

Figure 36. A linear regression graphic for a coned tip

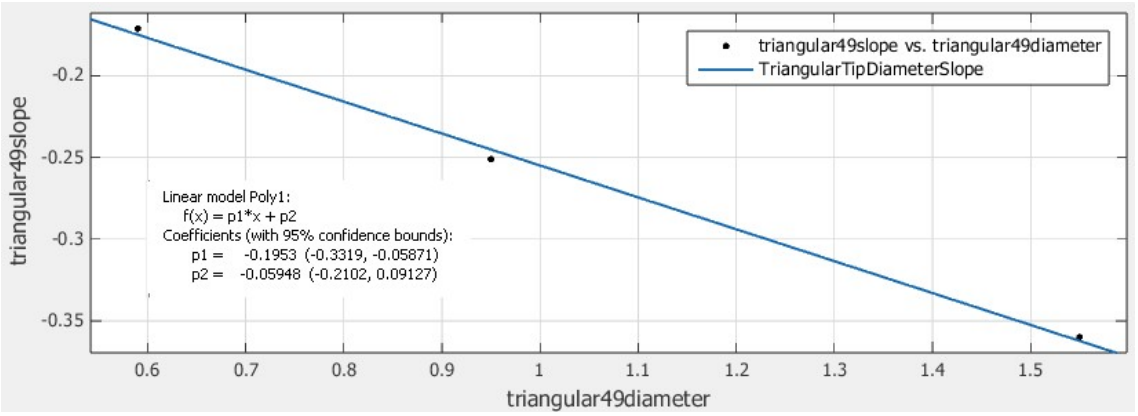

Figure 37. A linear regression graphic for a triangular tip

In Fig. 75, the epidural space is represented by dark gray color, where the anesthetic liquid is inserted and the other tissue of the body is illustrated by a light gray color. We consider the inner radius (a_0) of the epidural space and the outer radius (b_0) of the body of the patient before the deformation *(not deformed configuration)* B_U. The

action of the force in the radial direction applied by the needle is denoted by f_r. Moreover, the configuration B_d is before deformation (*deformed configuration*) where the inner radius (a) of the epidural space and outer radius (b) of the patient body are denoted. This configuration can be deformed either by the compression of the neddle on the skin surface (i.e. $b \le b_0$) or by the inflaction, due to the injection of the anesthetic fluid into the epidural space (*i.e.* $a \ge a_0$). Besides, in Figure 38, the inner pressure P of the tissue over the needle and the haptic device reaction to this force denoted by N, the coordinate systems (ρ, ϑ, ζ) and (r, θ, z) of the position vector related to any arbitrary point in the not deformed and deformed configuration respectively are shown.

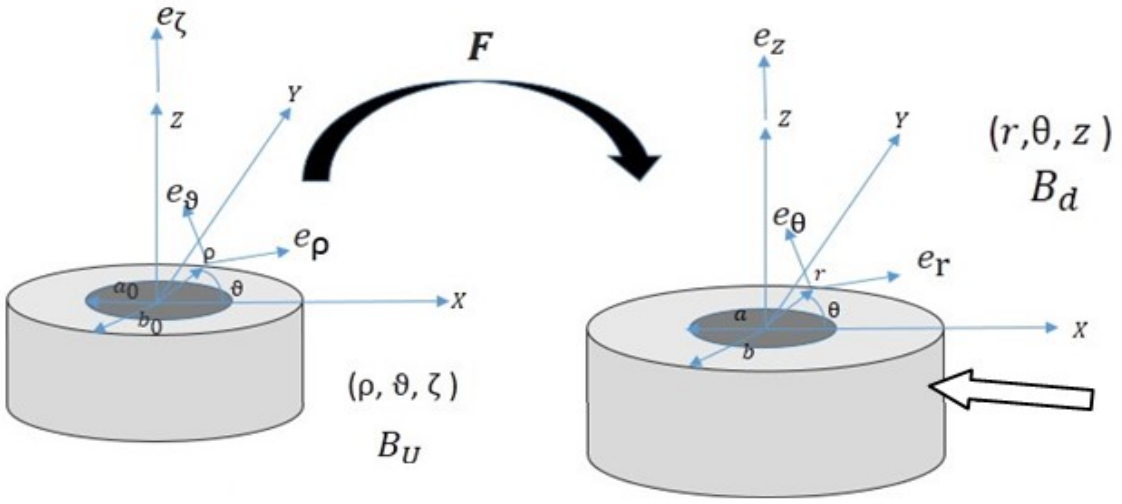

Figure 38. Geometrical representation of the epidural space and its surrounded tissue in undeformed cylindrical coordinate system B_U and deformed B_d configurations and the action of the forces (CONCI et al, 2015; BRAZIL et al, 2016).

4.4.1. KINEMATICS USING THE CONTINUUM APPROACH

For axisymmetric deformation, the position vectors to the point in the undeformed B_U and deformed B_d configurations are written in Taber (2004) as

$$\boldsymbol{\rho} = \rho e_\rho + \zeta e_\zeta, \quad \boldsymbol{r} = r e_r + z e_z. \qquad \textbf{(6)}$$

The extensión and inflation, from B_U to B_d, is defined by the relations

$$r = r(\rho), \quad \theta = \vartheta, \quad z = \lambda\zeta, \qquad \textbf{(7)}$$

where λ is the axial stretch ratio of the loaded tube (deformed position) relative to the unloaded tube (not deformed position).

Therefore, the deformation gradient tensor is written as:

$$\bar{\boldsymbol{F}} = r' e_r \otimes e_\rho + \frac{r}{\rho} e_\theta \otimes e_\vartheta + \lambda e_z \otimes e_\zeta. \qquad \textbf{(8)}$$

The Lagrangian strain tensor of B_d relative to B_U is given by

$$[E_{IJ}] = \frac{1}{2}[C_{IJ} - G_{IJ}] = \frac{1}{2}\begin{vmatrix} r'^2 - 1 & 0 & 0 \\ 0 & r^2 - \rho^2 & 0 \\ 0 & 0 & \lambda^2 - 1 \end{vmatrix}, \qquad \textbf{(9)}$$

and because the physical components of $\boldsymbol{E}$ can be calculated using $\hat{E}_{IJ} = E_{IJ} / (G_{II} G_{JJ})^{1/2}$,

we have $\left[\hat{E}_{IJ}\right] = \frac{1}{2}\begin{vmatrix} r'^2 - 1 & 0 & 0 \\ 0 & r^2 / \rho^2 & 0 \\ 0 & 0 & \lambda^2 - 1 \end{vmatrix}$. $\qquad$ ***(10).***

4.4.2. CONSTITUTIVE RELATIONS, GOVERNING EQUATIONS AND BOUNDARY CONDITIONS

Biological tissues are often modeling as hyperelastic materials. Hyperelastic media are types of materials where the mechanical properties are characterized completely by a scalar strain-energy density function W. With the epidural space assumed to be incompressible and pseudoelastic, the constitutive equation for the Cauchy stress tensor gives as:

$$\boldsymbol{\sigma} = \boldsymbol{F}\frac{\partial W}{\partial \boldsymbol{E}}\boldsymbol{F}^T - p\boldsymbol{I}. \qquad \textbf{(11)}$$

for a general W. Since these coordinates are orthogonal the stress tensor related to the deformed body is written as $\boldsymbol{\sigma} = \hat{\sigma}_{ij} e_i \otimes e_j$, where the unit vectors e_i are defined by the expression $e_i = g_i / (g_{ii})^{1/2}$ and the notation "$\hat{}$" denotes the physical components and in the case of Cauchy tensor has the form:

$$\hat{\sigma}^{rr} = \bar{\sigma}^{rr} - p, \quad \hat{\sigma}^{\theta\theta} = \bar{\sigma}^{\theta\theta} - p, \quad \hat{\sigma}^{zz} = \bar{\sigma}^{zz} - p. \qquad \textbf{(12)}$$

where

$$\bar{\sigma}^{rr} = r'^2 \frac{\partial W}{\partial \hat{E}_{\rho\rho}}, \bar{\sigma}^{\theta\theta} = \left(\frac{r}{\rho}\right)^2 \frac{\partial W}{\partial \hat{E}_{\vartheta\vartheta}} + \lambda^2 \frac{\partial W}{\partial \hat{E}_{\varsigma\varsigma}}, \bar{\sigma}^{zz} = \lambda^2 \frac{\partial W}{\partial \hat{E}_{\varsigma\varsigma}}. \qquad \textbf{(13)}$$

The symmetry in this problem demands that stress must be independent of θ and z. In the absence of inertial and the action of the body forces in the radial direction f_r due to the needle impinged the equilibrium equation can be expressed as

$$\frac{\partial \hat{\sigma}^{rr}}{\partial r} + \frac{\hat{\sigma}^{rr} - \hat{\sigma}^{\theta\theta}}{r} + f_r = 0, \qquad \textbf{(14)}$$

$$\frac{\partial (r^2 \hat{\sigma}^{r\theta})}{\partial r} = 0, \quad \frac{\partial (r \hat{\sigma}^{rz})}{\partial r} = 0. \qquad \textbf{(15)}$$

The boundary conditions are considered as follows. The inner wall $r = a$ of the epidural space in the deformed configuration is subjected to an internal pressure *P,* the outer wall is free of loads and a reaction force N as a response to the f_r force applied, we have,

$\hat{\sigma}^{rr} = -P$, $\hat{\sigma}^{r\theta} = \hat{\sigma}^{rz} = 0$ at $r = a$; $\hat{\sigma}^{rr} = \hat{\sigma}^{r\theta} = \hat{\sigma}^{rz} = 0$ at $r = b$ and $\pi a^2 P + N = 2\pi \int_a^b \hat{\sigma}^{zz} r\, dr.$

4.4.3. SOLUTION OF THE PROBLEM

Because the stresses depend only on r the equations ***(14)*** and ***(15)*** can be integrated, using the boundary conditions thus $\sigma^{r\theta} = \sigma^{rz} = 0$ everywhere. Because the epidural space is assumed to be incompressible $J = det\, \boldsymbol{F} = 1$ we obtain $r^2 = 2\lambda^{-1}\left(\rho^2 + a_0^2\right) + a^2$ in which the integration constant was found from the condition $r\left(a_0\right) = a.$ If the axial stretch ratio λ, and the deformed inner radius a are known, then the deformed outer radius can be computed using the relation $b = r\left(b_0\right) = \left[2\lambda^{-1}\left(b_0^2 + a_0^2\right) + a^2\right]^{1/2}$. With r(R) now known, the deformation gradient and strain components can be calculated. Then, with $W\left(\hat{E}_{IJ}\right)$ specified, Eq. ***(12)*** gives the stress components in terms of the yet unknown Lagrange multiplier p. To determine p, we substitute ***(12)*** into the radial equilibrium equation ***(14)*** and integrate to get

$$p(r) = (r')^2 \frac{\partial W}{\partial \hat{E}_{\rho\rho}} + \int_r^b \left[\left(\frac{r}{\rho}\right)^2 \frac{\partial W}{\partial \hat{E}_{\vartheta\vartheta}} + \lambda^2 \frac{\partial W}{\partial \hat{E}_{\zeta\zeta}} - r'^2 \frac{\partial W}{\partial \hat{E}_{\rho\rho}} - r f_r\right] \frac{dr}{r}. \quad \textbf{(16)}$$

The internal pressure required to maintain the deformation now can be found by substituting the resulting expression for ***(16)*** into the final boundary condition on the curved surfaces,

$\hat{\sigma}^{rr}(a) = -P$, to obtain

$$P = \int_a^b \left[\left(\frac{r}{\rho}\right)^2 \frac{\partial W}{\partial \hat{E}_{\vartheta\vartheta}} + \lambda^2 \frac{\partial W}{\partial \hat{E}_{\rho\rho}} - r'^2 \frac{\partial W}{\partial \hat{E}_{\rho\rho}} - r f_r\right] \frac{dr}{r}. \qquad \textbf{(17)}$$

Finally, the applied force N can be computed from the relation $\pi a^2 P + N = 2\pi \int_a^b \hat{\sigma}^{zz} r\, dr.$

For a general form of W, this integral must be evaluated numerically. Computing N, therefore, involves evaluating the above integral for p within the integral. Although this procedure is relatively straightforward, it may be more convenient to write the equation

for N in a form that does not involve p. Thus, using this last integral, integrating and applying the boundary conditions $\hat{\sigma}^{rr}(a) = -P, \quad \hat{\sigma}^{rr}(b) = 0$ we obtain

$$\pi a^2 \mathrm{P} + \mathrm{N} = \pi a^2 \mathrm{P} + \pi \int_a^b \left(2\hat{\sigma}^{zz} - \hat{\sigma}^{rr} + \hat{\sigma}^{\theta\theta} \right) r\, dr = \pi a^2 \mathrm{P} + \pi \int_a^b \left(2\bar{\sigma}^{zz} - \bar{\sigma}^{rr} + \bar{\sigma}^{\theta\theta} \right) r\, dr. \qquad \textbf{(18)}$$

Since the physical parameters and energy of the epidural space is not well known, the results presented here are based on the parameters used in Taber (2004) for the artery aorta. They assumed that the artery wall is cylindrically orthotropic, homogeneous, incompressible and hyper-elastic, with the strain-energy density function having the form of

$W = C\,(e^{Q} - 1)$ where $Q = a_1 \hat{E}_{\rho\rho}^2 + a_2 \hat{E}_{\vartheta\vartheta}^2 + a_3 \hat{E}_{\zeta\zeta}^2 + 2\left[a_4 \hat{E}_{\rho\rho} \hat{E}_{\vartheta\vartheta} + a_5 \hat{E}_{\vartheta\vartheta} \hat{E}_{\zeta\zeta} + a_6 \hat{E}_{\zeta\zeta} \hat{E}_{\rho\rho} \right]$ **(19)**

4.4.4. ANALYSIS OF NUMERICAL RESULTS

The analysis of the results are based on ***(13)***, ***(18)*** and ***(19)***. The numerical results are implemented in Matlab where firstly we obtain,

$$\frac{\partial W}{\partial \hat{E}_{\rho\rho}} = 2Ce^{Q}[a_1 \hat{E}_{\rho\rho} + a_4 \hat{E}_{\vartheta\vartheta} + a_6 \hat{E}_{\zeta\zeta}],$$
$$\frac{\partial W}{\partial \hat{E}_{\vartheta\vartheta}} = 2Ce^{Q}[a_2 \hat{E}_{\vartheta\vartheta} + a_4 \hat{E}_{\rho\rho} + a_5 \hat{E}_{\zeta\zeta}], \qquad \textbf{(20)}$$
$$\frac{\partial W}{\partial \hat{E}_{\zeta\zeta}} = 2Ce^{Q}[a_3 \hat{E}_{\zeta\zeta} + a_5 \hat{E}_{\vartheta\vartheta} + a_6 \hat{E}_{\rho\rho}].$$

The input parameters used for numerical implementation are:

$$C = 11.2kPa, a_1 = 0.0499, a_2 = 1.0672, a_3 = 0.4775,$$
$$a_4 = 0.0042, a_5 = 0.0903, a_6 = 0.0585, a_0 = 3.9mm, \qquad \textbf{(21)}$$
$$b_0 = 4.5mm, \rho = 4.5mm,$$

the inner radius values a of the deformed configuration varies and different fixed values of the parameter λ are taken for the numerical analysis (Figures 39 and 40).

This teoretical model can be used in the formulations replacing the based in experiments used. The epidural tissues modeling as tridimensional cylindrical objects allow the application of this model and its formulations on the simulator.

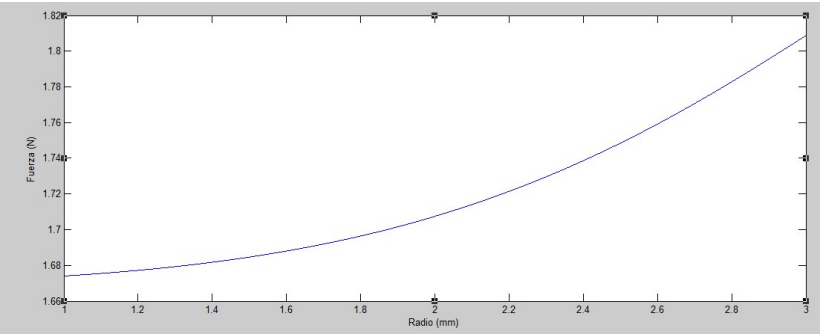

Figure 39. Force in Newtons (N) vs Internal deformed radius (mm), when λ=1,5 (BRAZIL et al, 2016).

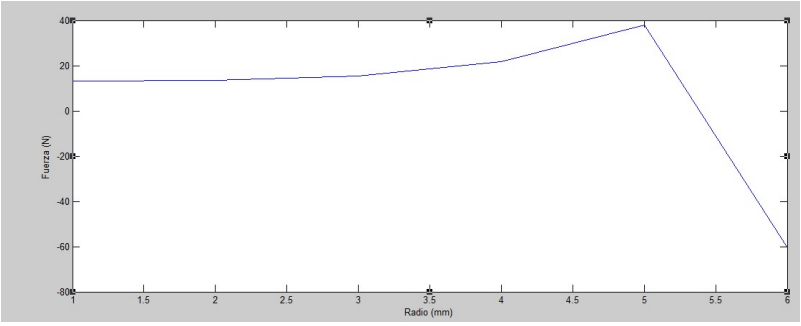

Figure 40. Force in Newtons (N) vs Internal deformed radius (mm), when λ=1,75 (BRAZIL et al, 2016).

4.5. A MODEL FOR VISUAL DEFORMATION ON TISSUES

Displacements are calculated based on the nodes (vertices) motions from the tridimensional mesh representing the patient body (the skin tissue), used as basic structure for the nodal displacement operations. Figure 41 shows the mesh of the patient body in use, composed by triangular flat surfaces joined at vertices.

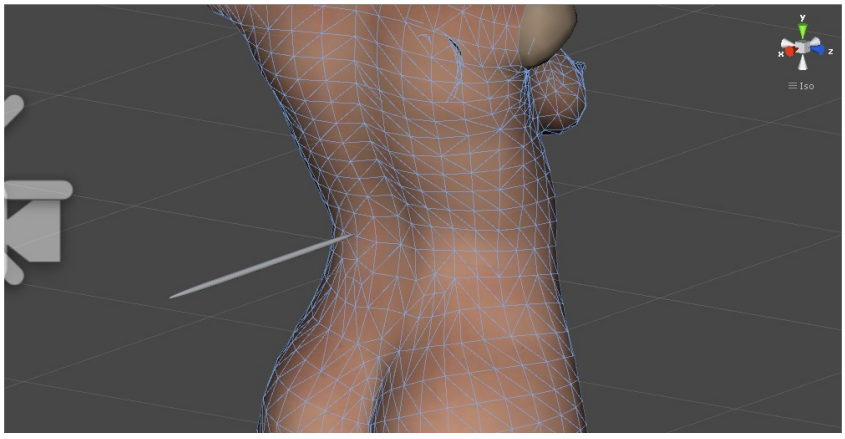

Figure 41. Tridimensional body mesh composed by triangular surfaces and vertices.

The deformation results can be achieved by considering a neighborhood area, composed by a group of nodes (vertices) near to the surface region being pressed by the needle tip and the Gaussian model represented in Figure 42 (right). The gaussian model can also be replaced by another existing model, in order to produce different results.

These nodes (proximal to the needle contact point) are the vertices from the 3D mesh to be affected by the displacement and they are considered with radial distances but interlinked by triangular flat surfaces to $P_{contact}$. Using the symbol M_d for the resultant displacement in each distance, i.e to be applied on each node, it has a magnitude that can be aproximated by the expression:

$$M_d = Z_{tip} / (N_{cd}^{\,2} + 1) \qquad (22)$$

where Z_{tip} references the needle tip depth and N_{cd} is the distance from a given node to contact point: $P_{contact}$.

For instance, see how to compute the $\mathbf{M}_d$ for nodes 2 and 4 in Figure 42. On stage **1**, there is no contact and so no deformation occurs. On stage 2**,** Z_{tip} is the relative displacement on the first point of contact i.e. on $P_{contact}$, because on stage 2 needle contacts tissue at node 3, then neighborhood nodes displace according their proximity to 3 assuming the curve represented in Figure 42 (right) or by equation ***(22)***. For nodes 2 and 4 N_{cd} are 2, then nodal displacement percentage M_d for these nodes (2 and 4) can be accounted as $M_d = Z_{tip} / (N_{cd}^{\,2} + 1) = 1 / (2^2+1) = 1/5 = 0.2$ that is nodes 2 and 4 suffered a displacement of 20% of node 3 displacement (i.e. they are displaced by 0.2 from their original position). Using same idea, for nodes 1 and 5, their N_{cd} are 4 and their displacement are 10% of node 3 displacement (i.e. its displacement multipled by 0.1).

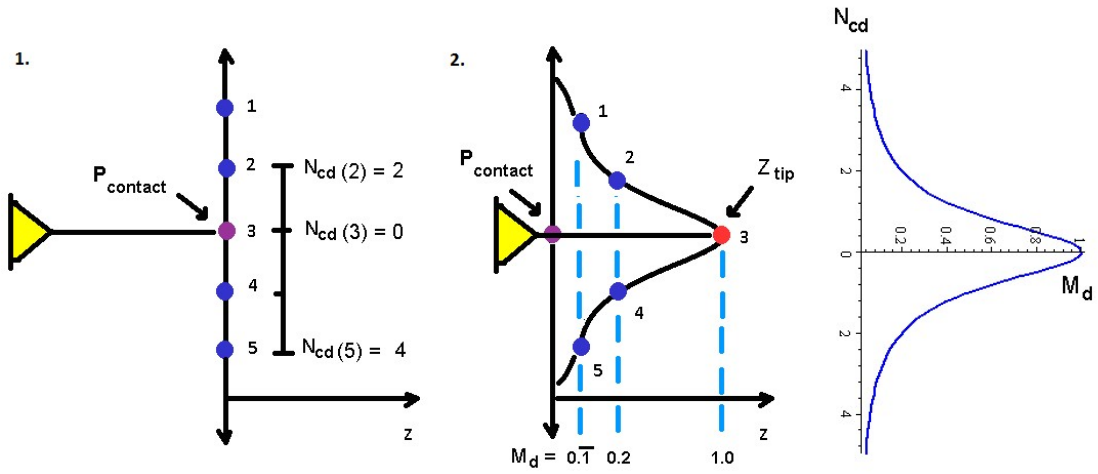

Figure 42. Displacement of nodes in a mesh based on $P_{contact}$ and distance (BRAZIL et al, 2017).

Note that the example from Figure 42 only considers the distance from $P_{contact}$ to the neighbor nodes (1-5) on the y-axis for N_{cd} calculations. This proposal can be used to calculate the nodes displacement when considering the neighboring nodes distant from contact point on any direction (radial), as well. Implementations on tridimensional environment should consider the relative distance on the 3D space between $P_{contact}$ and the neighbor nodes. Implementation results are available in Figure 69 (Section 6.10).

To enhance the real-time calculations performance, only a neighbor area on tissue mesh around $P_{contact}$ should be considered by the displacement effect. Farther nodes location has less displacement effect magnitude (M_d) upon the node. A node very distant from the contact point will only be affected by a smaller displacement from its original position, or not affected at all, depending on the displacement factor resulting from function ***(22)***. If a node location is very distant from $P_{contact}$, the displacement influence upon the node will be so low that it can be ignored, avoiding changes on the surface mesh.

The graphical representation of this function generates a curve similar to the shape of a "bell" statistic curve from normal distribution, displayed in Figure 42 (right). In Figure 42, the needle movement was represented on the z (depth) axis, to exemplify the displacement effects calculations relative to the nodes distant from $P_{contact}$. Note that this model can be used to calculate the nodes displacement considering the nodes distant from $P_{contact}$ on any direction.

The idea of taking in account the amount of displacement of the nodes by tissue stiffness property value (S_t) is considered as well. A constant value for S_t, ranging from 0 to 1 (maximum stiffness), is used in this approach, based on each tissue layer characteristics. The magnitude of displacement on each tissue node (M_d) will then be inversely proportionally to the tissue stiffness property value (S_t). The final node displacement N_d is the calculated by M_d divided by the tissue stiffness (S_t), resulting in:

$$N_d = M_d / S_t \qquad (23).$$

5. THE SIMULATOR AND ITS INTEGRATED DEVELOPMENTS

This chapter presents a series of developments applied on the virtual simulator implementation for the practice of epidural nerve block procedures. It is focused on integration of three main aspects: haptic device feedback, force modeling, and gamification. Figure 43 illustrates the simulator architecture and the implemented features. The sections of this chapter specify more details about them.

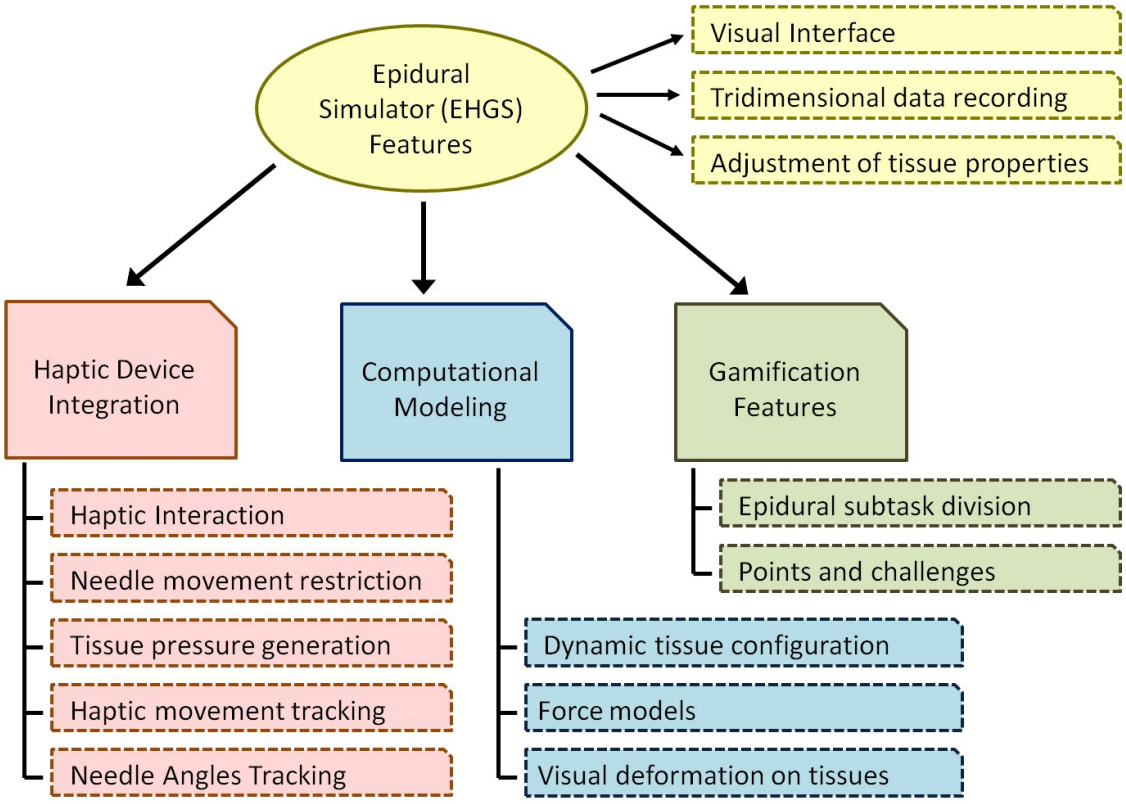

Figure 43. Main aspects and developed features from the implemented epidural simulator (EHGS).

Haptic device interation introduces more real movements and restrictions to the system and improves the outcome by adding physical sensations. The haptic device is an input-output instrument that provides force feedbacks in the virtual simulator. Section 5.2 of this chapter details the haptic device related features.

The central aspect includes the development and integration of computational models to support the epidural nerve block procedure in the simulator, considering as elements: the needle, the possible motions (degrees of freedom) with the haptic device, the tissues deformations and their answer in terms of force sensations from the haptic device to the hands. The main designed models are described on Chapter 4. Other computational models are detailed in Chapter 5. Such models are important to support

the simulation of needle insertions in the patient body. The implementation includes the design and use of models capable to dimension the epidural tissues, based on virtual patient attributes and the mapping of the forces and displacements involved on the epidural procedure steps, among other features.

The use of gamification elements help to turn the simulator into a playful experience. Significant elements and mechanics from games are used to motivate and engage the users. Details related to specified part of the implementation is the object of Section 5.3.

5.1. THE EPIDURAL SIMULATOR (EHGS)

In this work, an **E**pidural **S**imulator with **H**aptic device integration and **G**ame elements (EHGS) is implemented to integrate, validate and adjust the designed models. The integration of the haptic device in the system as an interaction device allows the introduction, in the computer implementation, of movements similar to the ones executed by the medical doctors and the transmission to the user adequated reactions to them improving the degree of realism in the simulation. A gamification strategy is included to engage and motivate the trainees. A secondary focus is the development of a lower cost solution for practices with epidural nerve block. The equipment and machinery used in this kind of training usually is costly, and involves the use of phantoms (i.e. physical mannequins), which have a limited lifespan and periodic fixed cost for maintenance of their replacement parts. Consequently, a number of hospitals in Brazil train the epidural nerve block directly on patients.

The following steps from epidural nerve block procedure are considered and included in the simulator: locate L4-L5 vertebral space, epidural needle placement, puncture and pressure measuring through LOR technique, catheter insertion, needle removal and catheter fixation (HARDAMA, 2013). This simulator focuses are epidural needle insertion and pressure measuring, both critical for reducing epidural failure rate.

The Unity3D (2016) engine is used for the simulator development, and it can be used for free on projects with a revenue lesser than U$100.000. Most of the 3D modelling software formats (Fbx, Autodesk, Blender, etc.) can be incorporated. It includes a visual interface for placement and adjustment of 3D objects in the implemented environment. Animations are easy to produce in this engine. Scripts in languages C#, Javascript and Python can be included in the program. However, C# is

chosen as the development language due to its versatility and previous personal background knowledge.

5.1.1. The Visual Interface

The visual interface handles the simulation interaction. A mental visualization of the 3D model of spinal anatomy is listed as one of the key factors for the epidural procedure success (BERNARDS, 2001). An intuitive interface to visualize the simulation data and integrated with the use of a haptic device is designed. Figure 5 in Chapter 1 shows the visual interface.

The virtual simulator includes 3D models to represent the patient body and a spine. The woman body model used for this implementation is generated with FUSE ™ software. The spine was extracted from a free skeleton 3D model (TF3DM, 2010).

Internal tissues are modeled as cylindrical shapes, and part of this work was presented in (CONCI et al, 2015; BRAZIL et al, 2016). A Tuohy needle and a pressure syringe are also included. The 3D model for a Tuohy needle was designed using Blender (Figure 44, left). A syringe 3D model was also incorporated, for the application of a local anaesthesia on the simulator (Figure 44, right). A video with syringe use on the simulator is available as well (BRAZIL, 2016b).

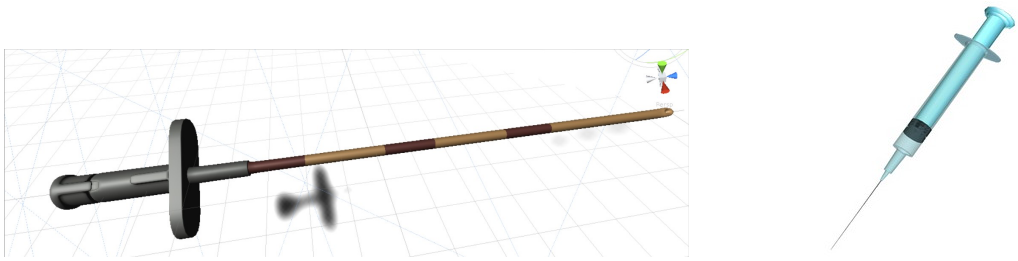

Figure 44. A custom designed model of a Tuohy Needle (left). A syringe free 3D model (JARRET, 2017) (right)

Internal lumbar body tissue layers are represented by cylindrical shapes generated in the engine. The cylindrical shapes are used considering the equations developed in Section 4.4. Textures from real tissue samples are applied to the tissue being represented in a given time for the system as in the needle tip (Figure 45).

Body models of patients are generated using Fuse 3D software (MIXAMO, 2016). These body models are used after customizations to represent specific details, as:

height, body mass, and skin colour. More implementation details and results can be visualized on Chapter 5.

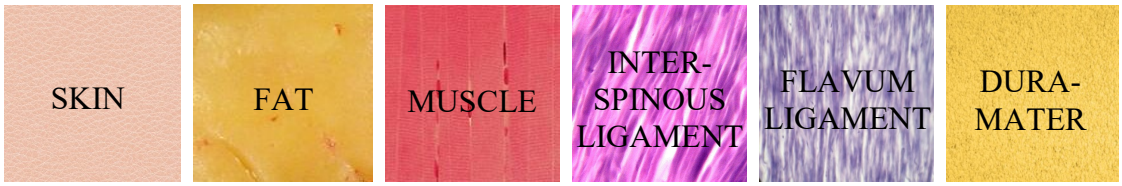

Figure 45. Textures from real tissue samples: skin (SEAMLESS PIXELS, 2017), subcutaneous fat (KENDALL FIT KITCHEN, 2017), muscle (PRO-ANABOLIC STEROIDS, 2017), interspinous ligament (CONNOR et al, 2013), ligamentum flavum (WEDENSBERGPENG, 2012) and dura-mater (CHOI et al, 2016).

The representation of triaxial models and calculations adopts the plane representations commonly used on medical field, displayed in Figure 46, where yz axis correspond the sagittal plane, xy axis are mapped by the coronal plane and xz axis indicate the transverse plane.

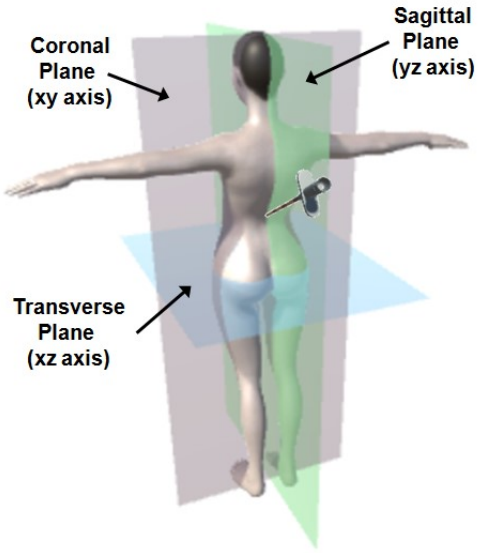

Figure 46. Visual representation of orientation planes used in the developed simulator.

5.1.2. THREE-DIMENSIONAL DATA RECORDING

Storage of simulation data, as forces and results are important for monitoring players' performance results. They can be accessed later for analysis, comparison and reproduction. Applied axial forces and needle depth data can be captured and organized generating graphical output related to real tissue experiments. These are useful for simulations evaluation and adjustments. Acquired data can also be used for needle tracking, movement reproduction and verification of the influence of tissue properties.

Three-dimensional recording and mapping of forces constitutes a significant advancement over former works. Previous experiment data focused only on a single axis (z) force mapping. Features like needle movement restriction, angles and deflection will perform better with a three-dimensional approach.

Recording of axial forces and additional haptic device data is based on two events on the haptic device simulation: the time passage and the needle depth variation (needle penetration). Performance registration are realized once per second of time elapsed, and once at each millimetre of needle depth advancement, in separate time and depth log files. Such information is written into text files separated by commas (";") characterizing the CSV files. Stored information includes: the needle three-dimensional position and orientation, haptic device applied axial forces, time interval on simulation and needle depth. There are, in stored line, the elements: Time (s); current tissue name; needle depth (mm); applied forces (N) (components in x, y and z axis); needle position (x, y, z); needle orientation (x, y, z); needle torque (x, y, z); tissue properties (stiffness, damping, static and dynamic external frictions, resistance to penetration, static and dynamic internal frictions; thickness (mm); depth location (z); saline and air pressures (kPa); needle depth (mm) and needle angles (x, y ,z) in degrees.

Data are stored for tracking and reproduction of needle movement (Section 5.2.5) and verification of the three-dimensional force modelling adequacy and its relationship with tissue properties (Section 6.8).

5.1.3. Tissue Properties Configuration and Calibration

A wide revision on material properties of the biological tissues was conducted. Specific values concerning the biomechanical properties of the human epidural tissues were found for the tissues thickness, listed on Table 2, from Section 2.2.1, and the saline pressures, listed on Table 14 (Section 5.2.6). Other properties values were mostly obtained from experiment data from Holton and Hiemenz (2001) and Clinkscales et al (2007).

Force feedback is achieved through communication between the epidural simulator and the integrated haptic device, by using API resources (SENSABLE, 2009). The contact between the needle and a tissue surface triggers in the implementation a message for the haptic device. Each 3D object representing a tissue in the developed simulator contains a configuration of values for its biomechanical properties. These values are converted into axial forces to be exerted by the integrated

haptic device. Figure 47 illustrates this communication process and the involved project components. Haptic device communication and API are detailed in Section 5.2.

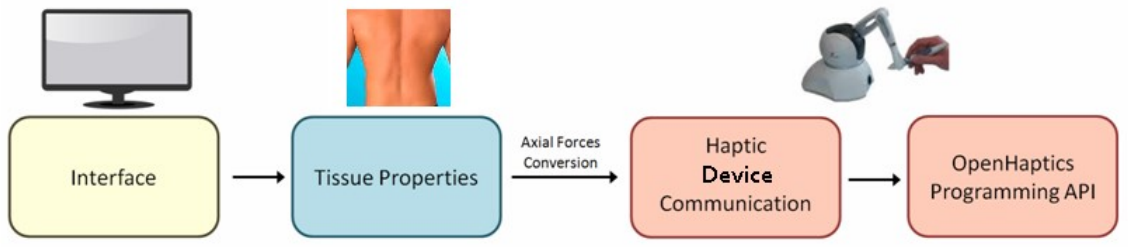

Figure 47. Tissue properties configuration diagram with project components

Tissue properties are real numbers, i.e. represented by floating point values in the program; they represent stiffness, static and dynamic friction, damping, thickness, depth, air and saline pressures. Values for these properties are associated to each 3D tissue trespassed. The game objects representing the tissue layers are stored in a vector structure.

Biomechanical properties values can be associated to the tissue layers to enable a real-time adjustment of them on the simulator. The changes of these properties values will guide by force results and feedbacks emulated from the haptic device. The display and adjustment of these tissue properties occurs on the virtual interface. Interactive sliders allow the scaling of each biomechanical property influence, from 0 (minimum influence) to 1 (maximum contribution). The display of currently axial forces applied on the haptic device is also shown on the visual interface. Implementation results can be visualized in Figure 55, in Section 6.1.

5.2. HAPTIC DEVICE INTEGRATION

Haptic devices enable sensations simulating physical restrictions and reactions of forces and moment to movements and rotations realized by operator hands.

The implementation integrates a force model with the restrictions, motions and feedback transmitted from and through the device to emulate what physically happens on the procedures. Movement on the simulator is transformed by input data from the Geomagic Touch haptic device (Figure 2), that allows six (6) degrees of freedom (DOF). The haptic device extremity, visible in Figure 2 (right) on Chapter 1, resembles a pen, and allows the simulation of needle rotations in 3 orthogonal directions, related to the x, y and z axis, by the gimbals numbered from 1 to 3. This device also offers 3 directional movements with force feedback, associated to its arm (3 DOF)

displacements. The arm movement with force feedback is provided by angular movements on the elements named “rotation”, identified by numbers 1 to 3. The rotation 1 is around z axis and rotations 2 and 3 are around x direction in Figure 46. The gimbals represent free rotations from the haptic device (without reation feedback in the implementation). The earlier implementation versions of this work has used a Novint Falcon (Figure 2 - left) for haptic device response.

The communication between the implementation and the haptic device hardware uses displacements and resistance sensations as feedbacks to the user motions through the use of program scripts. The OpenHaptics Toolkit Application Program Interface (API) from Sensable Technologies Inc. (2009) and a dynamic library link file (hd.dll) contain specifications and functions for reading and updating the device information. They enable the configuration and representation of biomechanical properties for the tissues. A haptic plug-in for Unity from Poyade et al (2015) is used as a reference.

This implementation includes epidural tissues parameters and simulation of their biomechanical properties. Stiffness stands for tissue hardiness and resistance to deformation. Damping measures elastic (spring) resistance. Static friction, dynamic friction and viscosity are tied to motion reply. All tissue properties influence the force model outcome for the used movements that will result in forces or movement restriction by the haptic feedback.

5.2.1. HAPTIC DEVICE INTERACTION

The implementation of the haptic device interaction uses the Unity engine and programming scripts associated to the engine working pipeline, including diverse calls to the haptic device application program intergace (API) from Sensable Technologies Inc. (2009). These API calls continually read the haptic device position and force data and the program scripts update the information on the simulator interface, at the speed of frame rate update provided by the computer system (usually 60 updates per second).

The haptic device extremity looks like a pen. It represents the needle movements and is associated to a 3D needle object in the simulator. The coordinates and other relevant information are adjusted in accordance to the haptic device position.

The movements executed by the user on the haptic device are captured by scripts that continuously update the values from the haptic device position and its angles. The scripts store them in a Vector3 structure. The object’s angular data is updated by the

LookRotation function available on the *Quaternion* library in the engine, based on current position, angle and torque information obtained from the haptic device.

The interactions between the 3D needle (controlled by the haptic device) and the other 3D objects on the implemented environment occurs by the flagging (marking) of all interactive objects as “touchable” (i.e. the patient body and all modelled tissue layers). Each of these flagged objects is considered by the interaction script, being associated to a transformations matrix and having its mesh information stored. The interaction script updates this data in the haptic device memory, using the API communication resources. The haptic device then becomes “aware” of these objects and is able to virtually interact with them. The player can physically "feel" them through the haptic device feedback.

The tissue detection and manipulation are mapped by the contact between the 3D needle object and the 3D female body and the cylindrical shapes representing the epidural tissue layers. The contact is detected through scripts, to program the collision tests between these objects.

The forces applied on haptic device extremity are read, mapped and converted to a Vector3 structure. Such a type of data is available from Unity engine and consists of 3 floating-point variables, proper to store the force components, in directions x, y and z. A programmed script uses the API resources to read these data and convert the values into floating-point (real numbers).

5.2.2. NEEDLE DEPTH CALCULATION

The needle depth calculation is associated with the position of the haptic device extremity, and starts soon after the 3D needle touches the patient body (skin) on the virtual environment. This location is related to the puncture point position in Figure 48. The surface of the patient body is considered on the coronal plane or xy, and the orthogonal z direction as that of the needle on penetrating the body. The difference between needle current position and this puncture point is the needle depth. Figure 48-1 shows first needle contact with skin tissue, determining an initial contact point between the skin tissue surface and the needle on what it is named $\boldsymbol{Z_{contact}}$ position in the model. Figure 48-2 illustrates the needle displacement (depth) and z axis ($\boldsymbol{\Delta z}$) calculation. It is measured as the distance from ($\boldsymbol{Z_{contact}}$) to the current needle tip position ($\boldsymbol{Z_{tip}}$). Same proposition is used for computation of displacement along other axis. The

implementation considers both ($Z_{contact}$) and (Z_{tip}) as tridimensional positions, and measures the relative distance between them.

5.2.3. NEEDLE MOVEMENT RESTRICTION

The needle movement restriction simulates a tissue answer to the needle movement when the needle is inside the tissue and along its penetration path. Figures 34 and 35 illustrate stages and simbols importants in the developed model. Elements before penetration are represented in Figure 49, while Figure 50 shows details of needle movement inside the tissue. The drawing in Figure 49-1 represents the time when there is needle collision with tissue surface in the contact point ($Z_{contact}$). Tissue surface has a surface normal (N_s). The drawing in Figure 49-2 shows the needle angle (A_r), relative to (N_s) in a needle penetration. A needle restriction path named V_r and is defined according the needle angle (A_r). Figure 50 shows the needle movement inside the tissues and the restriction path force (RP_f). The drawing with number 3 in Figure 50 shows a needle insertion with an applied force (A_f) and what happens if the needle inside the patient body follows V_r. The drawing with number 4 in Figure 50 right shows the case where the user forces the needle with an applied momentum (A_m), to deviate it from the restriction path (V_r), when a restauration-to-original-path force (RP_f) is generated by the internal tissues and related to an elastic effect.

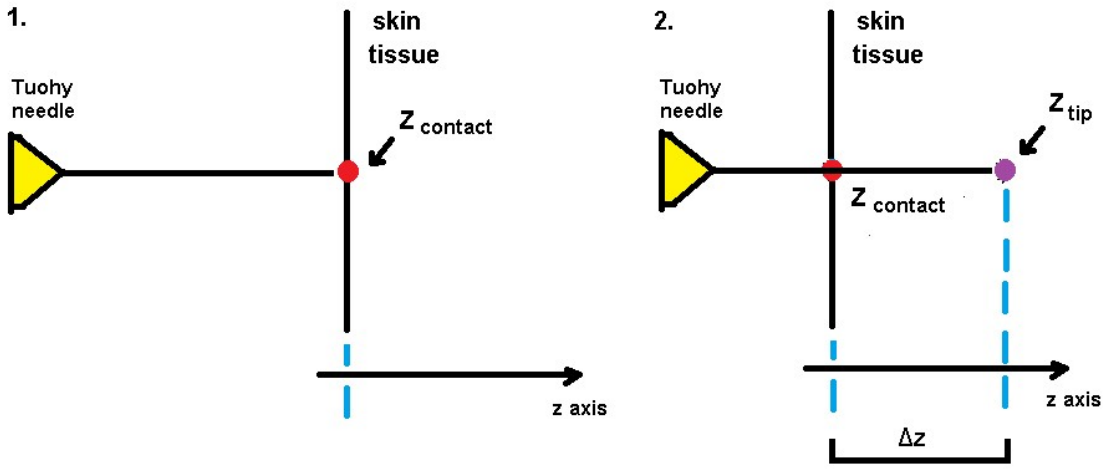

Figure 48. Elements for needle displacement calculation: 1. Initial needle contact with tissue, 2. Calculation of needle depth, based on distance from $Z_{contact}$ to needle tip position (Z_{tip})

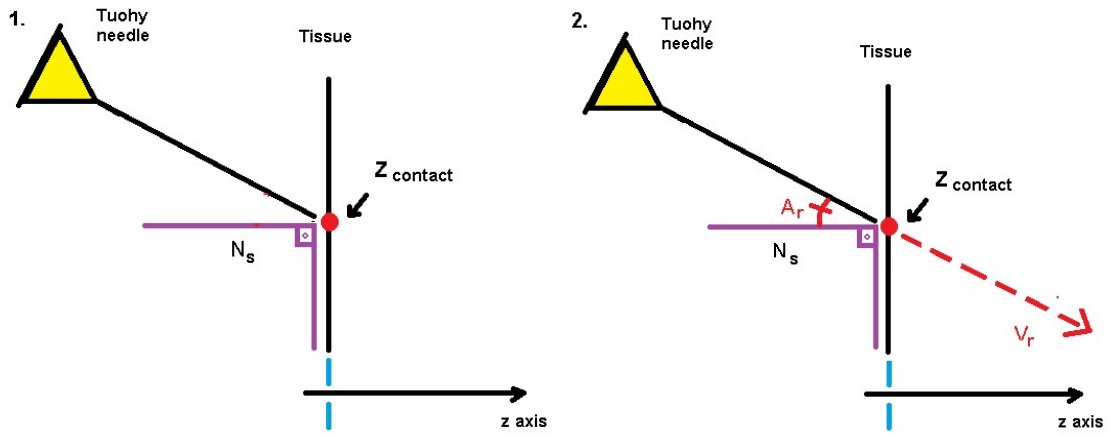

Figure 49. Needle movement restriction calculation: 1. contact with tissue surface, 2. path (V_r) and angle (A_r).

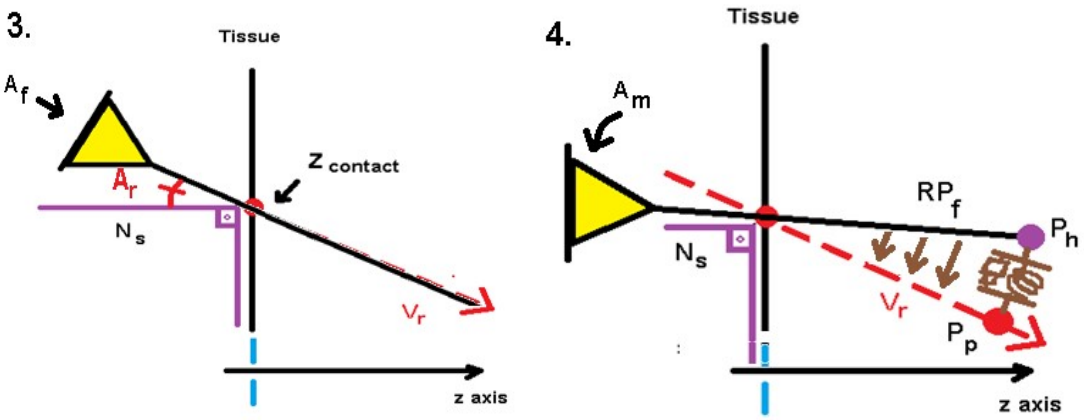

Figure 50. Needle movement inside tissue: 3. insertion following (V_r), 4. restrictions to transverse motion due internal tissues, represented by (RP_f).

In the proposed model, the tissue answer to the haptic device tip movement is represented by a virtual spring-elastic restauration force that is considered acting in the needle tip as represented in Figure 50 right (i.e. drawing number 4). It will try to restrain haptic device movement on the restriction path, where such continuous tissue characteristics are included by an elastic constant. The spring-elastic connects the haptic device current position ($\boldsymbol{P_h}$) (representing the needle tip in the virtual simulation) and the proxy position ($\boldsymbol{P_p}$). This last one is the position where the device should be, based on movement restriction according to the Hooke's Law ($F=k\delta$), where F represents the resulting force to be calculated, k represents the tissue stiffness, a tissue property value, obtained as defined in Section 5.1.2, and the δ parameter is the relative distance between the positions ($\boldsymbol{P_h}$) and ($\boldsymbol{P_p}$) in the force direction. This effect is incorporated in force

model in order to correct the haptic device orientation, based on the defined restriction path (V_r) and its corresponding inclination, relative to (A_r), as shown in Figure 50.

5.2.4. NEEDLE ANGLES TRACKING

The correct needle insertion angles are critical for epidural nerve block. They are formed by the relation between the needle and the skin. The vertical angle relates to the longitudinal axis in the sagittal plane and horizontal angle refers to transversal axis angle in the coronal plane. Needle insertion vertical angles must range from 10^o to 15^o (degrees), and horizontal angle must be around zero (none) for a midline needle insertion approach (Section 2.2.1), according to the plane orientations represented in Section 5.1.1 (Figure 46).

Angle calculation considers the needle tip position (Z_{tip}) when it becomes in contact with the skin tissue surface. A normal direction (N_s) is obtained, relative to the surface plane (P_s), as shown in Figure 51 (left).

The calculation of needle horizontal and vertical needle angles uses orthogonal projections of the needle in the sagittal (yz) and transverse (xz) planes (Figure 51, right). These needle projections will result in (V_{dy}) and (V_{dx}) respectively, as shown in Figure 52. Needle horizontal angle (A_h) will be calculated between (V_{dx}) and the surface normal (N_s). Vertical angle (A_v) is calculated between (V_{dy}) and the surface normal (N_s).

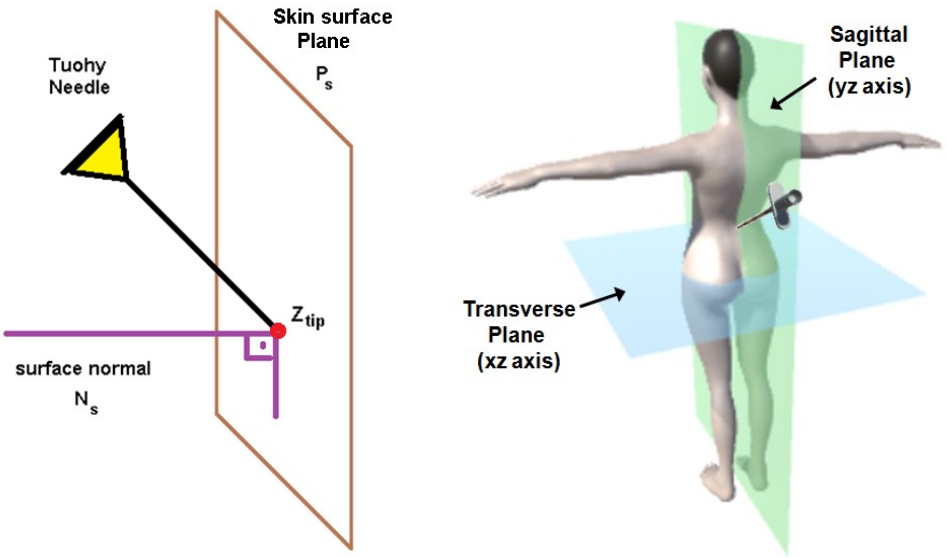

Figure 51. Needle contact with skin tissue and the surface normal (left). Transverse and sagittal planes (right)

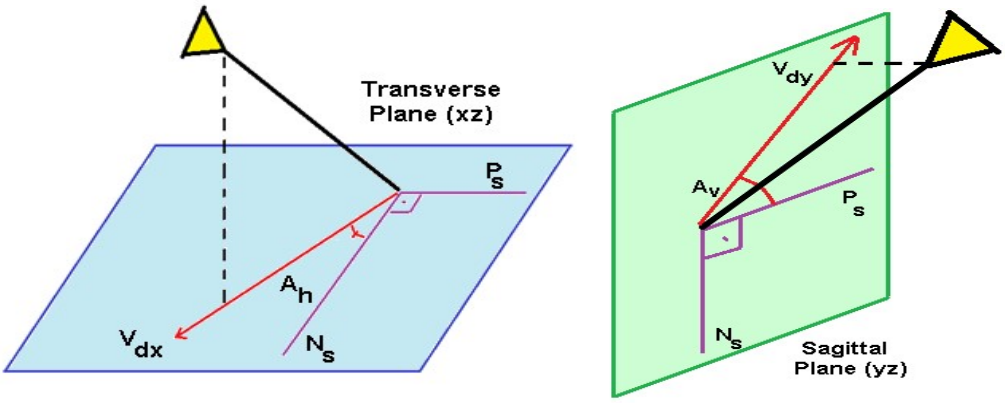

Figure 52. Orthogonal projections of the needle on transverse (left) and sagittal (right) planes.

5.2.5. NEEDLE MOVEMENT TRACKING AND REPRODUCTION

This functionality allows the tracking and visual reproduction of the haptic device movements done in a previous moment by the use of the simulator. It adds a wide range of possibilities to the project, including the tracking of expert player haptic device movements to be used as further tutorial step or help for new or apprentice players; or recovering of player executed movements for further evaluation from medical staff or experts. This is a desirable feature for virtual simulators (Section 3.1).

Haptic device movements executed in the simulator can be recorded as specified in Section (5.1.2), and reproduced afterwards, from needle position and orientation (direction and rotation parameters) information. Each register of needle position along the time is turned into a waypoint, which the virtual needle needs to arrive. Figure 53 illustrates the idea. Figure 59, in Section 6.5, shows the implementation results.

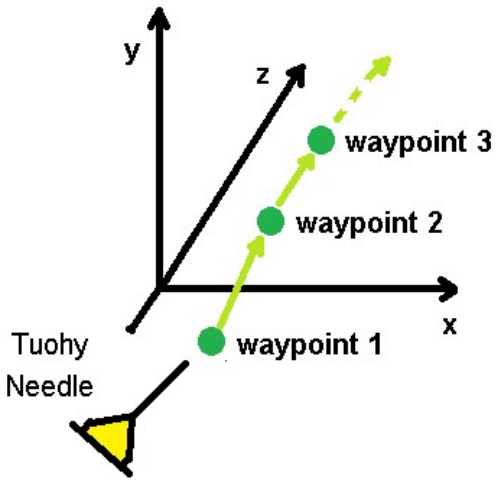

Figure 53. Needle positions are recorded and turned into waypoints, to orient needle movement reproduction on the simulator environment

5.2.6. TISSUE PRESSURE GENERATION

The evaluations of the air or saline pressures are critical for the epidural space detection: LOR technique uses them to identify tissue changes. The sudden pressure drop on tissue transition from ligamentum flavum to epidural space makes easier to identify epidural space location. This feature is important to simulate tissue detection by pressure. It enables pressure measurement simulation on the implementation by the use of a virtual syringe. The goal is to detect, by pressure measurings, if the virtual needle has already reached the epidural space region, which is represented by a very low tissue pressure value.

The implementation intends to emulate saline pressure for each relevant tissue in epidural nerve block procedure. The used values are generated at random, at the beginning of each simulation, using the average saline tissue pressures and their standard deviations from Table 14 as limits (average pressure ± standard deviation). The values listed on Table 14 are based on experiments from Tran et al (2009) and Lechner et al (2011). The randomly generated values are stored in a script class structure. They are defined for each tissue at the simulator start, and improve the simulations, because even an experienced specialist or a veteran player cannot preview the exact outcome.

Table 14. Average pressure values from epidural tissues to saline fluid and standard deviations.

Tissue Property	Tissue Layer						
	Skin	Fat	Muscle	Intersp. Ligament	Lig. Flavum	Epidural Space	Dura-Mater
Average Saline Pressure (kPa)	0	6	21	15.5	47.4	8.5	18
Std. Deviation for Saline Pressure (kPa)	0	1	10	12	14.7	1.2	9

5.3. GAMIFICATION OF THE SIMULATOR

In order to upgrade the virtual simulator into a ludic experience, points and challenges are incorporated as game elements. A tutorial mode is also included, for player supporting and basic understanding of the haptic device forces in the simulator.

The use of challenges and achievements is relevant for motivating the users on their quest by training, giving the evaluation of their state and current comparative reputation. These elements are important for orienting the trainees about the tasks already accomplished and remaining. This helps on motivating them to conclude the entire training procedure and store the best results, when comparing their results with other users' scores and reputations.

The strategy of this gamification is to identify the main steps to be executed by the physician in an epidural nerve block procedure and subdivide them into challenges. Three main steps from the epidural nerve block procedure in Hardama (2013) were considered for the gamification: local anaesthesia, epidural needle insertion and catheter placement. Each of these steps is implemented as a module in the EHGS simulator.

Each module is implemented in the simulator and includes its own set of challenges (Table 15). The tutorial, for example, includes two implemented challenges for vertebrae identification and other two, for the location of critical tissue layers.

The acomplishment of each task is tied to a set of actions to be executed by the user, by interacting with the simulator through the haptic device. The vertebrae identification tasks consist into moving the needle until hit the small purple spheres representing the vertebrae positions (Figure A5 in Appendix). The challenges to locate, achieve, pass, perforate or puncture a tissue layer require a needle insertion, trespassing all tissues and arriving at the specified location, as shown in Figure 5 (Section 1). The tasks of pressure measuring require the pressing of button 1 from the haptic device, to fit the syringe on back of the Tuohy needle, and the continuous pressing of button 2 from the haptic device afterwards, to measure the pressure resistance from the current tissue being penetrared by the needle (Figure 57 in Section 6.4). The local anaesthesia task requires the switch of the Tuohy for the anaesthetic syringe, by pressing the button 2 from keyboard, the insertion of the syringe into the skin and the pressing of the button 2 from the haptic device, to inject the anesthetic fluid (Figure 68 in Section 6.9).

Each challenge is composed of a name, a description and an associated achievement score. It corresponds to a specific set including movements and actions to be realized in the simulator environment with the right virtual medical tools, by the use of the haptic device. The points are earned by the player after the given challenge is accomplished. It facilitates the learning and tracking of player progress within the simulation. Another goal is to improve the trainee motivation.

The visual interface displays the current player score and messages after the conclusion of each task, including the challenge name and its awarded points, as a progression feedback to the player. Player score and performance are stored for future reference and comparison. These functions are linked to a game manager class.

The game manager is a persistent class required in most game-based simulations. It is important to specify details from game progress and gameplay related features. The proposal for this game manager is to keep track and provide feedback of

player progress within the simulation: score and all gaming challenges, together with their achievement status. Specific game related information, as patient data, visual and audio feedback for these elements are to be included in the game manager.

Some proposed challenges could not be implemented in the simulator. The challenges associated to the gamification of the catheter placement step would require the development of a new module with specific calculations for it. The first two challenges of local anesthesia step also require an implementation of a virtual hand contact with the patient back to sense and search for the spine structures of lumbar vertebrae, so time constraints also influenced this outcome.

Table 15. Epidural nerve block procedure main steps and proposed challenges

Main Step	Proposed Challenge	Achievement Points	Implemented (Y/N)?
Tutorial Mode	Identify L3 vertebra	100	Yes
	Identify L4 vertebra	100	Yes
	Locate the epidural space (ES)	250	No
	Locate and perforate the dura-mater (DM)	100	No
Local anaesthesia	Locate the L3-L4 inter-vertebral space	100	No
	Clean the needle insertion region	50	No
	Insert a syringe filled with anaesthetic fluid	100	Yes
	Apply local anaesthesia	150	Yes
Epidural needle insertion	Reach skin tissue	50	Yes
	Puncture subcutaneous fat	100	Yes
	Achieve muscle	150	Yes
	Measure pressure* (kPa) for muscle	100	Yes
	Reach interspinous ligament (ISL)	200	Yes
	Measure ISL pressure* (kPa)	200	Yes
	Pass ligamentum flavum (LF)	200	Yes
	Measure LF pressure* (kPa)	200	Yes
	Achieve epidural space (ES)	500	Yes
	Measure ES pressure* (kPa)	200	Yes
	Perforate dura-mater	-1000	Yes
	Reach bone	-250	No
Catheter placement	Insert catheter inside Tuohy needle	250	No
	Remove Tuohy needle from body	250	No
	Fixate catheter on patient body	200	No

* This is realized by a saline filled syringe fit on the back of the tuohy needle. The thumb presses the plunger afterwards (LOR)

6. RESULTS AND DISCUSSION

The implemented simulator is focused on the needle insertion for an epidural nerve block procedure with user movement and forces sensation integrated in the program by using a Geomagic Touch haptic device. It also includes a local anesthesia application before the needle insertion procedure, and the saline pressure tracking, by the use of the haptic device buttons. It is developed in the version 5 of Unity3D (2016) engine. The programming scripts are written in C# language and the developed 3D models imported from the Blender (.blend) or the Autodesk (.a3d) formats. A desktop computer with a Geforce GTX 960 1GB Videoboard is used for development.

6.1. THE VISUAL INTERFACE OF THE SIMULATOR

The visual interface is constructed with customized Unity 5 engine components, including a canvas, graphic bars, sliders, text fields and buttons. Figure 54 shows an initial view of the visual interface of the developed simulator. A video with an overview of the interface fuctionalities, detailed in section 5.1.1, is available (BRAZIL, 2016a).

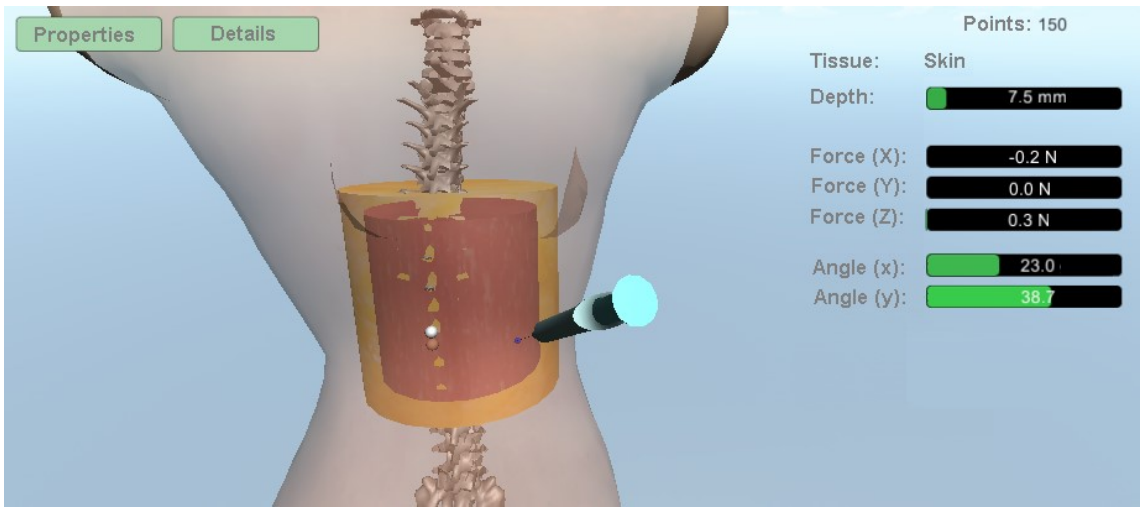

Figure 54. The initial view of the visual interface of the developed simulator.

The visual display area shows two buttons on its top: *Properties* and *Details*.

The *Properties* button, when clicked, lists all tissue relevant properties: static and dynamic friction (p) (internal: on tissue perforation), perforation resistance, stiffness, damping, and static and dynamic friction (external: on surface). The graphical sliders alow real-time adjustment of biomechanical properties values for each epidural tissue available on the simulator.

The *Details* button is used to display details and information about the needle insertion simulation: Needle depth, current exerted forces (*Force: X, Y, Z*), and the needle orientation. The orientation is composed by the needle tip position (*Position: X, Y, Z*), its pointing direction (*Direction: X, Y, Z)*, and its rotation (*Rotation: X, Y, Z*). Saline pressure from current tissue is also displayed. These data are visible in Figure 55.

The right side of interface is composed by a heads-up display (HUD) showing: (1) player points (score), obtained by the conclusion of the epidural procedure tasks defined in Section 5.3, (2) current needle depth, (3) applied axial forces, (4) tissue contacted, (5) needle angles obtained from orthogonal projections in the transverse and coronal planes, corresponding to the horizontal (X) and vertical (Y) axis. These values are updated in real time according to the haptic device tip position and user motions.

The interface from developed simulator also includes a number of others features detailed on the Chapter 4. A video showing the visual interface with the axial forces (Figure 55 - right) being applied on the simulator by the user interaction with the haptic device is available (BRAZIL, 2016a).

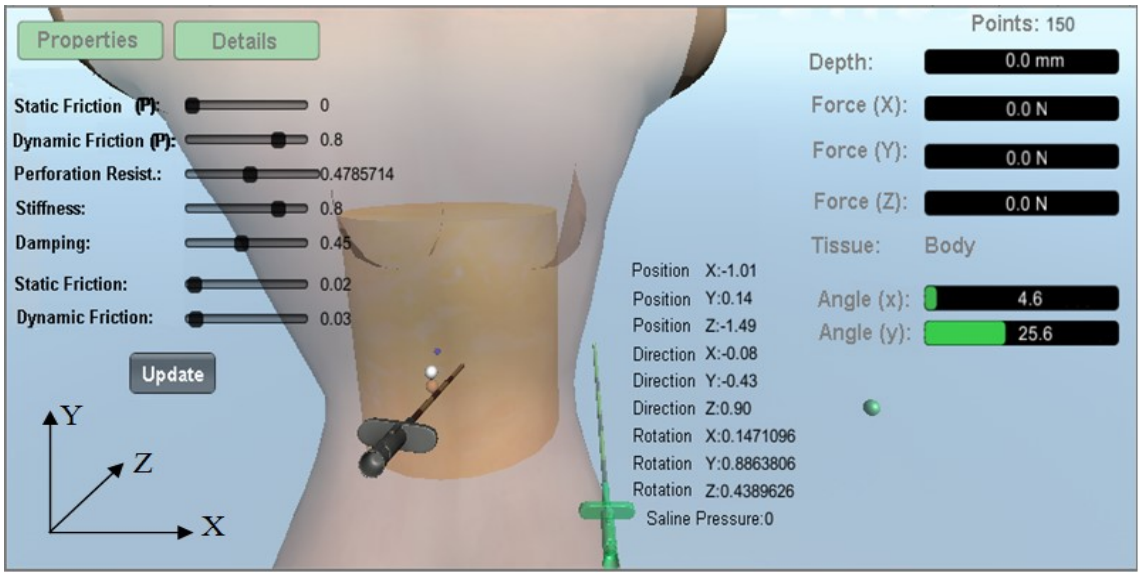

Figure 55. The visual interface from developed simulator, with *Properties* and *Details* activated.

6.2. DYNAMIC TISSUE DIMENSIONING AND POSITIONING

The implemented simulator allows a configuration of the patient data (height, weight and age) as parameters for different simulation setups, as mentioned in the model described in Section 4.1. They influence the standard tissues thickness values and are calculated in the beginning of the simulation. Each tissue in the simulator is tied to two previously defined properties: mean thickness and mean depth. Cylindrical shapes

associated to the tissues are dynamically resized, based on these properties values and the results from thickness calculations.

Tissues positional strategies involve the centring of tissue layers around the 3D spine position, using its location (its position property from the transform component associated to the game object) and considering the developed equation described in Section 4.4. In the screen presented in Figure 54, the subcutaneous fat and muscle tissues are represented already resized and positioned inside the virtual body, previously dimensioned by the equation designed and commented in Section 4.1.

Some tests and investigations revealed that the tissues positioning strategy did not fully correspond to real tissue simulation, as mentioned in Pouliot et al (1994). Tissue volume distribution usually is uneven, when related to the spine position. The tissue volume on patient's back usually should be more reduced than the frontal volume. The tissues position can be adjusted to take this volume difference of back and frontal direction into account. Results from this adjustment are presented in Figure 56, which shows a 3D view of the dimensioned tissues for a thin patient (left) and an obese patient (right), where the placement of the tissue cylinders has been repositioned, not being centered at spine anymore. The use of real textures for representation of internal epidural tissues improves the graphical quality of the simulator, approximating the experience to reality. None of previous works or investigated simulators employed this.

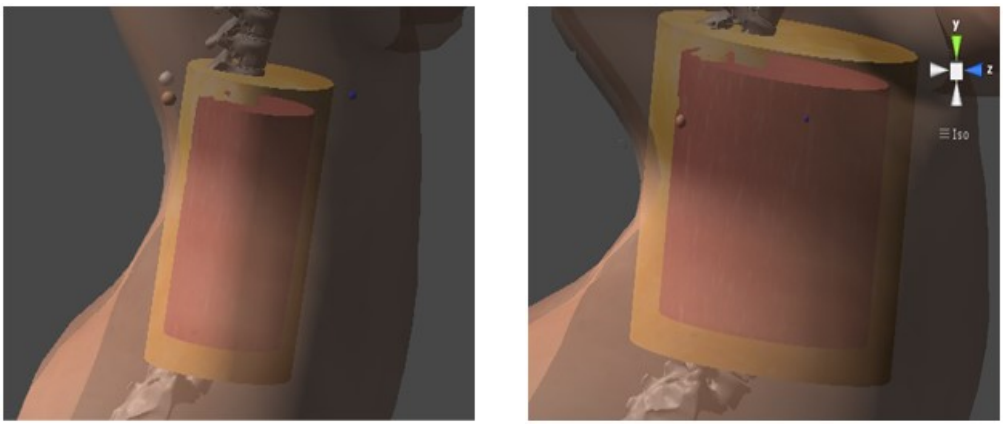

Figure 56. Dynamic tissue dimensions for a thin patient (left) and a obese (right).

6.3. NEEDLE MOVEMENTS RESTRICTION PATH

The direction of the needle along the penetration was modeled to be in-line with the needle angles from the perforated tissue surface. This direction was obtained through the use of a ray casting function from the engine, in order to trace a directional path (a line) from the current needle object to the punctured point position, as explained

in Section 5.2.3. A movement restriction script is programmed to use this path information on order to restrain all needle movement inside the body when the user deviates it from this direction, after skin perforation, by applying restrictive and reversal forces to the haptic device (ex. the script forces the haptic device back into the directional path, so it ensures the player "stays on the line"). These resistance forces are calculated as detailed in Section 5.2.3. The identification of tissues trespassed by the needle is based on this directional path and the current position from the needle tip. All the tissues crossed by the restriction path line are identified and stored in a vector structure, considering the needle tip position as the end point of this scanning. A demonstration video of needle insertion in tissues is available (BRAZIL, 2016c).

6.4. TISSUE PRESSURE GENERATION

A pressure generator was implemented defining saline and air pressure levels for each tissue at the beginning of the simulation, according to Section 5.2.6 specifications. This provides a different patient tissue setup for running each time the simulator is used.

The pressure measurement is activated by pressing the button 2 from the haptic device. The player must keep the button pressed to see the pressure values on the interface. This action represents the "syringe plunger being pressed by the thumb", described in Chapter 2. It emulates the use of LOR technique to identify the epidural space. It also requires the fitting of a saline filled syringe into the Tuohy needle (Figure 57), an action triggered by the pressing of button 1 from the haptic device.

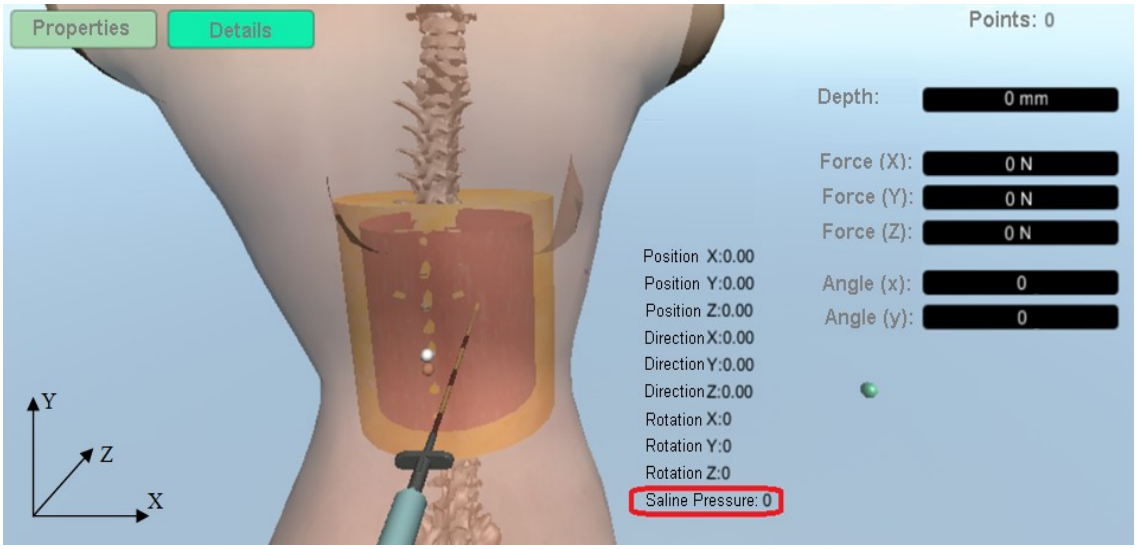

Figure 57. Saline filled syringe fit into Tuohy needle for evaluation of current pressure (LOR).

The pressure values are created inside an interval between each tissue average pressure values and their standard deviations, ranging from lower to upper limits. The pressure values used on simulator are listed on Table 5.

Pressure simulations were also included in Vaughan et al (2014), but the pressure values were not generated neither displayed by the visual interface of their simulator. A demonstration video is provided for this development (BRAZIL, 2016d).

6.5. TRACKING AND REPRODUCTION OF HAPTIC DEVICE MOVEMENTS

Haptic device movements are recorded on previous uses of the simulator and reproduced from needle position, direction and angles data, within a time frame. These are read from a log file, specified in Section 5.1.2. A visual reproduction of maneuvers with the haptic device is processed by the conversion of each line record into a waypoint position inside the simulator environment. These positions become target points to be achieved by the movement of the virtual needle. The needle orientation is obtained from direction and rotation information. Figure 58 shows the parameters used in the movement reproduction script. A log filename (*NomeArquivo*) is required to load a previously recorded simulation session. A 3D object (ex.: green needle) is associated to the script for movement reproduction. Figure 59 illustrates the ongoing process, indicated by the green line path.

The "Traceback" script reads the log file and sets the first recorded point as a waypoint for destination of the needle object. It reads the needle information, rotating and positioning the needle accordingly. Afterwards, it moves the needle to the waypoint, and reads the next waypoint in sequence upon the arrival. When the last waypoint is reached by the needle object, the process restarts, in a loop.

The needle trajectory is achieved with the use of the Trail Renderer component. This effect is programmed to be visible for five seconds before its disappearance. When the last waypoint is reached by the needle, the process restarts, and the needle moves back to the first waypoint. A demonstration video is available (BRAZIL, 2016e).

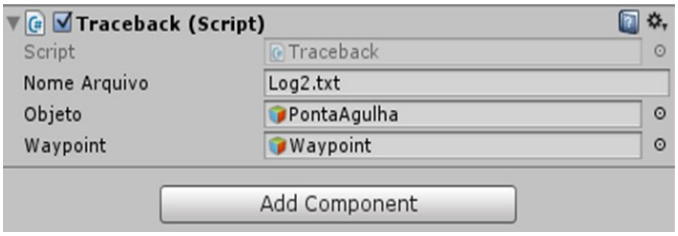

Figure 58. Traceback script parameters.

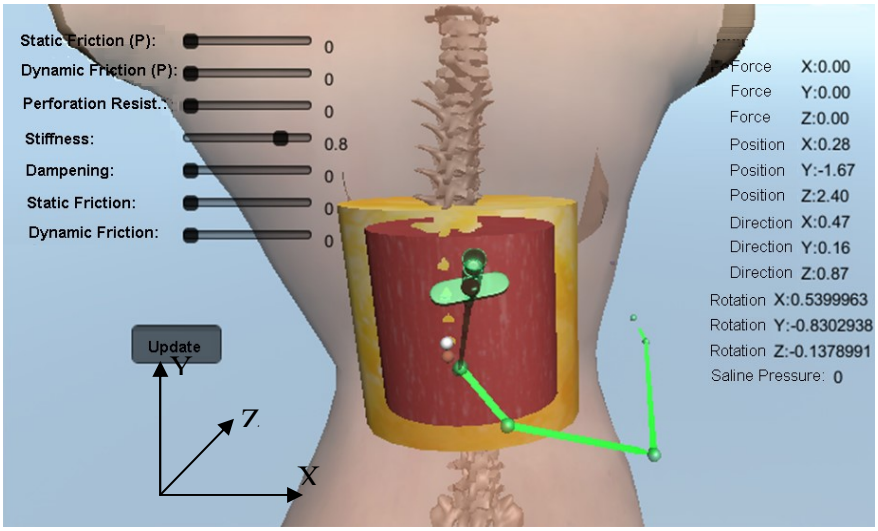

Figure 59. Movement reproduction by trace back functionality.

6.6. NEEDLE ANGULATION TRACKING

Needle vertical and horizontal angles are calculated from two line paths: the direction that the haptic device is currently pointing at (its orientation) and a normal direction. The needle orientation (yellow line in Figure 60 left) is traced by a ray casting function. The normal (red line in Figure 60 left) is obtained from a surface plane from the patient body 3D mesh, i.e. the surface to be perforated by the needle. The needle angles calculations use orthogonal projections from the needle direction, as defined in Section 5.2.4. Magenta and ciano lines in Figure 60 (right) show its horizontal and vertical projections.

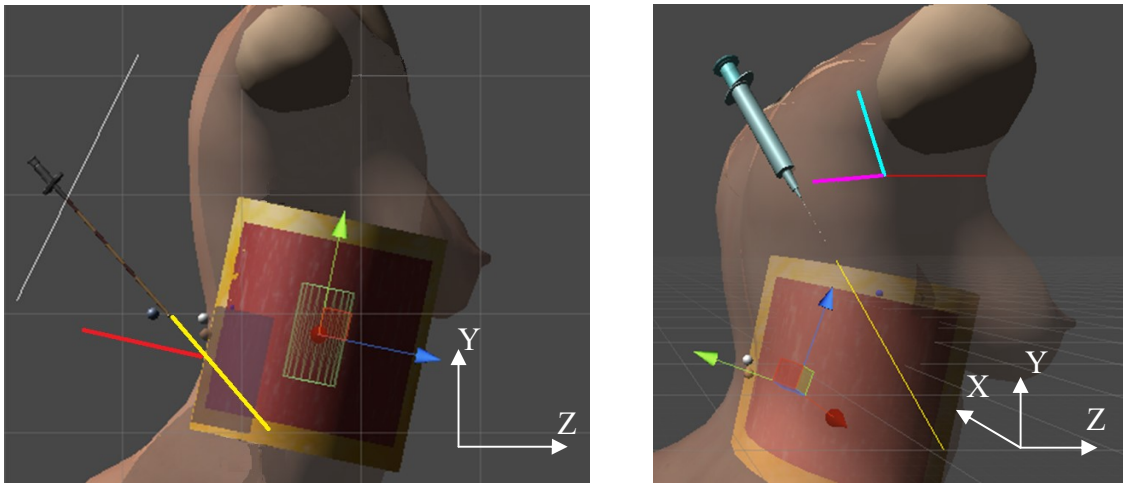

Figure 60. Directions paths for needle angles calculation (left). Lines representing orthogonal projections from the needle direction (right).

Initial tests have shown sudden changes on needle angles upon needle movement. This happened because the used body mesh is composed of many small surfaces (triangles), each one with a different normal. After preliminary tests, this functionality was simplified. The normal direction now is always obtained from a single surface plane that represents the whole body surface. The coronal plane is used (Figure 46, Section 5.1.1). This resulted into stable needle angles. A demonstration video of needle angles display is available (BRAZIL, 2016f).

6.7. FORCE MODELLING RESULTS

The designed force modelling for the virtual simulator employs the construction of a force model based on experiment data as mentioned in Section 4.2. Needle depth is obtained as a distance between two positions: first contacted point of body surface and the current needle tip location.

A first experiment consisted of generating a plotted force curve using the designed force model with the experiment data from needle insertions in bovine livers provided in Okamura et al (2004), and comparison of the obtained results with the original graph reported in Okamura et al (2004). The designed model used the parameters listed in Tables 16 and 17 for the development of the graphic. Results are shown in Figure 61. The curves in the graphic plotted from the designed model (right) present a similar behavior to the curves drawn from the experiment data results (left).

Table 16. Tissue parameters before puncture from bovine liver (OKAMURA et al, 2004)

Tissue	c_0 (N)	c_1 (N/mm)	c_2 (N/mm^2)	c_3 (N/mm^3)	Max. Stiffness Force (MSf) (N)
Skin (bovine liver)	0	0.048	0.0052	0	2.241

Table 17. Tissue parameters after puncture from bovine liver (OKAMURA et al, 2004)

Tissue	cp_0 (N)	cp_1 (N/mm)	cp_2 (N/mm^2)	Thickness (mm)	Transition Force (Tf) (N)
Skin (bovine liver)	0.94	0.00623	0.00021213	16.6514	1.0472

A second and more complete experiment, involves the use of the designed model considering all the relevant epidural tissues, with the experiment data from porcine cadavers and human subjects from Holton and Hiemenz (2001). The designed model used the data from Table 4 to generate a force x displacement graph, and compared them with results in Holton and Hiemenz (2001). The depth versus force curves from the developed model are plotted in Figure 34 (Section 4.2) and the original data reported

in Holton and Hiemenz (2001) is visible in Figure 31 (Section 3.2). The graphs obtained by simulation results nearly match those generated from experiment data and show the stiffness, friction and cutting forces and their individual contributions to the resulting force. The tissues from this second experiment are visible on the simulator as cylindrical based shapes, with a transparency effect applied on them after perforation, as shown in Figure 54.

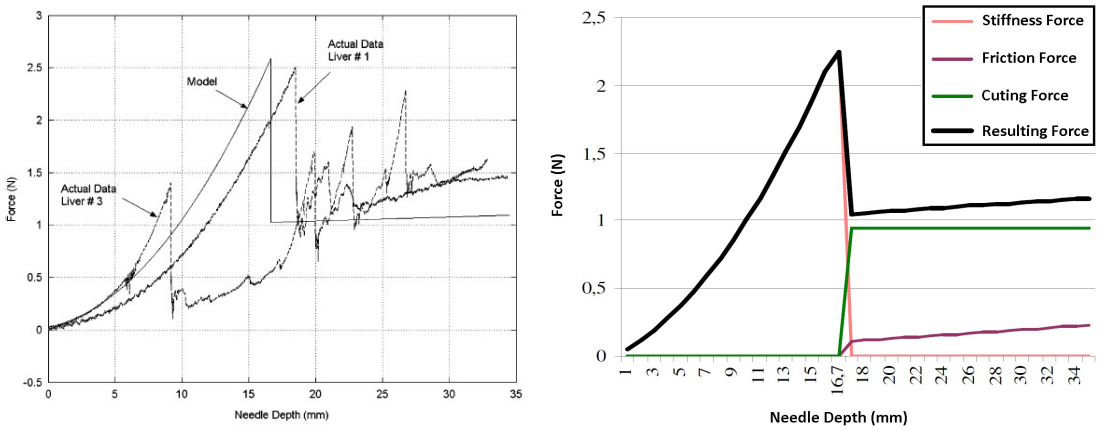

Figure 61. Needle Force (N) x Depth (mm): Experiment data from Okamura et al (2004) (left) and graph from developed model (Section 4.2) in Conci et al (2015) (right).

Two inconsistencies were found when testing the data from Ligament Flavum tissue of Holton and Hiemenz (2001). They reported a force of 12.1330 N necessary to perforate this tissue, but the graphic in Figure 31 (Section 3.2) shows a different value (14 N). The second issue was related to pos-puncture force for Ligamentum Flavum (LF) tissue represented in Holton and Hiemenz (2001):

$$F(X) = 6.1330 - 3.4693\,(X - Xp) - 0.7177\,(X - Xp)^2 + 6.0 \qquad (24)$$

where the use of equation ***(24)*** causes a force decay, does not corresponding to the LF descendant curve in Figure 31 (Section 3.2). Consequently, adjustment of LF forces was necessary to better reproduce this curve behaviour. The updated values for calculations to obtain the adjusted resulting forces are listed on Tables 13 and 14. The format used in the implementation with this corresponding force versus displacement curve is that of Figure 34 (Section 4.2).

Most works commented in Section 2.2 reported experiment data from needle insertions, but did not design a proper force model for them. They only plotted incomplete force-related curves, not showing all the tissues relevant for an epidural nerve block procedure. Figure 62 (top-left) shows one of these: a force x displacement curve from Brett et al (2000), of porcine cadavers and human lumbar samples, not

including all epidural tissues. Figure 62 (top-right) shows a curve mapping only skin, fat, muscle and bone tissues from Kwon et al (2001). Figure 62 (bottom) shows a force x displacement curve listed in Lee (2013), of an epidural simulator from Delft University of Technology, where the bold line shows the forces included in their the simulator, which presented a plastic behavior (constant force on displacement) until reaching ligamentum flavum. After this, it have shown an elastic (linear relation between force and displacement) behaviour until 16N, with a sudden drop to 9N (LOR) in the epidural space.

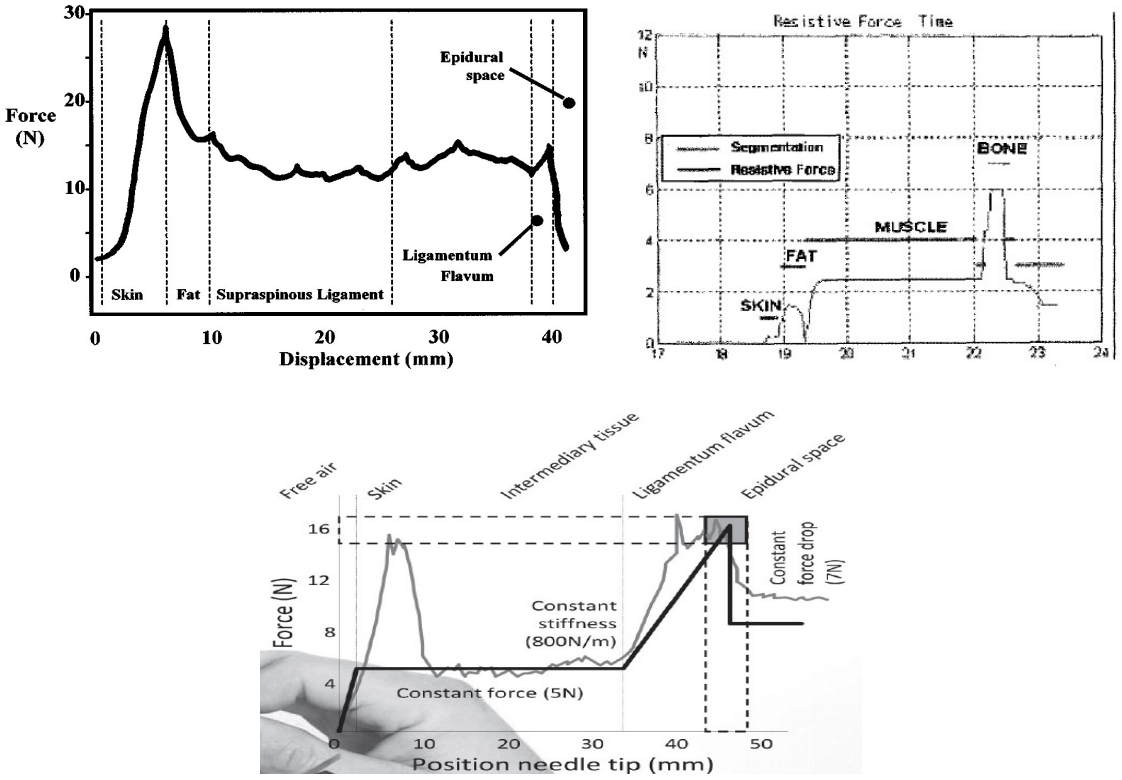

Figure 62. Two force x needle displacement curves from Brett et al (2000) (left) and Lee (2013) (bottom), and a force x time curve (KWON et al, 2001) (right).

Results for bending forces are calculated as defined in Section 4.3, and displayed on a previous version of the simulator interface (Figure 63). The force results are based on the type of the virtual needle tip on use by the implementation in a given simulation (bevelled, coned or triangular), its diameter and speed. Figure 63 shows the configuration parameters.

A work comparison between the force model and the results presented in Vaughan et al (2014) shows they had a relatively simple force model for calculating the insertions forces, which consider only stiffness and damping forces for the tissues, and

have only four tissues in the simulations (skin, fat, muscle and bone). Their visual feedback is based on a 2D image representing the tissues (Figure 6 - centre), and their work was not specifically directed at epidural procedures, with the use of a 1 DOF haptic device for simulation, against the 6 DOFs used in the developed simulator, limiting the outcome and possibilities.

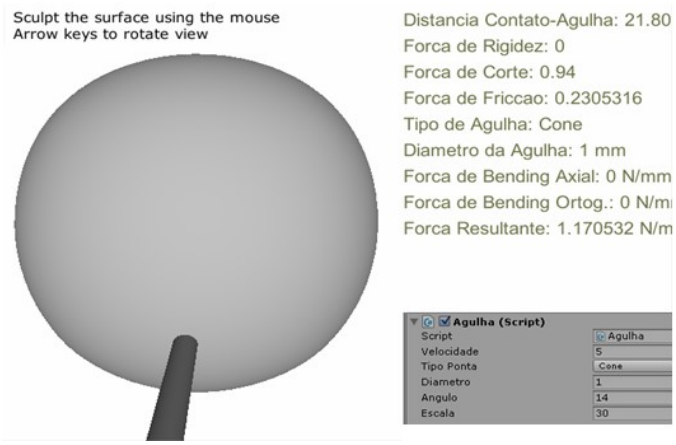

Figure 63. Needle bending forces calculation results on a previous version of the simulator interface.

6.8. TISSUE PROPERTIES CONFIGURATION AND CALIBRATION RESULTS

Biomechanical tissue properties are mapped and stored as values on a script class structure. They are linked to each tissue layer (cylindrical 3D shape) available on the simulator. Figure 64 shows an example of the tissue properties associated with the game object representing the epidural space tissue. These values are used to update the forces applied on the haptic device, when the needle reaches this tissue. API available resources are used to configure and set these values, for adjustment and emulation of the tissue properties by the haptic device. Each tissue property has a slider associated to it, displayed on the simulator interface, and accessible through the *Properties* button (see Figure 55). This adjustment has not been included in any other work until now. The sliders update the values for the current tissue in contact with the needle. They indicate the range of the influence of a property. A video containing the manipulation of the tissue properties on the simulator is available (BRAZIL, 2016g).

Two scripts were developed to handle each tissue layer in the simulator. They are used to specify the biomechanical properties for each tissue. An example of these properties and their association with the epidural space tissue can be visualized in Figure 64.

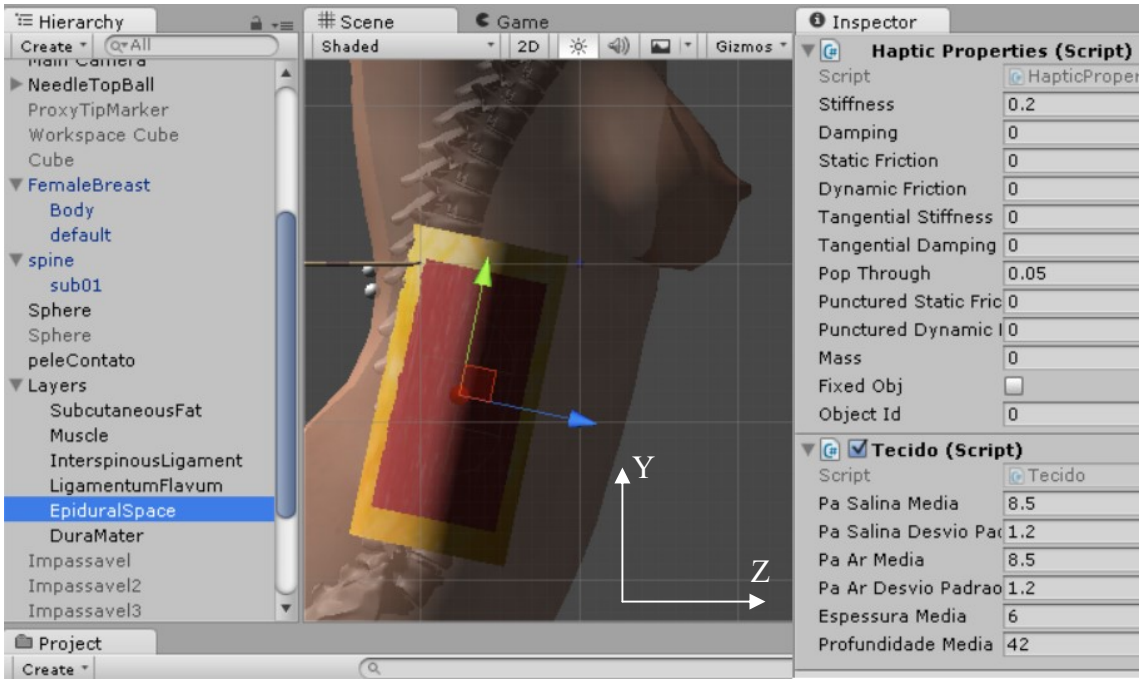

Figure 64. Tissue layers properties associated to the game object of epidural space tissue.

Configurable tissue properties include: average thickness (mm), average depth (mm), average saline and air pressure (kPa) and their standard deviation. Generation of current patient stress (kPa) for each tissue on the simulator environment is based on these properties. Tissue thickness and depth are important for correct tissue positioning and dimensioning inside the patient body. The pressure related parameters are relevant for generation of current virtual patient kPa of each tissue on the simulation environment. The calibration of tissue properties values uses the force model developed as a reference, reflecting the resulting forces achieved by the model. Table 18 shows adjusted properties for all relevant epidural tissues. Most of these properties range from 0 to 1, with exception of: pressure, thickness and depth.

A study on the influence of the tissue properties over resulting forces is achieved by isolating a property on simulation and retrieving three-dimensional axial forces recorded on the log file, aiming at mapping these properties influence on the resulting force outcome. A biomechanical property value is set to its maximum and all the other properties values are set to zero. A subsequent recording of the forces applied on the simulation is executed, as defined in Section 5.1.2. Force versus needle depth graphs are then plotted, based on result data (Figures 65 and 66). This strategy allows a behavioural mapping from a given property along needle insertion and may help in the calibration and combination of the biomechanical properties values for the tissue layers.

Table 18. Tissue properties influence values used for the simulations.

Tissue Property	Tissue Layer						
	Skin	Fat	Muscle	Interspinous Ligament	Lig. Flavum	Epidural Space	Dura-Mater
Stiffness (%)	0.8	0.2	0.8	0.8	0.9	0.2	0.2
Damping (%)	0.45	0.1	0.25	0.25	0.6	0.1	0.1
Static Friction (%)	0.02	0.22	0	0	0	0.22	0.22
Dynamic Friction (%)	0.03	0.21	0	0	0	0.21	0.21
Tangential Stiffness (%)	0	0	0	0	0	0	0
Tangential Damping (%)	0	0	0	0	0	0	0
Pop through (%)	0.05	0.05	0.15	0.25	0.2	0.05	0.05
Punctured Static Friction (%)	0	0.33	0.5	0.6	0.7	0.33	0.4
Punctured Dynamic Friction (%)	0.8	0.4	0.96	0.995	0.997	0.4	0.4
Average Saline Pressure (kPa)	0	6	21	15.5	47.4	8.5	18
Std. dev. for Saline Pressure (kPa)	0	1	10	12	14.7	1.2	9
Average Air Pressure (kPa)	0	6	21	15.5	47.4	8.5	18
Std. dev. for Air Pressure (kPa)	0	1	10	12	14.7	1.2	9
Average Thickness (mm)	3	6	4	26	3	6	15
Average Depth (mm)	0	3	9	13	39	42	48

Plotted graphs of axial force curves versus needle depth were obtained for stiffness, damping, static and dynamic friction properties. Figures 160 and 161 show these: it is possible to observe the influence of properties upon the tissue penetration action. The needle insertion speed was 3 mm/s.

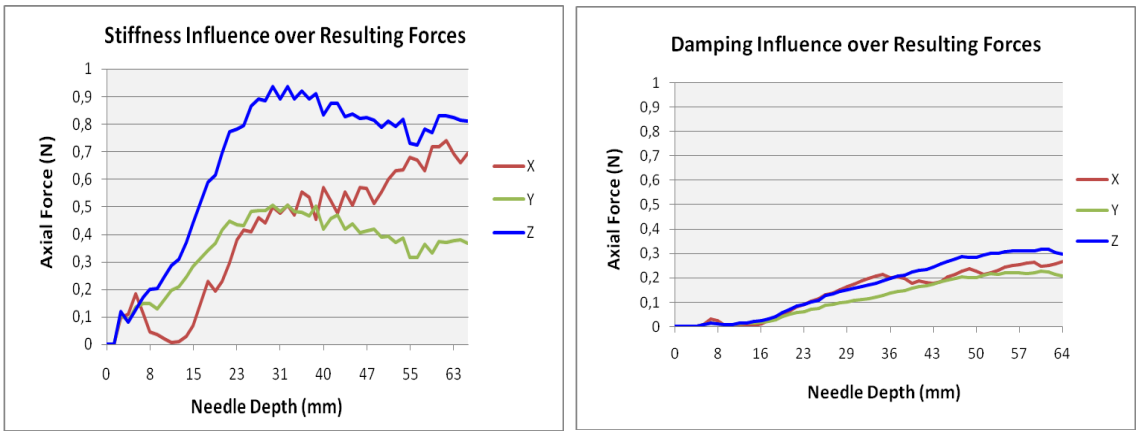

Figure 65: Stiffness (left) and damping(right) influence on axial forces x needle depth plots.

6.9. GAMING FEATURES

The gamification features implemented provide visual feedback of player score and concluded tasks on the interface. These features are linked to a game manager class.

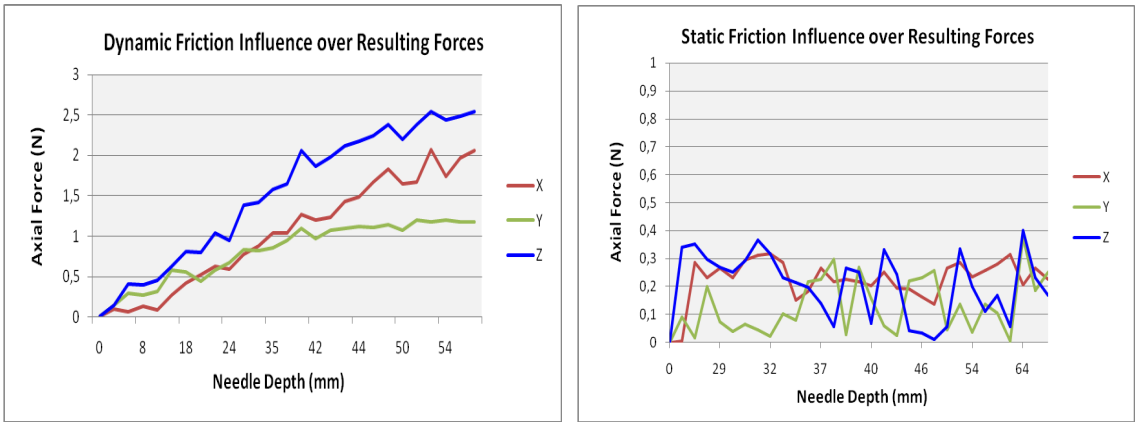

Figure 66: Dynamic (left) and static (right) friction influence on axial forces x needle depth plots.

The game manager from the developed simulator defines and keeps track of the following game resources: virtual patient data (height, weight, age, waist size and area), body and tissue layers (game objects and 3D meshes), their positions and properties. It uses a global parameter for: dimensioning all game objects, store and update the player score, control a list of challenges and their completion status and shows these feedbacks on the game interface (HUD). At the beginning of the simulation, the game manager dimensions and positions the tissue layers in the virtual simulator. At run-time, it constantly updates the current needle angles. Figure 67 shows the game manager properties and Figure 68 displays the gamified interface with points, challenges and HUD display (current layer and depth, exerted axial forces and needle inclination).

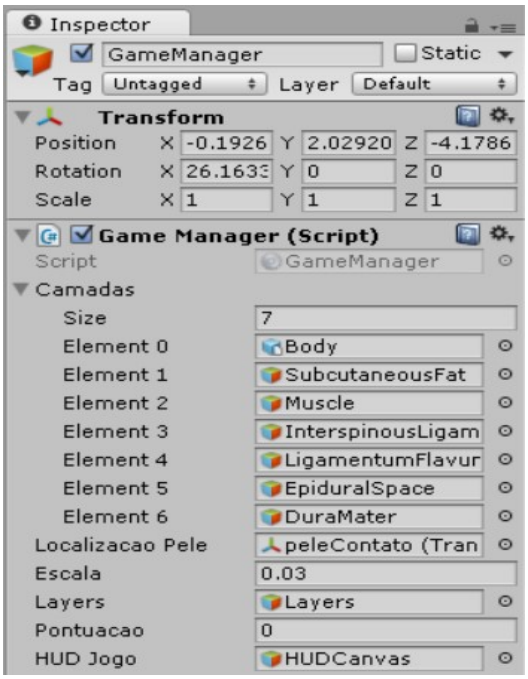

Figure 67. Game Manager class with properties shown on Inspector from Unity engine.

A challenge conclusion feedback is also displayed, each time a player succeeds in a task. A visual message is shown on lower right corner of the visual interface, with the task name and the total of points awarded. A demonstration video displaying the conclusion of challenges in the simulator interface is available (BRAZIL, 2016b).

The list of game challenges implemented, with their associated achievement score is available on Table 15 (Section 5.3). The simulation covers the majority of tasks related to the local anaesthesia and epidural needle insertion steps proposed for the gamification strategy. The developed simulator also implemented a tutorial mode, with L3 and L4 vertebrae identification tasks and audio feedback (details are available in the Appendix A). Vertebrae identification tasks in tutorial mode marked each vertebra location by adding a small purple sphere on the simulator environment. It disappears and launches an audio conclusion feedback when virtually "touched". Feedback sound and game music were also incorporated into the simulation.

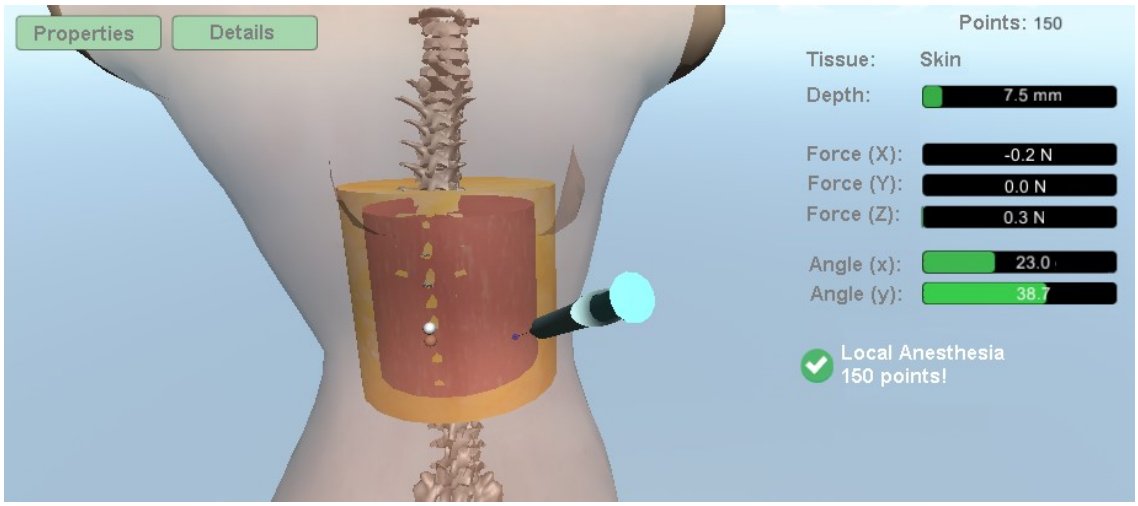

Figure 68. Gamified interface (current layer and depth, exerted axial forces and needle inclination).

6.10. Dynamic Tissue Deformation

The simulation of a visual tissue puncture effect is achievable using calculations specified in Section 4.5 and the use of the component "interactive cloth" available from unity engine version 4. This component is attached to a 3D object and enables real time body mesh geometry change, based on adjustable parameter values. Interactive configuration parameters include: friction, density pressure and collision response (Figure 69-left).

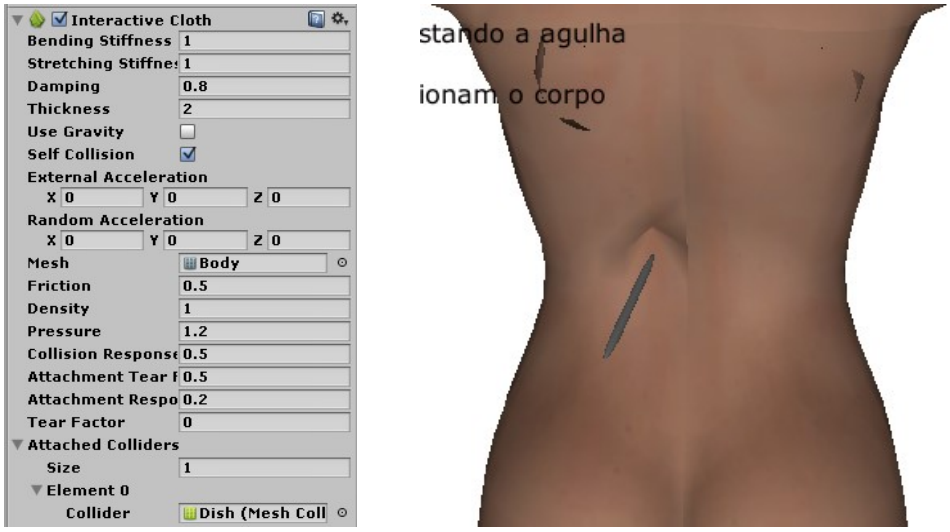

Figure 69. Interface from "interactive cloth" unity engine component (left). Woman 3D skin tissue deformation (CONCI et al, 2015; BRAZIL et al, 2016) (right).

Deformation tests are conducted in the simulator, with the 3D woman body object. A skin tissue deformation effect is shown in Figure 69 (right). The needle deforms the virtual patient body soon after it virtually hits the surface mesh. A breast tissue deformation example is shown in Section 6.11. The degree of this deformation can be modified as commented in Section 4.5.

Real time mesh geometry modifications computed on the developed simulator demonstrated a high computational cost for this feature after its implementation. The use of this feature caused a performance interference with other features concerning the haptic device force feedback, so its use was not enabled for all versions of the simulator.

6.11. SIMULATORS COMPARISON AND FEATURES EVALUATION

The current implementation of the simulator (EHGS) is compared to six other simulators with haptic device support. The features available on them are listed on Table 19. The descriptions and details about these features are available afterwards, in the following texts that describe and present the results obtained from comparisons between the simulators. Figures 71-74 show the graphical results plotted from the comparisons of features present on the simulators. Interface-related features are compared in Figure 71. Interaction features comparison results are shown in Figure 72. Results from the features associated to the tissues are presented in Figure 73, and a needle information comparison is shown in Figure 74.

Table 19. Features from epidural simulators with haptic device support.

Feature	3D HS (DUBEY et al, 2012)	2D HS (GEROVICH et al, 2004)	PBS (VAUGHAN et al, 2014)	HYS (AKASUM et al, 2016)	DNG (DANG et al, 2001)	EPI (FRAZETTO, 2011)	EHGS
Low resolution Interface	● (3D)	● (2D)		● (2D)	● (2D)	● (3D)	
High resolution interface			● (3D)				● (3D)
Patient display	●		●	●		●	●
Needle insertion display (skin)	●	●	●	●	●	●	●
Needle insertion display (fat, muscle)		●		●	●	●	●
Needle insertion with internal tissues					●	●	●
Tutorial mode							●
Local anaesthesia							●
Movement tracking	●	●	●	●	●	●	●
Movement reproduction					●	●	●
Haptic device - Degrees of Freedom (DOF)	3	1	3	3	6	6	6
Resulting forces simulation (number of directions)	1	1	1	1			3
Data recording (number of axes)		2					3
Needle depth	●	●	●	●	●	●	●
Needle position display (coordinates)		● (x, y)					● (x,y,z)
Needle insertion point	● Free	● Fixed	● Fixed	●Limited	● Fixed	● Fixed	● Free
Needle orientation (pointing direction and rotation)					●	●	●
Needle movement restriction on penetration							●
Needle angles mapping							●
Tissue properties configuration (real-time)					●	●	●
Tissue dimensioning					● manual	● manual	● auto
Tissue Pressure measuring (LOR)					●	●	●
Virtual patient body dimensioning (parametric)			●				
Gamification (points, challenges, subtasks)							●

The simulators used on this comparison are those of references Dubey et al (2012), Gerovich et al (2004), Vaughan et al (2014), Akasum et al (2016), Dang et al (2001) and the EpiSIM in Vaughan et al (2013) and Frazetto (2011). Figures 49 and 103 show the visual interfaces of those epidural simulators. Figure 6 (top-left) shows a 3D low resolution interface (named 3D HS) from Dubey et al (2012), where few simulation

data is displayed, and the virtual patient in the back position only includes the skin tissue and the spine. The 2D simulator interface from Gerovich et al (2004) (named 2D HS) can be visualized in Figure 6 (top-right), where some forces and tissues information are presented, but only four tissues (skin, fat, muscle and bone) are displayed. An epidural simulator (named PBS) from Vaughan et al (2014) with parametric body but few data simulation displayed can be visualized in Figure 6 (bottom-left). A hybrid simulator for needle insertions on soft tissues, combining the use of a phantom mannequim with a haptic device (named HYS) from Akasum et al (2016) is visible in Figure 6 (bottom-right). Its visual interface is described by authors, but no pictures of the computer screen display are included.

Figure 70 shows the interface for the simulator from Dang et al (2001) (named DNG) at left, and the EpiSIM simulator from Frazetto (2011) (named EPI) at right. They are also included in the comparison among the simulators. These two simulators both present some advanced configuration features, as a manual slider control for the adjustment of properties and thickness for the epidural tissues, but not the thickness dimensioning according to the patient weight, height and age, neither the inclusion of game elements, as provided by the implemented EHGS simulator. They also have a fixed point for needle insertion, which limits the possibilities for the epidural practice (VAUGHAN et al, 2013). The interface from the developed simulator displays more details about tissues and relevant simulation forces than the other investigated epidural simulators integrated with a haptic device.

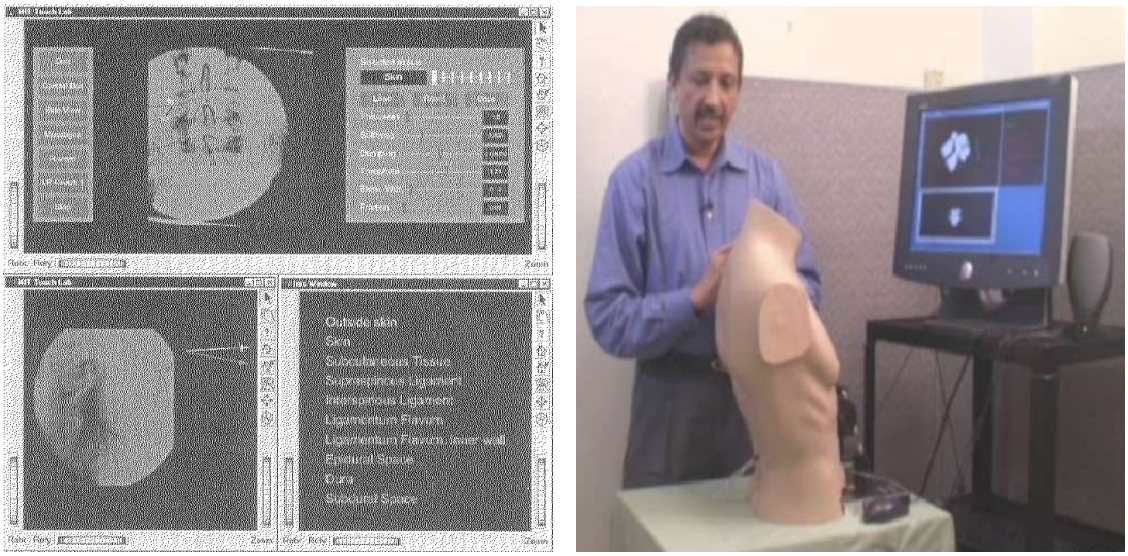

Figure 70. Interfaces of simulator from Dang et al (2001) (left) and the EpiSIM simulator (FRAZETTO, 2011) (right).

The interface features comparison (Figure 71) considers the interface resolution, the patient display and the use of game elements.

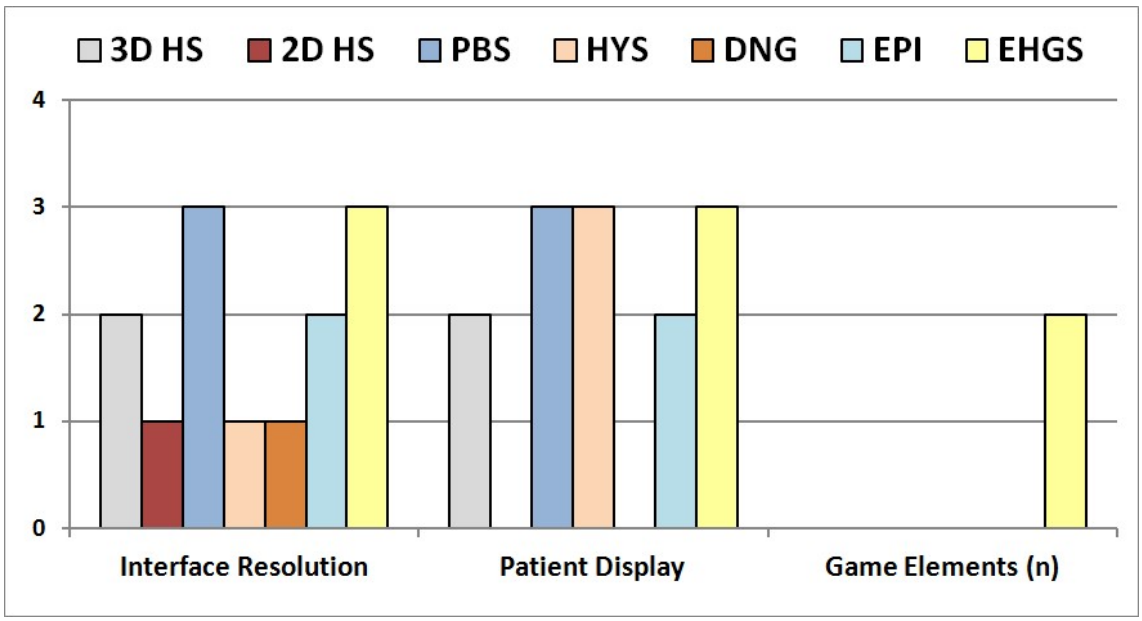

Figure 71. A comparison of interface-related features available on the simulators.

The interface resolution corresponds to the graphical display quality and the level of detail from the visual interfaces. The Sections 5.1.1 and 6.1 detail the EHGS interface. The PBS and EHGS interfaces scored highest (3), due to a 3D view and a high resolution. The 3D HS and EPI both include a tridimensional display with a lower resolution, as in Figure 6 (top-left) (ex.: a display screen of 640 x 480 pixels or less, with a pixelated resolution), attaining a score of (2). The interfaces of 2D HS, HYS and DNG are bi-dimensional (2D), so a score of (1) is assigned to them.

The patient display considers the graphical quality of the virtual patient body displayed on the simulator. The PBS, HYS and EHGS simulators have received the highest score available (3), once PBS and EHGS both present a 3D detailed body model for the virtual patient, and HYS includes a visual display attached to a phantom mannequim (Figure 6 - bottom-right). The score associated to the 3D HS is (2). It presents a lower resolution body model for the virtual patient. The EPI only presents a detailed view (3D) of patient vertebrae L4 and L5, so it received a score of (2). Both the 2D HS and DNG simulators scored (zero), due to an abscence of the patient display.

The game elements feature relates to the number of game elements available on the simulator interface. The EHGS gamified interface (Section 6.9) includes two: points and challenges, totalizing a score of (2). The other simulators do not present this feature.

The interaction features comparison (Figure 72) includes: haptic device interaction (DOFs), tracking, reproduction and restriction of movements, and the tutorial and local anesthesia interaction modes. Most of these are detailed in Section 5.2.

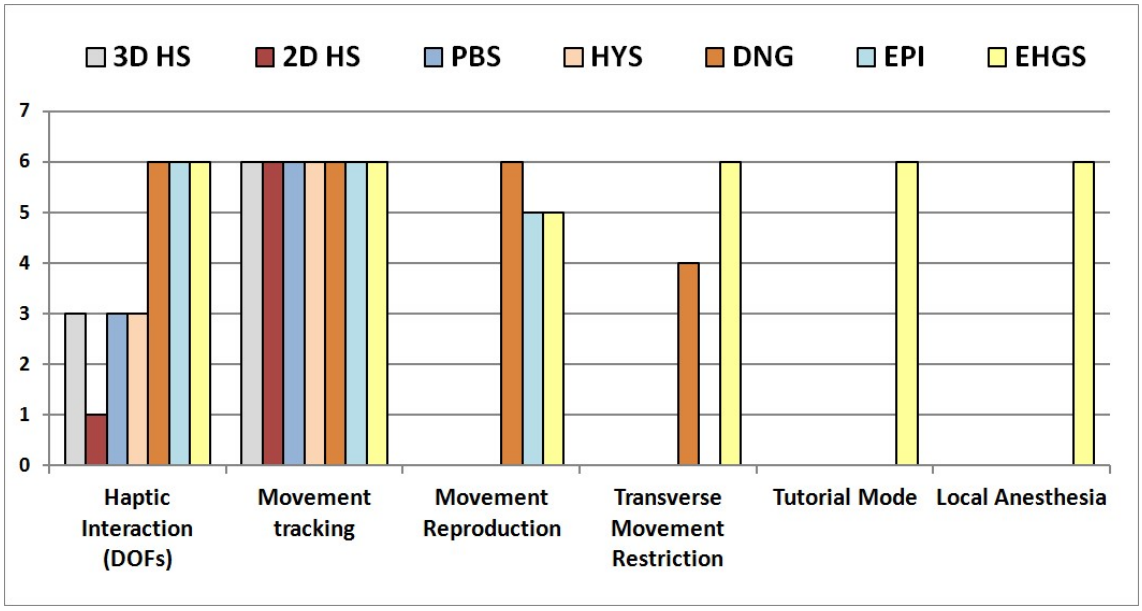

Figure 72. A comparison of interaction-related features available on the simulators.

The haptic device interaction (DOF) feature score corresponds to the total number of degrees of freedom available for the haptic device employed by the simulator. The EHGS, EPI and DNG use haptic devices with 6 DOFs: Geomatic Touch, Phantom Premium and Phantom Desktop. The 2D HS includes a 1 DOF haptic device and the other two simulators are integrated to the Novint Falcon (3 DOF).

The movement tracking feature is associated to the user interactions with the haptic device and their corresponding needle displacement on the visual interface. All simulators visually track user interactions, so the highest score (6) is assigned to them.

The feature of movement reproduction refers to the feature described in Sections 5.2.5 and 6.5, available only in EHGS, EPI and DNG simulators. The DNG has a specific movement reproduction mode called "tunneling guidance", not available on EPI or EHGS, where the haptic device movement becomes solely possible following the movement reproduction path in Dang et al (2001), so a highest score (6) is attained to DNG. Both EPI and EHGS present the movement reproduction feature, but not the "tunneling guidance", so a score of (5) is assigned to them.

The feature of transverse movement restriction on needle insertion is detailed in Sections 5.2.3 and 6.3. It is completely implemented in EHGS, so the highest possible

score is assigned (6). The DNG only restricts the haptic device movement when the "tunneling guidance" feature is activated for movement reproduction, so this feature use becomes limited, and a score of (4) is assigned.

The tutorial mode (Figure 5A in Appendix) and the local anesthesia simulation before the needle insertion (Figure 68 in Section 6.9) are only presented by the EHGS, so a score of (6) is assigned, while the other simulators do not present any of these features, having a score of zero (0).

A comparison of tissue-related features on simulators (Figure 73) includes the tissues display (n), dimensioning (n), configuration and pressure (LOR).

The score assigned to the tissues display (n) feature corresponds to the total number of tissues displayed on the visual interface of simulators. The 3DHS displays only two: the skin (body) and the bone (spine). The 2D HS interface shows four tissue layers: skin, fat, muscle and bone. The PBS only displays the skin (body). The HYS visually represent the skin, fat, muscle and liver tissues, totalizing (4). The DNG visually shows four (4) tissues on the screen and the EPI only shows the vertebrae on the interface, totalizing (1). The EHGS displays eight (8) lumbar epidural layers: skin, subcutaneous fat, muscle, interspinous ligament, ligamentum flavum, epidural space, dura-mater and bone.

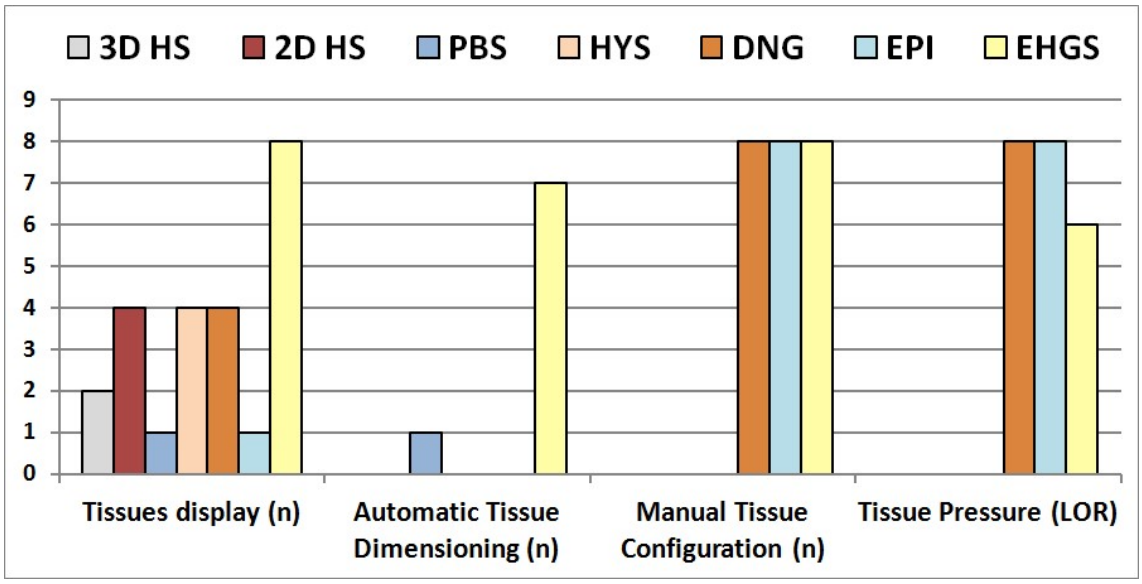

Figure 73. A comparison of tissue-related features available on the simulators.

The automatic tissue dimensioning feature relates to the dynamic adjustment of tissue thickness on the virtual patient body based on patient input parameters, as in

Section 6.2. Its score represents the number of tissues adjustable from input parameters for the patient: height, weight and age. The PBS is only capable to resize the skin tissue (1), represented by the patient body, while the EHGS adjusts the thickness of seven (7) epidural tissue layers (skin, fat, muscle, ISL, ligamentum flavum, epidural space and dura-mater) based on the calculation of a thickness scale factor (Section 4.1). The other simulators do not automatically resize any tissue layers based on input parameters.

The manual tissue configuration feature refers to the possibility of a real-time adjustment of the biomechanical properties values for the epidural tissues on the simulator, by the use of the visual interface, as detailed in Sections 5.1.3 and 6.8 and by the adjustment of property sliders (Figure 55-left). The DNG, EPI and EHGS present an interface for the manual adjustment for all the epidural tissues, so their assigned score is (8). The other simulators do not present this feature, so their assigned score is (0).

The feature of tissue pressure measurement (LOR) is associated to the measuring of pressure values for the epidural tissues, as described in Sections 5.2.6 and 6.4, critical for the simulation of epidural space detection by the use of LOR technique. This feature is available for the DNG, EPI and the EHGS simulators. Both the DNG and EPI include a physical syringe for the tissue pressure measurings, so their assigned score is the highest (8). The EHGS offers a automatic saline pressure values generation for all tissues, but does not include a syringe attached, so the pressure measuring is simulated by the pressing of haptic device buttons, so a lower score is assigned (6). The other simulators do not present this feature.

The needle-related features available on the simulators are grouped and compared in Figure 74. The comparison includes features concerning the information display of needle depth, position (n axis), orientation and angles. The freedom of needle insertion point, the data recording (n axis) and force mapping (n axis) features are also considered.

The needle depth information (Section 5.2.2) is available on all simulators, so the highest score (3) is assigned to them. The needle position information is only displayed on 2DHS and EHGS interfaces. The 2DHS displays two (2) axis (x and y) information, while EHGS shows the needle position on the three (3) axis (x, y and z).

The needle orientation information feature tracks its current pointing direction, and is available for the DNG, EPI and EHGS simulators, so the highest score (3) is associated to them. The other simulators do not present this feature and score of (0) is assigned to them.

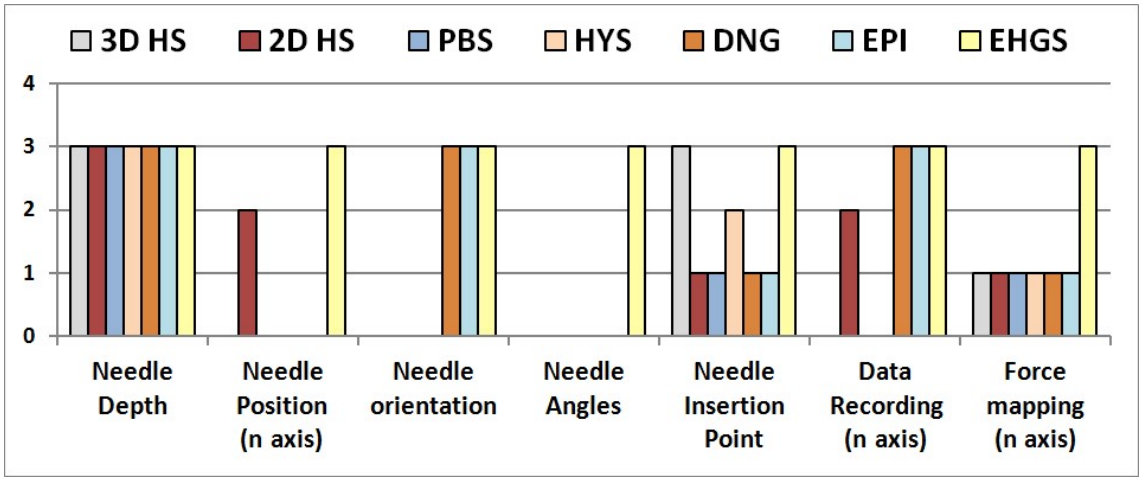

Figure 74. A comparison of needle-related features available on the simulators.

The needle angles feature, described in Sections 5.2.4 and 6.6, calculates its horizontal and vertical inclinations, both displayed on the interface, being helpful on the epidural needle insertion procedure. This information is only available for the EHGS, and it received the highest score (3). The other simulators available on the comparison do not present this feature so their assigned score is (0).

The data recording capability, detailed in Section 5.1.2, is available on the 2D HS, DNG, EPI and EHGS simulators. The DNG, EPI and EHGS simulators store the needle position information from three (3) axes (x, y and z), while 2D HS records in two (2) axes (x and y). Other simulators do not include this feature, so their score is (0).

The force mapping feature score relates to the total number of axial forces displayed by the simulators. All other investigated simulators, with exception of the EHGS, only display the forces applied on a single axis (z), while the EHGS maps and shows the forces applied on three (3) axes (x, y and z) (Section 6.1).

An evaluation of the EHGS implementation is done by its presentation to senior anestesysts. They consider the implementation helpful for epidural nerve block procedure practice and indicate, as necessary improvements: the use of plastic structures to represent the tuohy needle support wings, for a better holding, placement and positioning of the needle; and a syringe with a plunger, for pressure measuring along needle insertion. These plastic structures could be attached to the haptic device arm, and produced with the help of a 3D printer. They also suggested the inclusion of a 2D view for the epidural tissues on the interface, to facilitate the tracking of needle penetration and the visualization of the user progress along the procedure.

7. CONCLUSIONS

This work develops and integrates computational and mechanical models with relevant features and functionalities into an epidural nerve block simulator that incorporates the haptic device feedback and the use of game elements to improve the practice of epidural procedures, thus supporting the reduction of the epidural failure rate. The relevant tissues involved in this medical procedure were incorporated into the experience, associated with their biomechanical properties, to reflect and simulate the sensations from the needle penetration.

Tissues thickness dimensioning based on parturient experiment data becomes now possible: the designed model adjusts the thickness of all relevant epidural tissues at the start of each simulation, based on the configuration of a virtual patient by height, weight and age values. This provides more realistic scenarios for needle insertions providing different challenges for the medical team. Investigated works of simulators have not employed this feature for internal epidural tissues.

The epidural tissues are tied to their biomechanical properties values, adjustable in real time. These properties influence the haptic device behaviour and the user sensations in a simulated environment. This feature facilitates the calibration of values for these properties by the medical team, based on their own tactile expertise. It helps to improve the simulator realism for needle insertions on epidural nerve block procedures. The saline pressure, a critical element for the success of LOR technique, is also generated and tracked by the simulator, a feature not observed on previous works.

Developed force models consider and represent the axial forces and needle displacement on the patient body tissues from skin to the epidural space and bone. Needle tip type and diameter are also considered. Those parameters were not included in previous works. The curves plotted for the force model are similar to the epidural experiments data from Holton and Hiemenz (2001), confirming the precision of the designed force model. The force model accuracy is relevant, once real epidural procedure experiences provide limited or no visual real-time feedback, and the physicians must rely on the tactile feedback for their orientation on needle insertions (GEROVICH et al, 2004).

Force feedback mapping gains a three-dimensional aspect: the three axis (x, y, z) resulting forces are now tracked and graphed. They demonstrate the influence of the tissue properties over the total resulting forces upon needle depth advancement. Better

and more precise comparisons among results of different simulators can now be made. Previous works only considered a single axis (z) on their experiment data and results.

Needle movement restrictions to transverse movements are implemented inside the virtual patient body. Calculation of vertical and horizontal needle inclination angles and visual feedback on interface are included. These are relevant for the success rate of the epidural procedure practices and a better simulation of reality.

Tracking of the movements executed by the players allows the use of accumulated experience as a training background for new students. It opens possibilities for asynchronous or posterior evaluations of trainee performances in the simulator environment.

The investigated gaming works have shown that their use is an interesting resource to keep medical students practicing for a longer time. Many trials of epidural nerve block procedure are normally required by trainees, to improve the skill and proficiency needed to interact with real patients. Most of the Brazilian hospitals do not have simulators for practicing such a procedure, using directly real patients for it.

The gamification of the simulator subdivides the main steps required to perform a successful epidural nerve block into smaller and easier achievable challenges, tied to score awards and a visual conclusion feedback. The user's progress and practice results are continuously tracked by the simulator. These elements can act as motivators for the practice and improvement, aiming at the perfection of execution. Previous works on gamification applied to the training of epidural nerve block procedures were not found in the literature.

Three-dimensional representation of patient body and its tissue layers supports a mental visualization of the patient body anatomy by the physician, a critical step to succeed in a blind procedure as the epidural nerve block (BERNARDS, 2001).

Senior anesthetists considered the simulator presented by this work encouraging for the reduction of failure rate on epidural nerve block procedures and their practice. They indicated the need for: plastic wings, to represent the Tuohy needle support; a syringe with a plunger, for the pressure measuring; the inclusion of a 2D view on the interface for the epidural tissues, to facilitate the needle tracking; and the use of sound effects to warn the user after the occurrence of a dura-mater perforation.

7.1. FUTURE WORKS

This work developed models and implemented a simulator to support the reduction of the failure rate of epidural procedures. Some improvements can be added to enhance, validate and evaluate its use for the epidural practice.

Future works may include: the conduction of tests at the hospitals with the simulator and the medical team, to better validate and evaluate the current implementation and the designed models; an assessment of the effectiveness of the used game elements, with a balancing of the score points associated with the achievements, based on the difficulty of challenges and the feedback from the medical staff; the configuration of difficulty levels on the simulator (ex. patient spine flexion); inclusion of options for enabling or disabling the visual feedbacks avaliable to the user (ex. needle depth, visualization of the epidural tissues or game elements); the inclusion of a 2D view of tissues penetration (as suggested by the anesthetists); the use of a database to record the user's performance; the inclusion of a practice module for the palpation of back and column to locate the best spot for the needle insertion; the simulation of false positives in the LOR; the use of hospital environment sounds and patient speech to improve feedback; the enhancement of the needle forces model based on the continuum mechanic to consider all the epidural tissues; the validation of developed equations with material constants of in-vivo tissues from elastography experiments; a comparison of the developed equations with real epidural procedure in patients; the development of a needle prototype including strain gauges and sensible material to measure the resistance of the epidural tissues; an enhancement of the visual interface to better organize and display the relevant information; and, finally, the use of 3D models from patient CTs and MRI exams.

The simulator tests should divide the medical team into two or more experimental groups. This would help to map the simulator influence over learning and practice, and to evaluate the effectiveness of: game elements use, haptic device use, user advancement speed and each other implemented feature, for the reduction of epidural human related failures.

The implemented simulator could also be adjusted to expand its uses and take advantage of the already existing integration to the haptic device, to include the practice of other medical procedures related to the needle use, such as blood, tissues and bone marrow extractions, and the training of minimally invasive surgeries.

REFERENCES

ABOLHASSANI, N.; PATEL, R.; MOALLEM, M., Needle Insertion into Soft Tissue: A Survey. Medical Engineering & Physics 29 (2007) 413-431.

ANESTHESIOLOGY, A518. Study on Force Transducers (2002). http://www.asaabstracts.com/strands/asaabstracts/abstract.htm;sessionid=8782CDD7FAC9DE7799479FBCB837286?year=2002& index=7&absnum=1258 (accessed 15.1.15).

AGENCIACULTIVA, Lumbar Region Definition Anatomy, USA. http://www.agenciacultiva.com/lumbar-region-definition-anatomy/ (2016) (accessed 20.01.17).

AKASUM, G. F.; RAMDHANIA, L. N.; WIDYOTRIATMO, A., Integration of Soft Tissue Model and Open Haptic Device for Medical Training Simulator. In Journal of Physics: Conference Series 694.1 (2016).

BASSIAKOU, E., VALSAMIDIS, D., LOUKERI, A., KARATHANOS, A., The Distance from The Skin to The Epidural and Subarachnoid Spaces in Parturients Scheduled for Caesarean Section, Minerva Anestesiologica 77 (2011) 154-159.

BATKINGNZ, Unlock All Achievements in Minecraft XBOX360 Edition, VisiHow, USA. http://visihow.com/Unlock_All_Achievements_in_Minecraft_XBOX360_Edition (2017) (accessed 20.01.17).

BERNARDS, C. M., Epidural and Spinal Anesthesia, Clinical Anesthesia 5 (2001).

BOSSA STUDIOS, Surgeon Simulator, Wikipedia. https://en.wikipedia.org/wiki/Surgeon_Simulator_2013 (2013) (accessed 31.10.16).

BRAZIL, A. L. (a), Interface Options Overview - An Epidural Nerve Block Simulator, YouTube. https://www.youtube.com/watch?v=6mT1r5ouMO4 (2016) (accessed 20.12.16).

BRAZIL, A. L. (b), Syringe Use and Challenges - An Epidural Nerve Block Simulator, YouTube. https://www.youtube.com/watch?v=IVlRF9yuEJ0 (2016) (accessed 20.12.16).

BRAZIL, A. L. (c), Needle Insertion in Tissues - An Epidural Nerve Block Simulator, YouTube.https://www.youtube.com/watch?v=0OArwjJFP7U (2016) (accessed 20.12.16).

BRAZIL, A. L. (d), Force Details and Saline Pressure - An Epidural Nerve Block Simulator, YouTube. https://www.youtube.com/watch?v=mXOurEMrqi (2016) (accessed 20.12.16).

BRAZIL, A. L. (e), Movement Tracking and Reproduction - An Epidural Nerve Block Simulator. YouTube. https://www.youtube.com/watch?v=O_ZmZlkASuk (2016) (accessed 20.12.16).

BRAZIL, A. L. (f), Needle Horizontal and Vertical Angles - An Epidural Nerve Block Simulator, YouTube. https://www.youtube.com/watch?v=uAIKaZ5p1J4 (2016) (accessed 20.12.16).

BRAZIL, A. L. (g), Tissue Properties - An Epidural Nerve Block Simulator, YouTube, https://www.youtube.com/watch?v=NUXcgFU30_o (2016) (accessed 20.12.16).

BRAZIL, A. L., CONCI, A.; CLUA, E.; BITTENCOURT,L. K.; BARUQUE, L. B., A Virtual Environment for Breast Exams Practice with Haptics and Gamification, In: 5th

IEEE International Conference on Serious Games and Applications for Health - SEGAH 5 (2017).

BRAZIL, A. L.; CONCI, A.; RAMOS, R. R.; RODRIGUEZ-HERNANDEZ, N.; BITTENCOURT, L. K.; CLUA, E., Force Modeling and Gamification for Epidurial Anesthesia Training, In: 4th IEEE International Conference on Serious Games and Applications for Health - SEGAH 4 (2016) 110-118.

BRETT, P. N.; HARRISON, A. J.; THOMAS, T., Schemes for The Identification of Tissue Types and Boundaries at The Tool Point for Surgical Needles, IEEE Transactions on Information Technology in Biomedicine 4 (2000) 30-36.

BRUMMETT, C. M.; WILLIAMS, B. S.; HURLEY, R. W.; ERDEK, M. A., A Prospective, Observational Study of the Relationship Between Body Mass Index and Depth of The Epidural Space During Lumbar Transforaminal Epidural Steroid Injection. Regional Anesthesia and Pain Medicine 34.2 (2009) 100.

CHAWLA, J., RAGHAVENDRA, M., Epidural Nerve Block - Indications, Medscape, USA. http://emedicine.medscape.com/article/149646-overview#a2 (2015) (accessed on 20.01.17).

CHOI, J. Y.; CHUNG, J. H.; PARK, Y. J.; JUNG, G. Y.; YOON,T. W.; KIM, Y. J.; NAM, S. H., Extranodal Marginal Zone B-cell Lymphoma of Mucosa-Associated Tissue Type Involving The Dura, Cancer Research and Treatment: Official Journal of Korean Cancer Association 48.2 (2016) 859.

CLINKSCALES, C. P.; GREENFIELD, M. L. V. H.; VANARASE, M.; POLLEY, L. S., An Observational Study of The Relationship Between Lumbar Epidural Space Depth and Body Mass Index in Michigan Parturients, International Journal of Obstetric Anesthesia 16 (2007) 323–327.

COLES, T. R., MEGLAN, D., JOHN, N. W., The Role of Haptics in Medical Training Simulators: A Survey of The State of The Art, IEEE Transactions on haptics 4.1 (2011) 51-66.

CONCI, A.; BRAZIL, A. L.; BITTENCOURT,L. K.; MACHENRY, T.; PÉREZ, M. G.; HERNÁNDEZ, N. J. R.; RODRIGUEZ-RAMOS, R., Um Modelo para Representação das Respostas dos Tecidos Durante o Procedimento de Aplicação da Anestesia Epidural para Utilização em Ambiente de Realidade Virtual Associado ao Uso de Dispositivos Hápticos, Congreso Iberoamericano de Ingeniería Mecánica - CIBIM XII (2015) 164-171.

CONNOR, M. J.; NAWAZ, S.; PRASAD, V.; MAHIR, S.; RATTAN, R.; BERNARD, J.; ADDS, P. J., The Posterior Epidural Ligaments: A Cadaveric and Histological Investigation in The Lumbar Region. ISRN anatomy (2013).

CORRIERO, N.; DI BITONTO, P.; ROSELLI, T.; ROSSANO, V.; PESARE. E., Simulations of Clinical Cases for Learning in E-Health. International Journal of Information and Education Technology 4.4 (2014) 378.

CRAWFORD, C., The Art of Computer Game Design, Washington State University, Vancouver, 1984.

CYBERGLOVE SYSTEMS, The Cybergrasp, USA. http://www.cyberglovesystems. com/cybergrasp/ (2016) (accessed 20.12.16).

DANBRIDGE, T. C., Ceremony as an Integration of Work and Play. Organization Studies 7.2 (1986) 159-170.

DANG, T.; ANNASWAMY, T. M.; SRINIVASAN, M. A., Development and Evaluation of an Epidural Injection Simulator with Force Feedback for Medical Training. Studies in Health Technology and Informatics (2001) 97-102.

DETERDING, S., Gamification: Designing for Motivation, Interactions 19 (2012) 14-17.

DIGITAL HUMAN RESEARCH CENTER, Subscapular Skinfold Measurements, AIST, Japan. http://www.dh.aist.go.jp/research/centered/anthropometry/H_skinfold.html.en (2017) (accessed 20.01.17).

DUBEY, V. N.; VAUGHAN, N.; WEE, M. Y.; ISAACS, R., Biomedical Engineering in Epidural Anaesthesia Research, in: C. Constantinides, Practical Applications on Biomedical Engineering (2012) 387-410.

DREIFALDT, U.; KULCSAR, Z.; GALLAGHER, P., Exploring Haptics as a Tool to Improve Training of Medical Doctors in The Procedure of Spinal Anaesthetics. Eurohaptics 2006 (2006).

EFRONT, Badges - Gamification eFront Manual, USA. https://docs.efrontlearning.com/gamification (2017) (accessed 20.01.17).

FITZ-WALTER, Z.; TJONDRONEGORO, D.; WYETH, P., Orientation Passport: Using Gamification to Engage University Students, In Proceedings of The 23rd Australian Computer-Human Interaction Conference, ACM (2011) 122-125.

FARZAN, R., DIMICCO, J. M.; MILLEN, D. R.; BROWNHOLTZ, B.; GEYER,W.; DUGAN,C., When The Experiment is Over: Deploying an Incentive System to All The Users, Symposium on Persuasive Technology (2008).

FARZAN, R.; DIMICCO, J. M.; MILLEN, D. R.; DUGAN, C.; GEYER, W.; BROWNHOLTZ, E. A., Results from Deploying a Participation Incentive Mechanism Within The Enterprise, In: Proceedings of the SIGCHI Conference on Human Factors in Computing Systems, ACM (2008) 563-572.

FERRARA, J., Games for Persuasion Argumentation, Procedurality, and The Lie of Gamification, Games and Culture 8.4 (2013) 289-304.

FRAZETTO, J., Epidural Simulator - Haptics, Robotics and Prototyping in Medicine, Slideshare,USA. http://pt.slideshare.net/JoanFrazzetto/haptics-robotics-and-prototyping-in-medicine-1 (2011) (accessed on 20.01.2017).

GEROVICH, O.; MARAYONG, P.; OKAMURA, A. M., The Effect of Visual and Haptic Feedback on Computer-Assisted Needle Insertion. Computer Aided Surgery 9 (2004) 243-249.

GRANTCHAROV, T. P.; REZNIK, R. K., Teaching Rounds: Teaching Procedural Skills. British Medical Journal 7653.336 (2008) 1129-1131.

GRAU, T.; LEIPOLD, R. W.; CONRADI, R.; MARTIN, E., Ultrasound Control for Presumed Difficult Epidural Puncture, Acta Anaesthesiologica Scandinavica 45 (2001) 766-771.

GROENENDIJK, F., Global Videogame Sales Surpass Movie Industry in 2008!, Video Games Blogger. http://www.videogamesblogger.com/2008/04/09/global-videogame-sales-surpass-movie-industry-in-2008.htm (2008) (accessed 15.1.15).

HAKULINEN, L.; AUVINEN, T.; KORHONEN.A., Empirical Study on The Effect of Achievement Badges in TRAKLA2 Online Learning Environment, In: Learning and Teaching in Computing and Engineering - LaTiCE, IEEE (2013) 47-54.

HAMARI, J., Transforming Homo Economicus Into Homo Ludens: A Field Experiment on Gamification in a Utilitarian Peer-to-Peer Trading Service, Electronic Commerce Research and Applications 12 (2013).

HARDAMA (אתר "הרדמה"), Epidural Anesthesia and Analgesia Procedure - Including Placing Epidural Catheter, hardama.com. https://www.youtube.com/watch?v=qXbTEIV3t1o/ (2013) (accessed 16.10.16).

HOLTON, L.; HIEMENZ, L., Force Models for Needle Insertion Created from Measured Needle Puncture Data, Studies in Health Technology and Informatics (2001) 180-186.

HOTSCHEDULES, How Restaurants Can Use Gamification to Drive Sales and Culture - HotSchedules blog, USA, https://www.hotschedules.com/blog/how-restaurants-can-use-gamification-to-drive-sales-and-culture/ (2016) (accessed 20.01.17).

HUOTARI, K.; HAMARI, J., Defining Gamification: a Service Marketing Perspective, In Proceeding of The 16th International Academic MindTrek Conference, ACM (2012) 17-22.

IWATANI, T., The Pac-Man Game, Namco. https://en.wikipedia.org/wiki/Pac-Man (1980) (accessed 31.10.16).

JARRET, K., Syringe 3D Model, Archive.net, USA. http://archive3d.net/?a=download&id=6bad032e (2017) (accessed 20.12.16).

KENDALL FIT KITCHEN, Fat Cells, Wordpress, USA. https://kendallsfitkitchen.files.wordpress.com/2014/02/fat-cells-6.jpg (2014) (accessed on 20.01.17).

KERFOOT, B. P.; KISSANE, N., The Use of Gamification to Boost Residents Engagement in Simulation Training. JAMA Surgery 149.11 (2014) 1208-1209.

KEVINLIMD, Epidural Steroid Injection, Pain Management Doctor, Kevinlimd.com, USA. http://www.kevinlimd.com/treatment/interventional-procedures/epidural-steroid-injection/ (2017) (accessed 20.01.17).

KONRAD, C.; SCHUPFER, G.; WIETLISBACH, M.; GERBER, H., Learning Manual Skills in Anesthesiology: Is There a Recommended Number of Cases for Anesthetic Procedures? Anesthesia & Analgesia 86.3 (1998) 635-639.

KYOTO KAGAKU AMERICA INC., Training Models - Product Hystory, USA, https://www.kkamerica-inc.com/assets/1/7/MainFCKEditorDimension/MW3_Epidural_Anesthesia_Simulator_Photo_1_%281%29.jpg (2017) (accessed 20.01.17).

KWON, D. S., KYUNG, K. U.; KWON, S. M.; RA, J. B.; PARK, H. W.; KANG, H. S.; CLEARY, K. R., Realistic Force Reflection in a Spine Biopsy Simulator. IEEE International Conference on Robotics and Automation (2001) 1358-1363.

LECHNER, T. J. M.; VAN WIJK, M. G. F.; JONGENELIS, A. A. J.; RYBAK, M.; VAN NIEKERK, J.; LANGENBERG, C. J. M., The Use of a Sound-Enabled Device to Measure Pressure During Insertion of an Epidural Catheter in Women in Labour, Anaesthesia 66.7 (2011) 568-573.

LEE, R. A., Technical Development of Common Anesthesiology Techniques; Neuraxial Anesthesia and Laryngoscopy for Endotracheal Intubation. TU Delft, Delft University of Technology, New Zealand (2013).

LIM, M. W.; BURT, G.; RUTTER, S. V., Use of Three-Dimensional Animation for Regional Anaesthesia Teaching: Application to Interscalene Brachial Plexus Blockade, British Journal of Anaesthesia 94 (2005) 372-377.

MACARTHUR, C.; LEWIS, M.; KNOX, E. G., Accidental Dural Puncture in Obstetric Patients and Long Term Symptoms. British Medical Journal 6882.306 (1993) 883-885.

MALONE, T. W., What Makes Things Fun to Learn – A Study of Intrinsically Motivating Computer Games, In: Cognitive and Instructional Science Series - CIS-7. http://cci.mit.edu/malone/tm study 144.pdf (1980). (accessed 18.1.15).

MARCABRAHAM, Gamification - Motivation and Rewards, Wordpress, USA. https:// marcabraham.wordpress.com/2014/03/23/gamification-motivation-and-rewards/ (2014) (accessed 20.01.17).

MAUREL, W., 3D Modeling of The Human Upper Limb Including The Biomechanics of Joints, Muscles and Soft Tissues. PhD thesis, Laboratoire d'Infographie - Ecole Polytechnique Federale de Lausanne (1999).

MAURIN, B.; BARBE, L.; BAYLE, B.; ZANNE, P.; GANGLOFF, J.; DE MATHELIN, M.; FORGIONE, A., In Vivo Study of Forces During Needle Insertions, In: Proceedings of the Medical Robotics, Navigation and Visualisation Scientific Workshop, Ramagen, Germany (2004) 1-8.

MCCALLUM, S., Gamification and Serious Games for Personalized Health, Studies in Health Technoly and Informatics 177 (2012) 85-96.

MCGONICAL, J., Reality is Broken, TED2010 – Technology, Entertainment, Design – Session 6: Invention. http://www.ted.com/talks/jane_mcgonigal_gaming_can_make_ a_better_world.html (2010) (accessed 18.1.15).

MEDISCAN, Epidural Needle with Loss of Resistance Syringe, Alamy Stock Photos, USA. http://www.alamy.com/stock-photo-epidural-needle-with-loss-of-resistance-syringe-497728.html (2017) (accessed 20.01.17).

MIXAMO, Fuse 3D Character Creator. https://www.mixamo.com/fuse (2016) (accessed 31.10.16).

MYCO MEDICAL, Reli Epidural Needle, USA. http://www.mycomedical.com/ product/sterile-reli-epidural-needles-with-detachable-wing-and-metal-stylet-18g-x-2-12-pink-3/ (2017) (accessed 20.01.17).

MUNTEAN. C. I., Raising Engagement in E-Learning Through Gamification, In Proc. 6th International Conference on Virtual Learning ICVL (2011) 323-329.

NAIK, V. N.; DEVITO, I.; HALPERN, S. H., Cusum Analysis Is a Useful Tool to Assess Resident Proficiency at Insertion of Labour Epidurals. Canadian Journal of Anaesthesia 50.7 (2003) 694-698.

OKAMURA, A. M.; SIMONE, M. C.; LEARY, M., Force Modeling for Needle Insertion into Soft Tissue, IEEE Transactions on Biomedical Engineering 51 (2004) 1707-1716.

PEIRIS, R. L.; JANAKA, N.; DE SILVA, D.; NANAYAKKARA, S., SHRUG: Stroke Haptic Rehabilitation Using Gaming, In Proceedings of the 26th Australian Computer-

Human Interaction Conference on Designing Futures: The Future of Design, ACM (2014) 380-383.

PHILIPS LEARNING CONNECTION, Philips Medical Games - Online Learning Center. http://www.theonlinelearningcenter.com/free-online-medical-games.aspx (2016) (accessed 23.10.16).

POULIOT, M. C.; DESPRÉS, J. P.; LEMIEUX, S.; MOORJANI, S.; BOUCHARD, C.; TREMBLAY, A.; LUPIEN, P. J., Waist Circumference and Abdominal Sagittal Diameter: Best Simple Anthropometric Indexes of Abdominal Visceral Adipose Tissue Accumulation and Related Cardiovascular Risk in Men and Women. The American Journal of ardiology 73.7 (1994) 460-468.

POYADE, M.; KARGAS, M; PORTELA, V., *Haptic Plugin for Unity 5.x.,* Digital Design Studio, Glasglow School of Art (2015).

PRO ANABOLIC STEROIDS, Muscle Texture, USA. http://students.expression.edu/dunphypatrick/muscle-texture2-jpg/ (2017) (accessed 20.01.17).

RADOFF, J., Gamification. http://radoff.com/blog/2011/02/16/gamification (2011) (acessed 18.1.15).

RAVI, K. K.; KAUL, T. K.; KATHURIA, S.; GUPTA, S.; KHURANA, S., Distance from Skin to Epidural Space: Correlation with Body Mass Index (BMI). Journal of Anaesthesiology Clinical Pharmacology 27.1 (2011) 39.

RYAN, R.; RIGBY, C. PRZYBYLSKI, A., Motivational Pull of Video Games: a Self-Determination Theory Approach, Motivation and Emotion 30 (2006) 344-360.
WERBACH, K.; HUNTER, D., For The Win: How Game Thinking can Revolutionize your Business, Wharton Digital Press (2012).

SAWYER, B., From Cells to Cell Processors: The Integration of Health and Video Games. Computer Graphics and Applications, IEEE, 28.6 (2008) 83-85.

SCHELL, J., Design Outside the Box, DICE2010 - Digital Innovation, International Conference & Exibition. http://www.youtube.com/watch?v=9NzFCfZMBkU&noredirect=1 (2010) (acessed 15.1.18).

SEAMLESS PIXELS, High Resolution Seamless Textures, Brazil. http://seamless-pixels.blogspot.com.br/p/human-skin-textures.html (2017) (accessed 20.01.17).

SELTZ, B.; FEIL, J.; WOOD, J.; COOK, P.; LANGE, P.; LEPARD, S., Microsoft Flight Simulator X, Microsoft Studios. https://en.wikipedia.org/wiki/Microsoft_Flight_Simulator_X (2006) (accessed 31.10.16).

SENSABLE TECHNOLOGIES INC., OpenHaptics Toolkit Programmer's Guide - version 3.0, Geomagic, Woburn, MA (2009). http://www.geomagic.com/files/4013/4851/4367/OpenHaptics_ProgGuide.pdf (accessed 15.05.14).

SMITH, J.; LAABS, D., Life & Death Game, Wikipedia. https://en.wikipedia.org/wiki/Life_%26_Death (1988) (accessed 31.10.16).

SMITH, S. H., An Introduction to Gamification, HubPages: Business & Society, USA. http://awesome.hubpages.com/hub/Intro-to-Gamification (2011) (accessed 16.12.15).

SOTO-ASTORGA, R. P.; WEST,S.; PUTNIS,S.; HEBDEN, J. C.; DESJARDINS, A. E., Epidural Catheter With Integrated Light Guides for Spectroscopic Tissue Characterization. Biomedical Optics Express 4 (2013) 2619-2628.

TABER, L. A., Nonlinear Theory of Elasticity: Applications in Biomechanics, World Scientific Pub. (2004).

TF3DM, Skeleton 3D Model, tf3dm.com. http://tf3dm.com/3d-model/skeleton-94668.html (2010) (accessed 20.01.17).

THOM, J., MILLEN, D.; DIMICCO, J., Removing Gamification from an Enterprise SNS, In: Proceedings of the ACM 2012 conference on Computer Supported Cooperative Work, ACM (2012) 1067-1070.

TOPEND SPORTS, Subscapular Skinfold, USA. http://www.topendsports.com/testing/skinfold-subscapular.htm (2017) (accessed 20.01.17).

TRAN, D. K.; HOR, W.; KAMANI, A. A.; LESSOWAY, V. A.; ROHLING, R. N., Instrumentation of the Loss-of-Resistance Technique for Epidural Needle Insertion, IEEE Transactions on Biomedical Engineering 56 (2009) 820-827.

UNITY3D, Build Once Deploy Anywhere, Unity3D. https://unity3d.com/unity/multiplatform (2016). (accessed 31.10.16).

VAUGHAN, N.; DUBEY, V. N.; WEE, M. Y.; ISAACS, R., A Review of Epidural Simulators: Where Are We Today?, Medical Engineering & Physics 35 (2013) 1235-1250.

VAUGHAN, N.; DUBEY, V. N.; WEE, M. Y.; ISAACS, R., Parametric Model of Human Body Shape and Ligaments for Patient-Specific Epidural Simulation, Artificial Intelligence in Medicine 62 (2014) 129-140.

VIDEOGAMES BRASIL, vgBR Testa o Simulador do DETRAN na Campus Party 2013, vgBR, Brasil. https://www.youtube.com/watch?v=zCY3060PUzM (2013) (accessed 20.01.17).

VIRTUAL REALITY SOCIETY, The Novint Falcon Haptic System, United Kingdom. http://www.vrs.org.uk/virtual-reality-gear/haptic/novint-falcon.html (2016) (accessed 31.10.16).

VOGT MEDICAL, Epidural Needles, Germany. http://www.vogt-medical.com/en/products/regional-anaesthesia-systems/epidural-needles/ (2017) (accessed 20.01.17).

WATTERSON, L. M.; HYDE, S.; BAJENOV, S.; KENEDY, S. E., The Training Environment of Junior Anaesthetic Registrars Learning Epidural Labour Analgesia in Australian Teaching Hospitals. Anaesthesia and Intensive Care 35.1 (2007) 38.

WEDENSBERGPENG, Ligamentum Flavum, Mast Cell, Wordpress, USA. https://wedensbergpeng.files.wordpress.com/2012/05/h2-12-3.jpg (2012) (accessed 20.01.17).

WILSON, M. J. A., Epidural Endeavour and The Pressure Principle, Anaesthesia 62 (2007) 319-322.

APPENDIX A. THE EVOLUTION OF THE DEVELOPED SIMULATOR

Early simulator versions were developed in a Philco Notebook model PHN 15008, with a T6500 Intel Core 2 Duo processor, 4GB of DDR2 667Mhz ram memory, a 320GB hard disk and an ATI HD4650 Mobility Radeon with 512mb GDDR3 Videoboard, having a MMOPro Memory Card Interface slot which allowed the inclusion of a Firewire adapter for haptic device communication. Most recent versions used the computer system specified on the Chapter 4.

A1.1. VERSION 1

The 3D woman body model for the first implemented version was acquired freely on TurboSquid website (www.turbosquid.com). A real skin texture was applied on it. For the other simulator versions, the body models were generated with the help of the Fuse 3D software (MIXAMO, 2016), a tool for character creation usable at applications and games.

This first version of the simulator (Figures A1 and A2) was developed for testing movement restrictions and interaction with a 3D woman body bt using haptic force feedback of the Novint Falcon device (shown in Figure 2 - left) with 3 DOFs for movements and interactions inside the 3D virtual environment. In this version, the user was capable to effectively move the virtual woman body as a rigid body by using the haptic device and sensing the resistance of this acting as a reaction force feedback. This employs a tridimensional scene created in Unity3D engine (UNITY3D, 2016).

The simulator interface is composed by several scripts, coded in the C# language, and can be adjusted and applied to 3D objects in the scene, so these objects can be targets of a haptic device interactions, being influenced by the action of physical movement and displacement forces. Figure A1 (right) demonstrates an example of a 3D scene constructed for this purpose, containing a partial 3D model of an upper woman body as an interaction object.

One of the most important scripts to be associated to the scene objects is the Falcon rigid body script. The script presents several configuration parameters (variables) that adjust the experience of haptic interaction with the object. These parameters can be visualized in Figure A2. One important parameter is the physical object mass (the “Mass” parameter), which will regulate the haptic reaction force to be

employed on Falcon haptic device upon user interaction with the object inside the simulation environment.

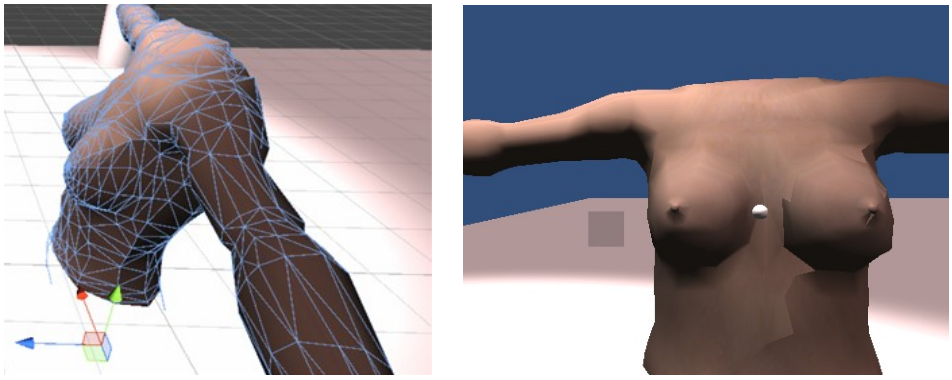

Figure A1. First version of developed simulator: woman 3D model (left), in execution, with a front view of the 3D scene (right).

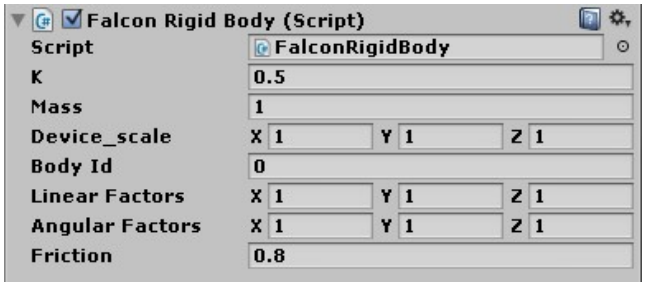

Figure A2. Configuration Parameters of Novint Falcon haptic device script for 3D object interaction

The first simulator version incorporates a special object inside the scene scene from Unity3D (2016) engine, named “Falcon”. This object represents the current location and positioning of the Novint Falcon haptic device inside the 3D interaction environment. This object is classified as a “prefab”, which means it is customizable by the developer and needs to be incorporated to the scene in order to allow interaction with other objects presented in the scene through the use of a haptic device. Figure A1 (right) evidences this object (a small white sphere), which represents the current position of the haptic device in its x, y and z axis inside the scene. Object interaction scripts can be associated to any 3D object inside the 3D scene, offering a wide range of interaction possibilities in the tridimensional environment by the use of a haptic device.

The initial experiment, implemented in the first simulator version, was intended to use the haptic device to react as physical resistance to user interaction with the 3D object, simulating a situation where a heavy object would being pushed in the real

world.

A1.2 . VERSION 2

The second version of the simulator (Figure A3) was developed using the Geomagic Touch haptic device (Figure 2), which is more expensive but offers 6 DOFs, where the first 3 DOFs are provided by the x, y and z axis movement by the device arm and also offering 3 additional degrees of freedom by allowing rotation movements with its outermost arm part.

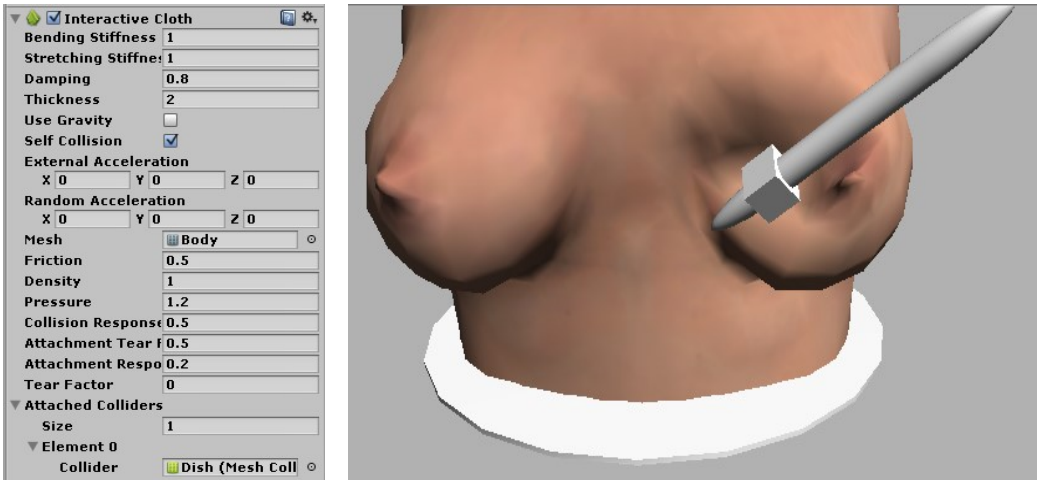

Figure A3. Interactive Cloth resource parameters from Unity3D inspector (left) and female 3D body tissue deformation with haptic interaction (right) (BRAZIL et al, 2017).

This second version of the simulator was intended to test the force feedback provided by the haptic device use. This second version uses a better modeled 3D woman body, composed of a higher number of polygons, generated with the help of the Fuse 3D software (MIXAMO, 2016), that facilitates the generation 3D human body models. This woman model has a flexible tissue, allowing interaction by partial simulation of the sensation of palpation on the outer skin, which is also used as a first step for locating the right spot to insert the needle in an epidural anesthesia medical procedure. Figure A3 illustrates the results obtained with this second version.

The main improvement for this simulator version was the implementation of flexible tissue, obtained by the use of a Unity3D (2016) engine component, called interactive cloth. This resource is very interesting, allowing the configuration of several interaction parameters, like friction, density pressure and collision response, to enable more realistic tissue reaction through the interactions. After configuring the parameters

of this resource accordingly (Figure A3 left), it is possible to visually perceive the reaction to the Geomagic Touch haptic device interaction, together with its programmed feedback, as visualized in Figure A3 (right).

A1.3. VERSION 3

The third version of the simulator uses the Geomagic Touch haptic device, and additionally allows interaction with the skin tissue of the body model, by trying to simulate sensations of needle penetration inside the skin through implementation of haptic feedback forces. A spine 3D model was incorporated into body for inclusion of resistance forces when interacting with bones. This first 3D model of the spine was obtained by editing a complete skeleton model and removing its other bone parts. The current level of implementation already provides a constant force of 2.0 Newtons as a haptic feedback, when interacting with the skin tissue, which can be sensed as a resisting reaction force soon after the haptic pen extremity (modeling the needle tip) penetrates thorugh the skin. Figure A4 displays the current scene of this developed version on the Unity 3D engine, with its tridimensional objects.

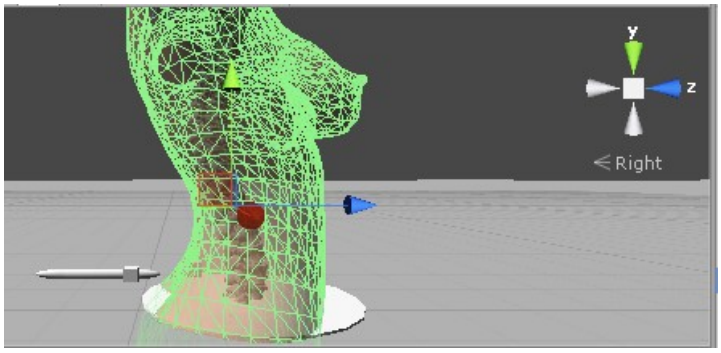

Figure A4. Version 3 of simulator, with spine model and constant haptic device forces (CONCI et al, 2015).

The haptic force feedback was coded by a C# script working on collision events between the needle and the woman body skin. A boolean variable controls if the needle is inside the body skin or not, while a float parameter sets a maximum value for haptic force feedback for the haptic device. The game object inside the scene in Figure A4 corresponds to the outer woman body trunk, including the body skin. When the needle becomes located inside this object, the script calculates a haptic force feedback to be exerted on the z axis, with an intensity of 2.0 Newtons, based on the value contained on

the float parameter. This haptic feedback is executed by the haptic device by the use of a SetForce method, programmed to call the API functions from Sensable Technologies Inc. (2009).

A1.4. VERSION 4

The fourth version of the simulator (shown in Figure A5) incorporated a tutorial for L3 and L4 vertebrae identification based on points represented by small purple spheres added to the spine 3D model. The aim of this tutorial is enable the player to scaffold and understand the haptic forces involved in the simulator environment. In this fourth version, the player was challenged to navigate through the virtual simulator and virtually "touch" the vertebrae points by moving a needle inside a patient body, with the use of the haptic device and some force feedback, after the user reaches the skin of the patient. The force applied to the haptic device was constant (2.0 N) and directed outwards the patient back, doing a sensation of "pushing" the needle out of the body, since there is not yet a force model use for this version. This version also incorporated audio feedback to indicate when an objective was achieved (vertebra touched with haptic device) and displayed a global achievement score, updated each time an objective was concluded in the simulator. The rewards are 100 points for each vertebra identified in the tutorial, totalizing 200 points in the player score.

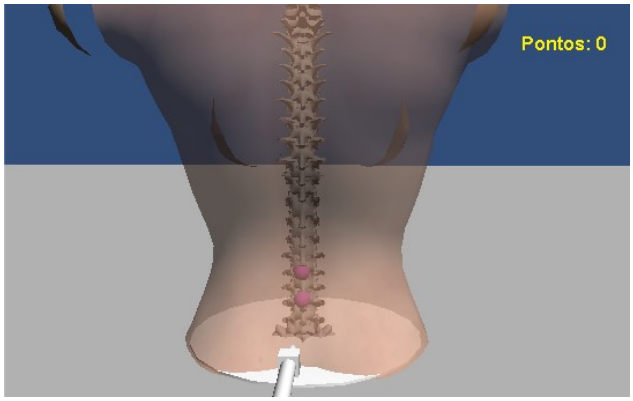

Figure A5. Version 4 of the simulator: L3 and L4 vertebrae plus audio and achievement score feedback (CONCI et al, 2015; BRAZIL et al, 2016).

A1.5. VERSION 5

The fifth version of the simulator was intended to test and simulate tissue deformation along the body. This version allowed the player to deform the virtual patient body by simulating a deformation effect upon clicking with the mouse button

over a surface area. An updated subversion (5b) included a needle to test body surface deformation by “touching” the needle in Figure 69 (right) shows the effect.

A1.6. VERSION 6

The sixth version of the simulator includes the calculations of resulting force, based on the proposed force model presented in Section 4.2. This implementation enables to see, in real-time, the resulting force as well as its components (i.e. stiffness, cutting and friction) and the distance from the needle tip to the surface contact point. Such a distance is necessary for some calculations and acts as an indicator of the length of the needle inside the tissue (after puncturing). Figure 63 shows the output interface with its force values. The sphere 3D object represents the body tissue and was used to facilitate the initial calculations for this developed version, being replaced by the woman body afterwards. For this version was necessary to develop additional classes to control the tissue, the simulator interface and the needle.

The script of tissue class contains several tissue properties, like stiffness, dynamic friction and damping coefficients. This class was directly associated to the 3D model object representing the body part (e.g. skin, in this case). This implementation assumes the following initial values for the skin tissue properties: 0.5 for stiffness, 0.2 for dynamic friction, 0.3 for damping and 0.27 for cutting through resistance constant.

Interface class is developed to allow the persistence and feedback for interaction of the user and the simulator. It was composed by visual outputs (labels) associated to the current force values shown on the game screen. The Needle class was implemented on a previous version of the simulator, and has been improved with collision events, to map the contact between the needle and each tissue associated to the 3D model from virtual patient. This class script also calculates the distance from the needle tip to the surface contact point, that is useful for force calculations defined in Section 4.2.

A1.7. VERSION 7

The seventh version of the simulator had improvements over version six related to the calculations for needle bending and deflection forces, based on the equations proposed in Section 4.3. This version was able to show, in real time, the resulting force as well its component forces calculated and the distance from the needle tip to the surface contact point, they are necessary for some computations and acting as an indicator of the length of the needle remaining inside the tissue (after puncturing).

Figure 63 shows the output interface and updated force values. In this version two new variables for force calculations were included: needle tip type (coned, beveled or triangular) and the needle diameter (mm).

A1.8. VERSION 8

The eighth version of the simulator was directed to calculate the resulting forces based on experiment data from needle insertions on bovine livers available in Okamura et al (2004). This version enables showing, in real time, the resulting force as well its component forces and the distance from the needle tip to the surface contact point. It is necessary for some calculation of the needle length inside the tissue (after puncturing). Figure 63 shows the output interface with its force values. For this version was necessary to improve the Needle class, adding the "Okamura" calculation method, as well as modifying the Tissue class, adding the bovine liver tissue parameters, based in Okamura et al (2004) experiment data. Some conversions on the properties values were necessary, in order to allow the calculations. A scale variable was also added to allow more precise simulation of needle depth during needle insertion calculations.

A1.9. VERSION 9

The ninth version of the simulator was dedicated to generate and plot relations of force x displacement for the resulting force and its components (stiffness, friction and cutting forces). The calculations were based on data from experiments using bovine livers in Okamura et al (2004), where the values used are listed on Table A1 and the results displayed in Figure 61 (right).

Table A1. Values used for the implemented simulation (OKAMURA et al, 2004).

Parameter (units)	Liver #1	Liver #2	Experiments with both tissues	Simulation (Model)
a1 (N/mm)	0.0480	0.0020	Tissues 1 and 2	0.0480
a2 (N/mm^2)	0.0052	0.0023	Tissues 1 and 2	0.0052
Force required to puncture tissue ***(N)***	2.600	1.400	2.304 (average) + 0.8286 (standard deviation)	2.241
z = Needle Displacement ***(mm)***	18.0000	9.0000	16.6514 (average) + 3.5470 (standard deviation)	16.6514
Resulting Force ***(N)***	1.0000	0.2000	0.6579 (average) + 0.5638 (standard deviation)	1.0472

The implemented model considered the following parameters: the needle penetration velocity of 1mm/s and (9) for stiffness force (S_f) calculations.

$$S_f = a_1 z + a_2 z^2 \quad (1)$$

For the friction force (F_f), was used:

$$F_f = z\,(SF_t + D_t.\Delta z.\Delta t) \quad (2)$$

where SF_t is the static friction from tissue, D_t is the tissue damping coefficient, and Δz is the relative needle depth change (current z - previous z), that multiplied by Δt (time) results in the speed of 1mm/s.

For tissue static friction the average value of 6.23 N/m was used (average listed value of 10.57 minus 4.34 value for standard deviation) in Okamura et al (2004). For tissue damping coefficient of 212.31 N/m^2 (average value reported). For cutting force, an average constant value of 0.94N was used.

A1.10. VERSION 10

The version 10 of the simulator (Figure A6) includes force modeling calculations based on experiment data from Holton and Hiemenz (2001), incorporating skin and subcutaneous fat tissues and the display of stiffness, cutting and friction forces. An improvement on the Needle class was necessary, by adding the Holton calculation method, as well as modifying the Tissue class, adding the skin and subcutaneous tissues parameters, based on experiment data from Holton and Hiemenz (2001). The main shape of body was also adjusted to a cylinder based shape in which one of the dimensions, representing its thickness was reduced to a quarter of its value. Inside this body shape was added another one, representing the subcutaneous fat tissue. A transparency effect also was added upon needle collision with the body shape, as can be seen in Figure A6.

In order to verify the response to the simulation accuracy and allow comparison of its results with the data reported in Holton and Hiemenz (2001), the resulting forces were recorded and plotted as a complete graphic curve in a force x needle depth graph, as shown in Figure A7. This graph only shows the forces actuating over the skin and subcutaneous fat tissues. The other tissues were not incorporated in the following versions.

Figure A6. Version 10 of the simulator, with force modeling calculations.

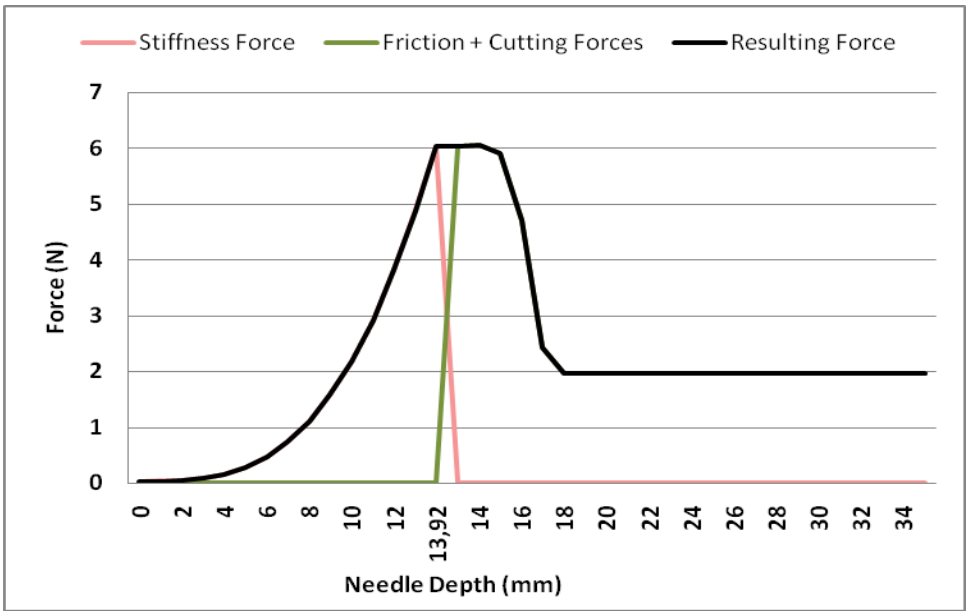

Figure A7. Skin and subcutaneous fat tissue force x needle depth model.

A1.11. VERSION 11

The eleventh version of the simulator (Figure A8) improved the Tissue class, adding parameters for the muscle tissue ("*MusculoHolton*") and two additional properties for every tissue: the initial depth and the perforation depth. Initial depth property is related to the initial position of this tissue inside the body, and perforation depth is related to the position (depth level) where the tissue becomes trespassed by the needle, which changes the force calculations from before to after puncture tissue stages. The perforation depth values were estimated from Holton and Hiemenz (2001) data, as

follows: 13.92 mm for skin tissue, where skin becomes perforated and subcutaneous fat is achieved, and 19.22 mm for reaching the muscle tissue, where the muscle was perforated, and the needle reached the interspinous ligament (ISL).

In order to verify the simulation accuracy and allow comparison of its results with experiment data from Holton and Hiemenz (2001), the resulting forces were recorded and plotted as force x needle depth graph. The first version of this plot only shows the stiffness, cutting, friction and resulting forces actuating in skin, subcutaneous fat and muscle tissues. The other tissues were incorporated in next versions. Figure 31 (Section 3.2) displays the complete force curve reported in Holton and Hiemenz (2001). The data obtained by simulation results (Figure 34 in Section 4.2) and curve behavior were similar.

Figure A8. Version 11 of the simulator, with force model based on experiment data (CONCI et al, 2015).

A1.12. VERSION 12

The version 12 of the simulator was focused into completing the Holton force model simulation, to build force model curves representing all the tissues mapped in Holton and Hiemenz (2001). It was necessary to improve the Tissue class, adding the width muscle for some tissues, and two links for every tissue, in order to map the next tissue to be found and the previous tissue. It was important because it was necessary to load the data from the next tissue, to continue the simulation after the current tissue being completely traversed by the needle tissue. Tissue data were added for the following tissues: Interspinous Ligament (ISL), Ligamentum Flavum (LF), Epidural

Space (ES) and Bone. A plotted force x displacement graph was generated (Figure 34 in Section 4.2). The inconsistencies reported in Section 6.7 were corrected in this version of the simulator.

A1.13. VERSION 13

The version 13 of the simulator was focused into the implementation of needle movement and haptic sensations after tissue perforation. An online demonstration video is available (BRAZIL, 2016c). The needle behavior after perforation was programmed to be in-line with the needle angles, i.e. presets same angle in relation to the normal of the surface being perforated. A Raycast command was set on programming code, with its starting point being the first contact point between the needle tip and the tissue surface being perforated. The puncture direction was then achieved as a function of the orientation of the haptic device, recorded on the last contact point. Setting a maximum depth for needle perforation was necessary, in order to map the tissue surfaces collision path, and calculate the needle inclination angles for setting needle movement restrictions into the needle behavior after the tissue puncture. A haptic plugin from Poyade et al (2015) is also included in the implemented simulator, to enable the haptic device position tracking and communication through the GetProxyPosition and GetProxyOrientation script commands.

A1.14. VERSION 14

The version 14 of the simulator included real-time configuration and adjustments for the following tissue properties: static friction, dynamic friction, stiffness, resistance to perforation, dampening, punctured static and dynamic friction (Figure A9). A 3D model for a Tuohy needle was also incorporated to the simulator, this model was created by the designer Arthur on LNCC lab on Petropolis-RJ, in order to provide more realism to the simulation (Figure 55).

A1.15. VERSION 15

The version 15 of the simulator was directed to calculation, display and recording of resulting haptic forces transmitted to the user by the haptic device, through the combination of tissue properties in action, while the user executes motions related to the simulation of the perforation process (Figure A10). The resulting axial forces on the needle were computed, and the current needle position, direction and torque values were

considered. In order to be able to effectively record the resulting forces, an implemented funtion periodically reads the values from the forces applied on the haptic device and shows them in the user interface. For this task, a Dynamic Library Link (DLL) was used. This DLL is provided as part of the OpenHaptics API from Sensable Technologies Inc. (2009), currently in version 3.0, developed by The 3DSystems (the firm responsible for the Geomagic Touch haptic device production).

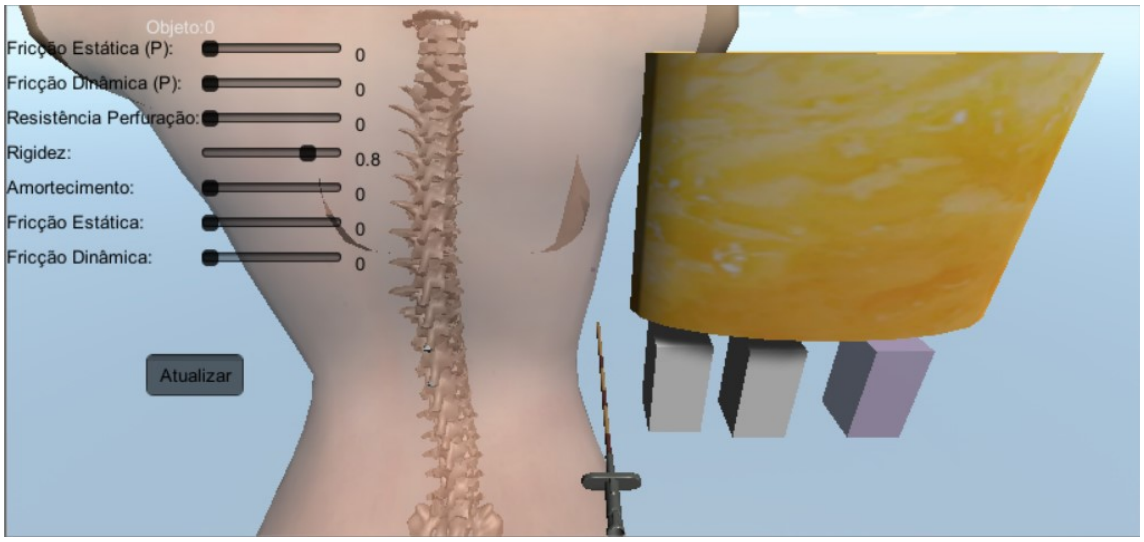

Figure A9. Version 14 of the simulator, including the real-time adjustment of the tissue properties and textures for some tissues.

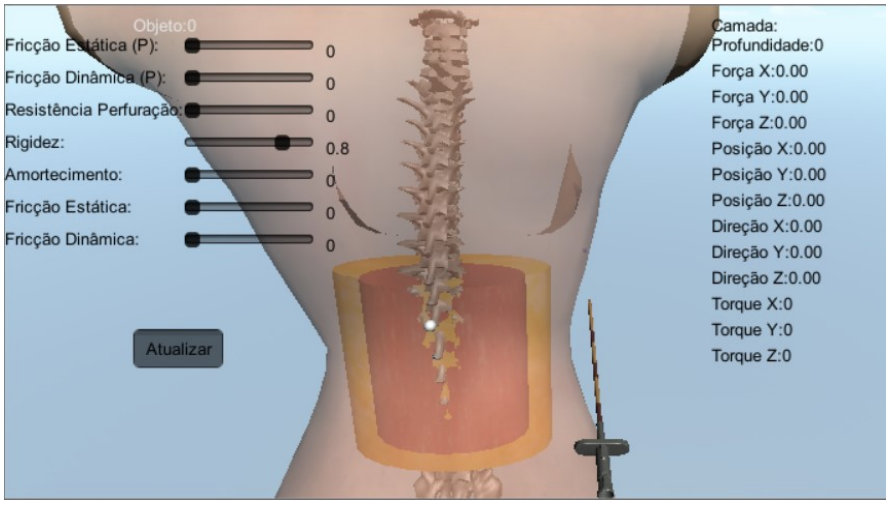

Figure A10. Version 15 of the simulator, including the information from haptic device: applied forces, position, direction and torque.

A large set of the type of data enumeration was configured as parameters for haptic communication and access to its resources. Diverse DLL calls for the available API in Sensable Technologies Inc. (2009) are used to access the haptic device related

functions. As an example, for reading the haptic forces applied to used hands by the device:

```
[DllImport("hd.dll")]
public static extern void hdGetDoublev(ParameterName paramName, [Out] double[ ]
                                                                        value);
```

The version 15 also implemented: the recording of elapsed time (in seconds), current tissue being penetrated and needle depth, forces, position, direction and torque values into a CSV log text file, for further reference and result comparison. An example of a line of recorded data in the log file is:

[8;Muscle;0.2417205;-0.3233308;0.1360251;0.6376453;-0.9209223;-0.2137753;-0.5135543;-0.4209476;-0.9052995;-0.05688529;0.6460515;-0.2895775;-0.7062311]

A1.16. VERSION 16

The version 16 of the simulator emulated the removal of needle mandril and the subsequent insertion of a saline filled syringe, in order to map and display the pressure (kPa) exerted in the current tissue being penetrated (shown in Figure 57). The syringe is currently represented by the 3D object above the needle and the saline pressure is displayed below other information values.

These features are important in order to simulate the LOR technique and enable to detect if the needle has already reached the epidural space region, which is represented by a very low tissue pressure value. The pressure reading was programmed to be displayed only if the player exchanged the mandrill by the syringe, by pressing the button 2 in the haptic device pen. After the syringe insertion, the player was able to read the current tissue pressure displayed on screen, available while pressing the button 1 from haptic device.

A generator of saline pressure values for the epidural tissues was also programmed on this simulator version, to provide different simulation experiences concerning the LOR technique. This implementation details are listed in Section 6.4.

A1.17. VERSION 17

The development of version 17 of simulator was focused on the dynamic dimensioning and positioning of the tissues involved in the epidural simulation (Figure 54). Dynamic tissue dimensioning was implemented based on patient parameters:

height, weight and age, as discussed in Sections 4.1 and 6.2. For dynamic positioning and dimensioning, it was necessary to implement two methods in the game manager class, in which all tissues were defined as a parameter vector of game objects (Figure 67). Details about game manager class can be found in Sections 5.3 and 6.9. Figure 54 shows a woman body with the subcutaneous fat and muscle tissues already dimensioned and positioned inside it. The tissue dimensioning issues mentioned in Section 4.1 could be detected after this implementation.

For specification of each tissue layer parameters, two class scripts were implemented and attached: HapticProperties and Tissue ("*Tecido*"). An example of these class parameters and their association to a tissue can be visualized in Figure 67. Many tests were executed with version 17, regarding additional haptic effects that could be applied when the needle was inside tissues along the simulation. These effects include haptic sensations of: constant forces, spring forces, friction forces and viscosity, defined in Sensable Technologies Inc. (2009).

A1.18. VERSIONS 18 TO 20

The version 18 of the simulator was implemented to track the user movement and a visual reproduction of the player movements executed within the simulator. Tracking and reproduction are listed as a desirable functionality for a virtual simulator (Section 3.1). Details and results from this implementation can be found in Figure 59 from Section 6.5, which illustrates the ongoing of the functionality.

The visual interface became improved on version 19, with the addition of two buttons (Propriedades and Detalhes) which allowed the toogling (displaying or hiding) of relevant information associated to tissues properties and the insertion procedure (Figure 68). A HUD, located at right, was also implemented to display specific information related to the simulation. More information available in Section 6.9. The version 19 also brought the configuration of gamification challenges inside the GameManager class and the logic of awarding score upon task conclusion.

The version 20 of the simulator was focused into the implementation and improvement of the data recording related to the needle advancement event. Section 5.1.2 includes these details. After analyzing the recorded information, it was possible to identify the need of storage for the needle angles in a file, because it strongly influences the axial forces output. Force comparisons were also used for checking the tissue properties influence rate (stiffness, damping, static and dynamic friction) related to the

needle depth. Needle depth x force displacement relations are based on results from Figures 55 and 56.